THESIS FOR THE DEGREE OF DOCTOR OF PHILOSOPHY (Ph.D.)

ION CHANNELS IN NATIVE ENVIRONMENT: CHARACTERIZATION OF ION CHANNELS IN DENDRITIC AND ENDOTHELIAL CELLS

by Emese Zsiros, M.D.

UNIVERSITY OF DEBRECEN

DOCTORAL SCHOOL OF MOLECULAR MEDICINE

DEBRECEN, 2011

Supervisor:

György Panyi, D.Sc.

Table of contents

Abbreviations

ACh	acetylcholine
Ag	antigen
APC	antigen presenting cell
α-GA	18-alfa-glycyrrhetinic acid
BK_{Ca}	large conductance Ca^{2+} activated K^+ channel
CCE	capacitative Ca^{2+} entry
ChTx	charybdotoxin
CNG	cyclic-nucleotide-activated non-selective cation channels
COX	cyclooxigenase
CRAC	Ca^{2+} release activated $Ca2^+$ channel
CTL	cytotoxic T lymphocyte
Cx	connexins
DC	dendritic cells
EC	endothelial cells
EDHF	endothel-derived hyperpolarization factor
eNOS	endothelial nitric oxide synthase
ER	endoplasmic reticulum
GM-CSF	granulocyte-macrophage colony-stimulating factor
HLA	human leukocyte antigen
HPC	hematopoietic progenitor cells
IbTx	iberiotoxin
IC	intracellular
IDC	immature dendritic cell
IK_{Ca1}	intermediate-conductance Ca^{2+} activited K^+ channel
IL	interleukin
IFN	interferon
IP_3	inosithol trisphosphate
K_{ATP}	ATP-sensitive K^+ channel
K_{ir}	inwardly rectifying K^+ channel

LPS	lipopolysaccharide
MEGJ	myoendothelial gap junctions
MDC	mature dendritic cell
MgTx	margatoxin
MHC	major histocompatibility complex
Mo	monocyte
NK	natural killer cells
NO	nitric oxide
NSC	non-selective Ca^{2+}-permeable cation channels
PKC	protein kinase C
PMA	phorbol 12-myristate 13-acetate
PSS	physiological salt solution
RCF	remaining current fraction
SERCA	sarco/endoplasmic reticulum Ca^{2+} ATPase
SK_{Ca}	small-conductance Ca^{2+} activited K^+ channel
SMC	smooth muscle cells
SOC	store-operated Ca^{2+} channels
STX	saxitoxin
VEGF	vascular endothelial growth factor
VRAC	volume-regulated anion channel
VGPC	voltage gated potassium channel
VGSC	voltage gated sodium channel
VSM/VSMC	vascular smooth muscle/ vascular smooth muscle cell
TEA	tetraethylammonium
TCR	T cell receptor
Th	T helper lymphocyte
TNF-α	tumor necrosis factor α
TTX	tetrodotoxin
18β-gly	18β glycyrrhetinic acid

I. Preface

Ion channels as integral membrane proteins provide low-energy pathways for ions to cross cellular membranes. Since the introduction of the patch clamp technique two decades ago the study of ion channels has progressed enormously, allowing one to characterize the ion channel expression in almost every cell type. Ion channels can be characterized by their ion selectivity, conductance, gating properties and pharmacology. Several specific ion channel blockers are now used in clinical therapies, underlying the importance of ion channel research. In our study we focused on the characterization of ion channels in two different cell types, the human dendritic cells (DC) and the endothelial cells (EC) of the arteria mesenterica superior in rats. As cells modulate their gene and ion channel expression rapidly upon the change of extracellular environment in both cases our goal was to characterize the ion channels of these cells in the most physiologic circumstances, thus our results can be further used in clinical investigations.

DC, as well as EC, has been intensively studied in the last 10 years due to their key role in several pathophysiological processes and their potential in new clinical applications. Recent success of DC therapy in cancer treatment have opened new horizons, therefore the study of their maturation and the changes of ion channel expression pattern during this process can have significant impact on developing new treatment protocols. The introduction of DC differentiation from blood derived monocytes (Mo) with cytokines several years ago made it possible to obtain larger amount of DC for research purposes. This made it possible to study the ion channels of DC during the maturation process and compare the ion channel expression to the most frequently used DC model cell, KG-1.

EC dysfunction has also been extensively studied for its pivotal role in hypertension, atherosclerosis, immune response or hemostasis. The function of EC could be considerably altered during the process of isolation and cell culturing; therefore one of the aims of the present study were to set up a method that allows identifying and characterizing the activity of ion channels present on the EC *in situ* and therefore avoiding the alterations induced by cell dispersion or cell culture. The presented method allows evaluating the electrophysiological characteristics of the ion channels expressed in the EC *in situ*.

II. Scientific background

A. Dendritic cells and their role in the immune response

Dendritic cells are located between the boundaries of inner and outside world and are created to bridge the innate and adaptive immunity (Reid, Penna et al. 2000; Schuurhuis, Fu et al. 2006). These cells are able to induce, sustain and regulate immune responses by the translocation of antigens (Ag) from periphery to lymphoid niches (Jonuleit, Schmitt et al. 2001). They represent a rare and phenotypically diverse population of white blood cells with high functional heterogeneity and flexibility (Stockwin, McGonagle et al. 2000). DC originate from $CD34^+$ hematopoetic stem cells and differentiate into multiple different circulating subsets, such as myeloid, lymphoid or plasmacytoid cells (Banchereau and Steinman 1998; Ardavin, Martinez et al. 2001). DC subsets can be found in both lymphoid organs (thymus, bone marrow, lymph nodes and spleen) as well as in non-lymphoid organs (such as blood, skin and other peripheral tissues). They can be further characterized by their surface phenotype or by their function – such as migratory -, tissue-resident -, inflammatory - or tolerogenic DC (Ju, Clark et al. 2010).

DC are the transporters of pathogen-related information within the immune system as they continuously uptake particles and soluble compounds from their tissue environment. They are the only type of antigen presenting cells (APC) that are capable of priming naïve and resting memory T cells as they can migrate from the periphery to the lymph nodes providing them Ag-specific, co-stimulatory and polarizing signals. Pathogen-induced tissue damage as well as multiple environmental factors in the periphery are able to induce DC maturation, which will result in transient increase of Ag uptake, shortly afterwards the loss of endocytic/phagocytic receptors, followed by the presentation major histocompatibility complex (MHC) molecules. DC maturation also includes the production of immunostimulatory cytokines, which are essential for the differentiation and induction of effectors functions of $CD4^+$ (T helper - Th) and $CD8^+$ (cytotoxic – CTL) T lymphocytes, as well as for their protection from apoptosis (**Figure 1)**.

In the development of this cell-mediated immunity the interaction between CD40 and CD40 ligand (CD40L) is one of the key elements. CD40 is widely distributed and is expressed on B

lymphocytes, Mo and DC, but also on EC and epithelial cells (Van Kooten and Banchereau 1997). The CD40L has a more restricted distribution, being mainly expressed by activated $CD4^+$ T lymphocytes (Roy, Waldschmidt et al. 1993). Ligation of CD40 on DC results in maturation of the DC (Cella, Scheidegger et al. 1996), which is crucial for the priming of efficient T cell responses (Schuurhuis, Laban et al. 2000).

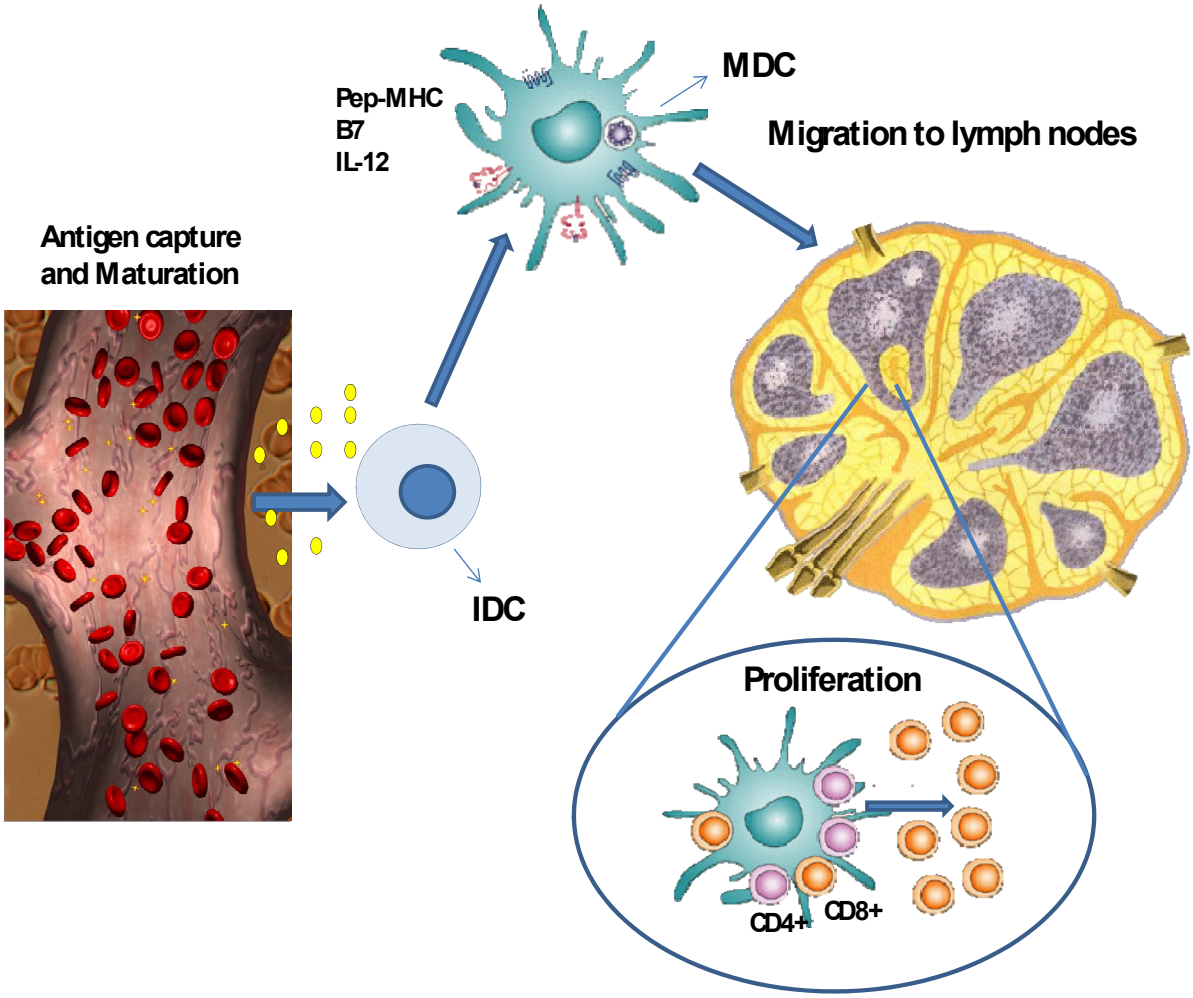

Figure 1 T cell priming by DC

The recruitment of DC precursor Mo into peripheral tissue and the maturation of DC in response to pathogens or cytokines result in migration to the draining lymph node of large numbers of DC carrying high levels of peptide-MHC complexes and B7. By physical interaction through an immunological synapse, naïve T cells achieve stimulation and become committed to proliferate. Sustained T cell receptor (TCR) stimulation by continuous contact with DC and polarizing cytokines promote T cell differentiation to non-lymphoid tissue-homing effector cell. T cells receiving a shorter stimulation do not acquire effector function and retain lymph node-homing capacity.

In the 'license to kill' model (Guerder and Matzinger 1992; Bennett, Carbone et al. 1998; Lanzavecchia 1998) Th cells induce maturation of APC, thereby "licensing" them to directly activate CTL. In addition to Th cells, inflammatory cytokines [tumor necrosis factor α (TNF-α) or interleukin (IL)-1], bacterial components (such as lipopolysaccharide, LPS) or Ag-Antibody immune complexes can induce DC maturation. Once this maturation is complete it is irreversible and will eventually be followed by the death of DC (Wan and Dupasquier 2005).

DC not only play a vital role in adaptive immunity, but they are also crucial in the innate immunity as they play role in the activation of major innate effector cells, the natural killer (NK) cells. NK cells represent less than 10% of peripheral blood lymphocytes and are characterized by their CD56+/CD3- phenotype and their large granular lymphocyte morphology. They have the unique immediate ability to kill their targets without prior cell activation as they are rapidly recruited to the sites of pathogen entry and use the combination of germ line-encoded activating and stimulatory receptors to detect transformed or virally infected cells (Andrews, Andoniou et al. 2005).

Recent studies demonstrated a functional link between NK, DC and unprimed lymphocytes as lymphocyte activation can also take place via reciprocal activation through NK/DC interactions. Activated NK cells induce the maturation of myeloid DC into stable type-1 polarized DC by the production of interferon (IFN)-γ as well as TNF-α (Andrews, Andoniou et al. 2005). These maturated DC have the ability to produce pro-inflammatory cytokines and stimulate Th and CTL cells (Reschner, Hubert et al. 2008). Thus the interaction between NK and DC leads to lymphocyte activation, which has a dramatic impact on the quality and strength of the down-stream immune responses, mainly in the context of early response to tumor cells and infectious agents (**Figure 2**).

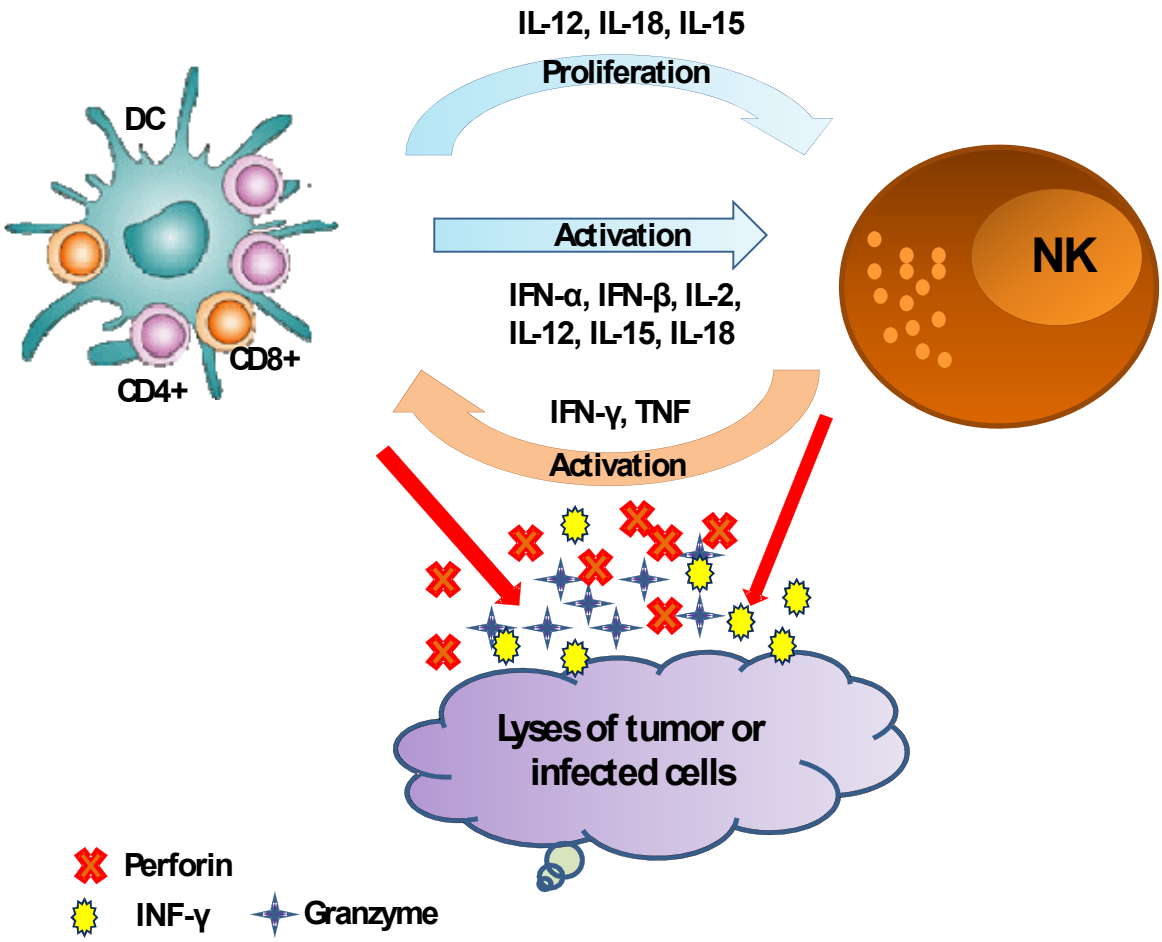

Figure 2 Schematic representation of NK, DC and lymphocyte cross-talk in the effector phase of the immune response

DC maturation by NK is relevant in early responses to tumor cells and certain viruses, when the absence of inflammation and pathogen-associated molecules do not result in DC maturation and subsequent antigen presentation. In addition, the interaction between MDC and NK results in lymphocyte proliferation, IFN-γ production and cytolytic activity against tumors, virus or infected cells. IFN: interferon; IL: interleukin

Although it is known that DC are essential in initiating T cell immunity, numerous pieces of evidence suggest that DC also play a role in tolerance, e.g. different DC subsets can regulate the Th subset balance. In addition with the constant recognition and uptake of apoptotic cells DC provide self-reactive T cells with the opportunity to take themselves out of the functional repertoire through physical elimination or functional inactivation (Steinman, Hawiger et al. 2003; Mueller 2010). Hence as they maintain peripheral tolerance DC seem to be the default mechanism for avoiding autoimmunity. Therefore, manipulating DC seems to be a potent way to treat chronic infections, allergies, autoimmune disease and cancer. In order to do so,

DC have to be obtained, either by isolating them directly from the body or by culturing them from isolated precursors.

1. In vitro differentiation of DC

DC were first described in 1973 by Ralph M. Steinman and Zanvil A. Cohn as a novel cell type found in peripheral lymphoid organs (Steinman and Cohn 1973). In the early years DC research mainly focused on identifying the cells responsibility for follicular antigens retention in the peripheral lymph nodes, but in the recent decades DC research has not been limited to basic immunology. The possibility of using DC for clinical application has generated a great interest and currently more than 6,000 papers are being published annually investigating different basic or translational aspects of DC biology (Trinchieri 2007). Until the discovery of granulocyte – macrophage colony stimulating factor (GM-CSF), which acts as the major factor for the growth and differentiation for DC precursors along with TNF-α, it was very difficult to purify and characterize a large number of these cell types.

In 1992 it was presented, that myeloid DC can be differentiated from $CD34^+$ progenitors of the human cord blood and bone marrow by GM-CSF and TNF-α mediated stimulation, which will result in a heterogeneous population of DC (Caux, Dezutter-Dambuyant et al. 1992; Inaba, Inaba et al. 1992). Further on it was shown, that blood Mo also possess the potential to differentiate into DC in the presence of GM-CSF and anti-inflammatory cytokines such as IL-4 or IL-13 (Romani, Gruner et al. 1994; Sallusto and Lanzavecchia 1994). When CD 14^+ peripheral Mo were cultured in the presence of GCM-CSF and IL-4 they neo-expressed CD1a, CD1b, CD1c, CD80, and CD5; they massively upregulated the expression of CD40 (>100-fold) and HLA-DQ and HLA-DP (~100-fold); as well as significantly (>5-fold) upregulated HLA-DR, CD4, CDllb, CDllc, CD43, CD45, CD45R0, CD54, CD58, and CD59 expression. With this method of differentiation there were no major changes observed for the expression of human leukocyte antigen (HLA) class I**,** CD11a, CD32, CD33, CD48, CD50, CD86, CDw92, CD93, or CD97 (Pickl, Majdic et al. 1996). These *in vitro* generated monocyte-derived DC were able to efficiently present tetanus toxoid as well as they had the ability to form clusters with resting T cells. Thus, based on the detailed phenotypic and functional characteristics (Pickl, Majdic et al. 1996) these cells resemble immature tissue resident DC. These immature DC (IDC) were then further activated by various stimuli such as inflammatory cytokines, bacterial LPS or CD40 ligand to obtain mature DC (MDC) (Caux,

Massacrier et al. 1994) (**Figure 3**). Activation with LPS and CD40 ligand resulted in important morphological changes with a reduction of cytoplasmic content and a remarkable increase of dendrite development as well as an altered phenotype. CD40 triggering induced the maintenance of high levels of MHC II and the up regulation of accessory molecules such as CD58, CD80 (B7-1) and CD86 (B7-2). Finally, CD40 activated IDC secreted a limited set of cytokines (TNF-alpha, IL-8, and macrophage inflammatory protein 1 alpha [MIP-1 alpha]) and were able to mimic physiologic interactions with activated T cells via CD40-CD40L (Caux, Massacrier et al. 1994).

The ability to generate a large number of DC made it possible to study DC biology and to use them in clinical trials and tumor therapy. Among numerous factors that control immune cells' function, ion channels are one of them that play an important role in the regulation of different functions of these cells.

A

B

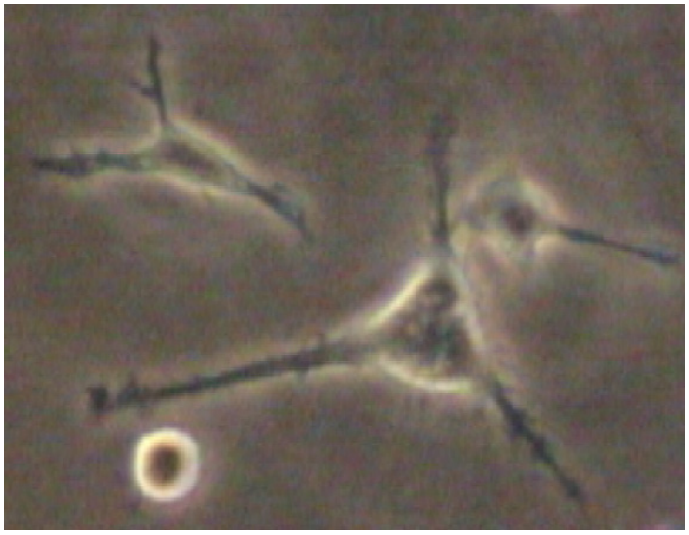

Figure 3 Immature and Mature DC

Panel A shows an IDC that was generated from peripheral blood Mo with GM-CSF and IL-4 during a 5 day incubation. Panel B shows the MDC obtained from IDC 1 day after activation with TNF-α, IL-1β, IL-6, GM-CSF and prostaglandin E2.

2. The characteristics of DC model cell lines and their role in DC research

As described above human DC is a heterogeneous cell population that *in vivo* arises from multiple distinct hematopoietic progenitor cells (HPC) along distinct differentiation pathways. These progenitors include $CD14^+$ Mo and $CD34^+$ bone marrow cells (Akagawa, Takasuka et al. 1996; Kiertscher and Roth 1996; Zhou and Tedder 1996). $CD34^+CD10^+$ HPC give rise to the lymphoid DC lineage (Galy, Travis et al. 1995), whereas $CD34^+CD86^+$ HPC are progenitors for myeloid DC as well as monocytes and macrophages (Ryncarz and Anasetti 1998). Despite of being able to activate some of signal transduction pathways involved in the differentiation, a number of obstacles make it difficult to generate large amount of homogenous human DC *ex vivo* from $CD34^+$ HPC (St Louis, Woodcock et al. 1999). The rarity of $CD34^+$ HPC (0.1–1% of bone marrow mononuclear cells) makes sufficient isolation for larger scale studies laborious, as well as $CD34^+$ HPC are heterogeneous population of progenitors that can be already committed to different lineages. The activation of these cells results in mixed population of cells (DC, Mo, neutrophils) that require additional purification of DC before definitive analysis (Hart 1997). Finally, $CD34^+$ HPC have been difficult to transfect and transduce (Sekhar, Kotani et al. 1996), which makes genetic manipulation less effective.

As mentioned in the previous section human myeloid DC can also be differentiated from peripheral blood $CD14^+$ Mo with GM-CSF+IL-4 (Romani, Gruner et al. 1994; Sallusto and Lanzavecchia 1994). This method has been widely used recently for experimental purposes as $CD14^+$ precursors are abundant in the blood (Thurner, Roder et al. 1999). Although it is possible to generate larger number of DC with this method, the stimulation of peripheral Mo by cytokines is still very arduous and expensive, which makes it difficult to obtain them on a daily base for experimental purposes.

To overcome these hurdles established leukemic cell lines, such as the pro-myelocytic HL-60 and the $CD34^+$ erythroleukemia cell line KG-1 were used to study DC function, maturation and differentiation in the past (Czerniecki, Carter et al. 1997; Ackerman and Cresswell 2003). Stimulation of these cell lines with calcium ionophor, cytokines and phorbol 12-myristate 13-acetate (PMA) results in morphological changes and the up-regulation of the expression of CD80, CD86, CD83, CD40, and CD54 (ICAM-1), the loss of CD14 and the delayed (48–96 h) acquisition of dendritic processes, as well as a capacity to sensitize T lymphocytes to

antigen (Caux, Massacrier et al. 1994; Ackerman and Cresswell 2003; Hajas, Zsiros et al. 2004).

KG-1 cells are described to be one of the closest models to human myeloid DC (St Louis, Woodcock et al. 1999). These cells can be activated by various stimuli and the differentiated cells resemble mature myeloid DC (Hulette, Rowden et al. 2001). As mentioned above this process can be induced by various cytokine cocktails or PMA alone or in combination with ionomycin and cytokines together with PMA (St Louis, Woodcock et al. 1999). The PMA-induced protein kinase C (PKC)-driven differentiation of KG-1 cells was shown to result in a DC-like phenotype as revealed by morphology and also by the appearance of the CD83 DC marker (St Louis, Woodcock et al. 1999). It was also suggested that this PKC activation was required to initiate cell differentiation, and the rise of intracellular free Ca^{2+} was necessary for the terminal differentiation and the apoptosis of KG-1 cells (St Louis, Woodcock et al. 1999). A small proportion of KG-1 cells were also induced to express the Langerhans cell marker CD1a when differentiated by a cytokine cocktail including GM-CSF and TNF-α (Hulette, Rowden et al. 2001; Ackerman and Cresswell 2003). PKC activation of KG-1 cells was shown to enhance their potential to induce allogenic T-cell proliferation (St Louis, Woodcock et al. 1999), whereas Suciu-Foca Cortesini et al. demonstrated that regulatory T cells induce the maturation of KG-1 cells into an immune suppressive type of APC (Suciu-Foca Cortesini, Piazza et al. 2001). In response to contact with T cells KG-1 cells upregulated 4-1BB ligand, FcγRIIa (CD32), FcγRI (CD64), downregulated Ox40ligand and CD43, a cell surface sialoglycoprotein of immature DC, which regulates cell adhesion and mediates DC cell maturation (Suciu-Foca Cortesini, Piazza et al. 2001). PMA and ionomycin induces a maturation process in KG-1 cells which is accompanied by changes of morphology, internalizing capacity, and cell surface expression of MHC class I molecules. Intracellular MHC class II trafficking and the potential to cross-present exogenous antigens for $CD8^+$ T lymphocytes was similar in monocyte-derived DC and in KG-1 cells (Ackerman and Cresswell 2003).

Based on the phenotypic and functional similarities of IDC, MDC and KG-1 cells we initiated experiments to characterize the ion channels expressed in unstimulated and activated KG-l cells and compare the results with those obtained for IDC and MDC. We aimed to determine if the KG-1 cell line could be used to understand the function of ion channels in dendritic cells and utilize as a model cell line in electrophysiological studies as well.

3. Ion channels in the immune system

Several studies demonstrated that the expression of ion channels in different immune cells - such as monocytes, macrophages and lymphocytes - varies during their activation and differentiation (Chandy, DeCoursey et al. 1985; Gallin and McKinney 1988; Ghanshani, Wulff et al. 2000; Vicente, Escalada et al. 2003; Villalonga, Escalada et al. 2007). These electrically non-excitable cells possess both voltage-dependent and secondary messenger-gated ion channels that are crucial for their antigen-dependent activation, proliferation and migration (Chandy, DeCoursey et al. 1985). Voltage-gated potassium channels (VGPCs) have been described to be the main ion channels controlling the resting membrane potential and tuning the intracellular Ca^{2+} signaling in Mo, lymphocytes, macrophages and mouse DC (DeCoursey, Chandy et al. 1985; Fischer and Eder 1995; Vicente, Escalada et al. 2003; Panyi, Varga et al. 2004). The dynamic change in the expression of ion channels, including VGPCs upon distinct EC stimuli is important in specific immune responses during the terminal differentiation and activation of these cells (Chandy, DeCoursey et al. 1985; Craner, Damarjian et al. 2005). Among the VGPCs the mammalian *Shaker* family (Kv1) contains at least eight different genes (Kv1.1 to 1.8) that can form functional homo- and heterotetrameric complexes (Gutman, Chandy et al. 2005). These Kv1 subunits can assemble promiscuously creating a wide variety of biophysically and pharmacologically different channels (Vicente, Escalada et al. 2005). The biophysical characteristics of these channels are further modified by presence of auxiliary subunits (Kvβ), which provide additional mechanism for fine-tuning K^+ currents to ever changing cellular conditions (Vicente, Escalada et al. 2005). A member of the *Shaker* family, Kv1.3 channel is extensively studied for its potential role in lymphocyte and macrophage activation. Kv1.3 channels are almost exclusively expressed in the immune system, and the blockade of these channels is associated with selective inhibition of T cell activation and proliferation (Chandy, Wulff et al. 2004; Panyi, Varga et al. 2004). Inwardly rectifying K^+ channels ($K_{ir}2.1$), Ca^{2+}-activated K^+ channels (IK_{Ca1} or $K_{Ca}3.1$) and Kv1.5/Kv1.3 heterotetramer channels have also been described in T cells and in cells of the mononuclear phagocytic system (Gallin 1991; Grissmer, Nguyen et al. 1993; Vicente, Escalada et al. 2003; Chandy, Wulff et al. 2004; Panyi, Varga et al. 2004).

Among the myeloid cell lines macrophages have been electrophysiologically well-characterized. Gallin and McKinney found that 35% of human macrophages, cultured longer than 7 days, exhibited whole-cell inward currents, whereas 85% of cultured cells expressed large conductance (240 pS in symmetrical K^+) calcium-activated K^+ channels (Gallin and

McKinney 1988) , but these channels were absent in freshly isolated monocytes. The group of DeCoursey identified the following types of ion channels in undifferentiated and differentiated monocyte-derived human THP-1 macrophage model cells: (1) delayed rectifier K^+channels (confirmed to be Kv1.3), (2) Ca^{2+}-activated K^+ channels (SK type), (3) non-selective cation channels, (4) Cl^- channels, (5) voltage-activated H^+ channels, (6) Ca^{2+}-activated maxi K^+ channels (BK channels) and (7) inwardly rectifying K^+ channels (DeCoursey, Chandy et al. 1985; Kim, Silver et al. 1996). The human myelomonocytic-model cell line HL-60 showed different ion-channel expression upon their differentiation into monocytes or polymorphonuclear cells (Brent, Rubenstein et al. 1996). The expression of different ion channels was reflected in the ATP- and ionomycin-induced change in the membrane potential: polymorphonuclear cells responded with depolarization, whereas the membrane of monocytes became hyperpolarized upon addition of ATP and ionomycin (DeCoursey, Chandy et al. 1985).

The hypothesized role of most of these channels is to maintain a hyperpolarized membrane potential, which enhances and sustains the Ca^{2+} signal upon activation. The intracellular Ca^{2+} signal is also influenced by the presence of Ca^{2+} release-activated Ca^{2+} channels (CRAC) in lymphocytes, macrophages and DC. These channels are responsible for the sustained Ca^{2+} signal required for the expression of numerous functionally important genes (Lewis 2001) that regulate immune responses.

4. Ion channels and Ca^{2+} signaling in DC

Similar to other immune cells, several crucial intracellular functions are coupled to the Ca^{2+} signaling pathway in DC. The rise of cytosolic Ca^{2+} concentration accompanies the differentiation of IDC to MDC. Various Ca^{2+} channels take part in controlling the intracellular Ca^{2+} level in DC: RyR1 receptors, P2Y receptors, L-type calcium channels and CRAC (Poggi, Rubartelli et al. 1998; Liu, Bohlen et al. 1999; Hsu, O'Connell et al. 2001; O'Connell, Klyachko et al. 2002). It is well documented that a prerequisite of proper CRAC function is a negative membrane potential, which is usually maintained by different K^+ channels. Fischer and Eder showed the presence of voltage-gated K^+ conductance in the membrane of murine DC, but limited or no information was available about the ion channel expression of DC differentiation models (such as KG-1) or human DC (Fischer and Eder 1995).

Based on the preliminary evidence regarding the role of ion channels in Mo and DC we designed experiments to identify and characterize the expression and functional activity of voltage-gated ion channels in DC generated *in vitro* from human peripheral blood monocytes and the DC model cell KG-1. We hypothesized that there's a switch of ion channel expression during DC maturation, which could contribute to the distinct functional activities of these cells associated with their different maturation states.

5. Biophysical characteristics of Kv1.3 and IK_{Ca1} channels

The Kv1.3 channel is composed of four identical, pore-forming alpha subunits, which are composed of six transmembrane α-helices connected by intra- and extracellular loops (Panyi 2005). The extracellular loop between the 5th and 6th transmembrane segments (S5 and S6) along with segments of the S6 helix from each subunit form the pore through which K^+ cross the membrane. The co-expression of auxiliary β subunits in cells alters several biophysical properties of Kv1.3 gating (Vicente, Escalada et al. 2005). The main structural element of the ion conduction pore is the selectivity filter that contains the signature sequence of K^+ channels (Panyi 2005). The selectivity sequence of Kv1.3 is K^+>Rb^+>>$NH4^+$>>Cs^+>>Na^+, overall, Kv1.3 is ~1000-fold selective for K^+ as compared to Na^+ (Cahalan, Chandy et al. 1985).

The Kv1.3 channel is a depolarization-activated voltage-gated K^+ channel. The activation threshold of Kv1.3 channels is between −50 mV and −60 mV, and the open probability of the channel increases steeply with depolarization (Cahalan, Chandy et al. 1985; Pahapill and Schlichter 1992). The midpoint of the voltage-dependence of steady-state activation measured in whole-cell patch-clamp configuration in human T cells is between −40mV and −30mV and the slope factor characterizing the steepness of the conductance-voltage relationship is around 10 mV (Panyi 2005). The voltage-dependence of steady-state inactivation of Kv1.3 has a midpoint between −60mV and −70mV and the slope factor of ~10 mV (Panyi 2005).

Upon depolarization of the membrane Kv1.3 channels open rapidly and the activation time constant of the current becomes shorter with depolarization reaching values of 1-1.5 ms at positive voltages (Cahalan, Chandy et al. 1985). The short rising phase of the whole-cell

current is followed by a slow decay during prolonged depolarization as a consequence of inactivation. Members of the *Shaker* K^+ channel family can be inactivated via N-type and the so-called "slow inactivation" (Panyi 2005). The N-type inactivation mechanism, which is the consequence of the occlusion of the open pore by an N-terminal "tethered cytoplasmic ball" (Hoshi, Zagotta et al. 1990), is missing in Kv1.3. The "slow inactivation" is related to the constriction or collapse of the selectivity filter near the extracellular mouth of the pore (Liu, Jurman et al. 1996; Loots and Isacoff 1998). The slow inactivation consists of the closing of the gate at the extracellular end of the pore (P-type inactivation), followed by the further conformational change in this region that stabilizes both the non-conducting state and the conformation of the voltage sensors (C-type inactivation) (Olcese, Latorre et al. 1997).

IK_{Ca1} is an intermediate conductance Ca^{2+}-activated K^+ channel. Similarly to other voltage-gated K^+ channels (Panyi 2005) IK_{Ca1} channels are composed of four non-covalently linked subunits, where each subunit consists of 6 transmembrane helices (Panyi 2005) with a pore architecture similar to Kv1.3 (Rauer, Pennington et al. 1999). The relative permeability ratios to K^+ determined from reversal potential measurements are: K^+ (1.0) > Rb^+ (0.96) > $NH4^+$ (0.17) > Cs^+ (0.07) (Grissmer, Nguyen et al. 1993).
Although the IK_{Ca1} current shows inward rectification, the activation of the channels is voltage-independent (Panyi 2005) and the channel is activated by the rise of the intracellular free Ca^{2+} concentration above ~100 nM (Grissmer, Nguyen et al. 1993). The Ca^{2+} concentration-dependence of the IK_{Ca1} conductance is very steep and it is characterized by a Hill coefficient of 4 and a midpoint of ~300 nM (Panyi 2005).
The channels are fully activated by 1 μM Ca^{2+} in the pipette solution at which most of the pharmacological experiments are conducted. The unitary conductance of the channel in symmetrical K^+ solution is 33-35 pS (Panyi 2005).

6. Pharmacological description of Kv1.3 and IK_{Ca1} channels

Based on their chemical structure molecules inhibiting Kv1.3 and IK_{Ca1} channels are classified as inorganic ions, small-molecule inhibitors and peptide blockers (Wulff, Calabresi et al. 2003; Panyi 2005). Most of the peptide blockers of Kv1.3 were isolated from scorpions and are composed of 23 to 64 amino acids (Price, Lee et al. 1989; Leonard, Garcia et al. 1992). The scorpion toxins peptides bind tightly into the external vestibule of the channels

with 1:1 toxin-channel stoichiometry and occlude the ion conduction pore (Goldstein and Miller 1993). Their structural hallmark is the presence of a cysteine-stabilized α/β motif in which disulphide bridges covalently link the antiparallel β-sheets located on the toxin's surface interacting with the channels to the α-helical segment on the opposite side of the molecule (Rodriguez de la Vega and Possani 2004). The most potent natural toxin blockers of Kv1.3 channels are characterized by equilibrium dissociation constants (K_d) in the low nM and pM range (Panyi 2005). Some of the important of these toxins are charybdotoxin (ChTx, K_d~0.5-1 nM (Price, Lee et al. 1989)), noxiustoxin (K_d~1 nM (Grissmer, Nguyen et al. 1994)) and margatoxin (MgTx, K_d~50 pM (Garcia-Calvo, Leonard et al. 1993)).

In addition to the scorpion toxins one of the most potent and most extensively studied blockers of Kv1.3, ShK, was isolated for the sea anemone Stichodactyla helianthus (Kalman, Pennington et al. 1998). The structure of sea anemone toxins is substantially different from those of scorpion toxins, however, the interaction surface between the toxins and the Kv1.3 pore is similar with a K_d ~11 pM (Dauplais, Lecoq et al. 1997).

Tetraethylammonium (TEA, K_d~12 mM) has also been demonstrated to reduce the peak amplitude of Kv1.3 current as well as to slow down the inactivation process by the foot-in-the-door mechanism (Grissmer and Cahalan 1989). This mechanism means that fast binding of TEA to the open channels impedes slow inactivation: blocked channels cannot be inactivated until TEA unbinds. This results in an apparent slowing of the rate of slow inactivation of Kv1.3 (Grissmer and Cahalan 1989).

The IK_{Ca1} current can be inhibited by clotrimazole (Logsdon, Kang et al. 1997) and its engineered analogue TRAM-34 (K_d= 20 nM) (Wulff, Miller et al. 2000), however it is insensitive to the SK_{Ca} blocker apamin (Grissmer, Nguyen et al. 1993).

Pioneering studies led to the discovery of peptide blockers having good selectivity for Kv1.3 over IK_{Ca1}, e.g. margatoxin and noxiustoxin and to the recognition that depending on the activation status of the T cells the contribution of the channels to the membrane potential control is different.

7. Biophysical and pharmacological characteristics of voltage gated sodium channels, including NaV1.7 channels

Voltage-gated sodium channels (VGSC) are described to be responsible for action potential initiation and propagation in excitable cells, however they are also expressed on non-excitable cells, where their physiological role is unclear (Catterall, Goldin et al. 2005).

Sodium channels consist of a highly processed 260 kDa α subunit which is associated with auxiliary β subunits (Catterall, Goldin et al. 2005). The pore-forming α subunit is sufficient for functional expression, however the kinetics and voltage dependence of channel gating are modified by the β subunits (Catterall, Goldin et al. 2005). The α subunits are organized in four homologous domains (I-IV), each of which contains six transmembrane α helices (S1-S6) and an additional pore loop located between the S5 and S6 segments (Catterall, Goldin et al. 2005). The pore loops line the outer, narrow entry to the pore, whereas the S5 and S6 segments line the inner, wider exit from the pore (Terlau and Stuhmer 1998). The S4 segments in each domain contain positively charged amino acid residues at every third position (Catterall, Goldin et al. 2005) (Fozzard and Hanck 1996). These residues serve as gating charges and move across the membrane to initiate channel activation in response to depolarization of the membrane. The short intracellular loop connecting homologous domains III and IV serves as the inactivation gate, folding into the channel structure and blocking the pore from the inside during sustained depolarization of the membrane (Fozzard and Hanck 1996; Terlau and Stuhmer 1998; Catterall, Goldin et al. 2005).

The nine mammalian sodium channel isoforms that have been identified and functionally expressed are all greater than 50% identical in amino acid sequence in the transmembrane and extracellular domains, where the amino acid sequence is similar enough for clear alignment (Catterall, Goldin et al. 2005). All of the pharmacological agents that act on sodium channels have receptor sites on the α subunits (Catterall, Goldin et al. 2005). At least six distinct receptor sites for neurotoxins and one receptor site for local anesthetics and related drugs have been identified (Cestele and Catterall 2000). Neurotoxin receptor site 1 binds the nonpeptide pore blockers tetrodotoxin (TTX), saxitoxin (STX) and the peptide pore blocker μ-conotoxin (Fozzard and Hanck 1996; Terlau and Stuhmer 1998; Cestele and Catterall 2000). The receptor sites for these toxins are formed by amino acid residues in the pore loops and immediately on the extracellular side of the pore loops at the outer end of the pore. Neurotoxin receptor site 2 binds a family of lipid-soluble toxins, including batrachotoxin, veratridine, aconitine, and grayanotoxin, which enhance activation of sodium channels, whereas neurotoxin receptor site 3 binds the α-scorpion toxins and sea anemone toxins, which slow the coupling of sodium channel activation to inactivation (Cestele and Catterall 2000). These peptide toxins bind to a complex receptor site that includes the S3-S4 loop at the outer end of the S4 segment in domain IV (Cestele and Catterall 2000). Neurotoxin receptor site 4 binds the β-scorpion toxins, which enhances activation of the

channels. The receptor site for the β-scorpion toxins includes the S3-S4 loop at the extracellular end of the voltage-sensing S4 segment in domain II (Cestele and Catterall 2000). Neurotoxin receptor site 5 binds the complex polyether toxins brevetoxin and ciguatoxin, which are made by dinoflagellates and cause toxic red tides in warm ocean waters (Cestele and Catterall 2000). Neurotoxin receptor site 6 binds δ-conotoxins, which slows the rate of inactivation like the α-scorpion toxins (Cestele and Catterall 2000).

Nav1.7 channels have been previously described in action potential initiation and transmission in peripheral neurons (DRG neurons, sympathetic neurons, Schwann cells, and neuroendocrine cells) (Sangameswaran, Fish et al. 1997; Rush, Brau et al. 1998), however they have not been described in the immune system. The activation threshold of the channel is at Va= −45 mV with a conductance of 19.5 pS on peripheral neurons. The current is blocked by: TTX (EC_{50} = 25 nM in human), STX and local anesthetic lidocaine (EC_{50} = 450 μM in resting state at −100 mV), which makes it a probable target of local anesthetics in the peripheral nervous system (Klugbauer, Lacinova et al. 1995; Chevrier, Vijayaragavan et al. 2004).

Mutations of the channel have been described in inherited erythromelalgia, which is a rare disorder characterized by burning pain and warmth and redness of the extremities (Yang, Wang et al. 2004).

B. Physiological functions of endothelial cells

Vascular endothelium is a multifunctional and highly specialized cell layer, lining the luminal surface of the entire vascular system. They provide a structural and metabolic barrier between the blood and the underlying tissues as they regulate a variety of vascular functions. They control vessel tone and adjust vascular diameter in response to hemodynamic needs and forces, such as changes in flow rate or in blood pressure (Beny 1999). This is governed by synthesizing and releasing vasoactive mediators in response to different chemical substances, such as acetylcholine (Ach) or bradykinin, which bind to specific receptors present on the luminal or abluminal surfaces of EC. Because of their complex function and pivotal role in numerous pathophysiologic conditions these cells have become the major focus of modern biomedical research (Davies, Olesen et al. 1988; Beny 1999). EC also regulate the permeation of various cell metabolites as well as the release of paracrine substances that are involved in blood coagulation and in the migration of various cell types (Esper, Nordaby et al. 2006). They initiate angiogenesis, wound healing and vascular remodeling, and as antigen presenting cells, they are involved in the immune responses as well (Mombouli and Vanhoutte 1999).

1. Calcium signals and ion channels in vascular response

The complex function of EC requires a rapid analysis and transduction of various signals that originate from the blood, from the adhering cells, or from the luminal surface of the vessel (Beny 1999). These extracellular signals activate various second messenger systems that are integrated in the EC membrane. Our knowledge about the intracellular signal transduction is still very limited, but among the second messengers Ca^{2+} signaling is known to be the most important (Oike, Droogmans et al. 1994). The control of the intracellular free Ca^{2+} concentration ($[Ca^{2+}]_i$) is the main regulating factor in the production and release of various vasoactive factors, e.g. nitric oxide (NO), prostaglandin I_2, endothelium-derived hyperpolarization factor (EDHF), angiotensin II, endothelin, superoxide anions and thromboxane A_2, and factors involved in blood clotting (Nilius and Droogmans 2001; Brakemeier, Kersten et al. 2003). In addition, Ca^{2+} entry is also involved in controlling intercellular permeability, EC proliferation and angiogenesis (Nilius and Droogmans 2001; Salomonsson, Sorensen et al. 2004).

Under physiological circumstances two types of Ca^{2+} signals can be distinguished in cultured EC: Ca^{2+} oscillations and biphasic increase in the $[Ca^{2+}]_i$ (Nilius and Droogmans 2001). Oscillations appear after the stimulation with a small concentration of agonist as a result of Ca^{2+} release from inositol trisphosphate (IP_3) sensitive intracellular stores (Jacob, Merritt et al. 1988; Oike, Droogmans et al. 1994). Biphasic responses occur after application of higher agonist dose, and consist of a fast peak followed by a long lasting plateau. During the biphasic response the fast Ca^{2+} peak represents Ca^{2+} release from the IP_3 sensitive intracellular Ca^{2+} stores, whereas the plateau level is the consequence of Ca^{2+} entry into the cells. The sustained plateau level is modulated by the mitochondrial Ca^{2+} buffering, the Na^+/Ca^{2+} exchanger located in the plasma membrane and by the sarco/endoplasmic reticulum Ca^{2+} ATPase (SERCA) (Nilius and Droogmans 2001).

Ca^{2+} entry into EC occurs via different pathways, but the mechanism of their activation is still poorly understood. Among these pathways Ca^{2+} entry channels, and channels that control membrane potential and tune the electrochemical gradient that provides driving force for Ca^{2+} play a major role. The main Ca^{2+} entry channels described so far are the non-selective Ca^{2+}-permeable cation channels (NSC), cyclic-nucleotide-activated non-selective cation channels, store-operated Ca^{2+} channels (SOC) like CRAC and capacitative Ca^{2+} entry (CCE) channels.

Store-operated CRAC channels are one of the most conserved and widespread route for triggering cytoplasmic Ca^{2+} rise in many cells - including EC (Parekh 2010). The cellular responses that are activated in response to Ca^{2+} entry through CRAC channels are include both short-term [safeguarding the Ca^{2+} content of the endoplasmic reticulum (ER), maintenance of cytoplasmic Ca^{2+} oscillations, enzyme activation, secretion] and long-term (gene expression) changes in cells (Zweifach and Lewis 1993).
These channels are activated by the emptying of the IP_3-sensitive ER, regardless of the mechanism how the ER are depleted (e.g.: physiological increase of IP_3 levels or by pharmacological mechanism -like IP_3 analogues, Ca^{2+} ionophores, and inhibitors of the SERCA pump such as thapsigargin) (Parekh and Putney 2005). It is the fall in Ca^{2+} levels within the ER and not the subsequent cytosolic rise in Ca^{2+} levels that initiates the cascade of events leading to CRAC channel activation (Parekh 2010). CRAC channels are not voltage-activated by themselves, but changes in the membrane potential affect the driving force for Ca^{2+} flux through the channels. The channels are exquisitely selective for Ca^{2+} and discriminate not only between monovalent and divalent cations, but also between the

different divalent cations (Parekh and Putney 2005; Prakriya and Lewis 2006). This high selectivity pairs up with a low single channel conductance, estimated to be as low as ~2 fS from fluctuation analysis (Zweifach and Lewis 1993). Nevertheless, after store depletion the channels have a high likelihood of being open and therefore of conducting Ca^{2+} (Parekh 2010). These channels are also highly conserved in terms of their gating, conductance and ionic selectivity thereby reinforcing the view that CRAC channels are an important and fundamental Ca^{2+} entry pathway (Parekh 2010).

The Ca^{2+} signal mediated by Ca^{2+} entry channels was proved to be important in the synthesis and release of NO, secretion of vasoactive compounds out of the vesicular compartments, and they also play role during the stimulation of EC by growth factors, such as vascular endothelial growth factor (VEGF). Voltage-gated Ca^{2+} channels (similar to the classical L- and T-type Ca^{2+} channels) have also been described in freshly dissociated capillary EC from bovine adrenal glands. They are involved in the depolarization induced Ca^{2+} transient, thus seem to play role in the endothelial Ca^{2+} signaling (Nilius and Droogmans 2001).

Channels that control the membrane potential are also important regulators for transmembrane Ca^{2+} fluxes. The membrane potential of vascular endothelial cells is negative compared to the blood and tissue compartments. Its value, as well as the cell capacitance and input resistance, varies considerably between different cells types and conditions of cell isolation and culturing. In general EC membrane potential is more negative in macrovascular than in microvascular EC (Daut, Standen et al. 1994; Zunkler, Henning et al. 1995; Nilius, Viana et al. 1997). According to our current knowledge the resting membrane potential is mainly controlled by K^+, Cl^- and Na^+ conductances. Their relative contribution to the resting membrane potential is K^+ : Cl^- : Na^+ = 27-95% : 9-35% : 3-30% (Himmel, Whorton et al. 1993; Vargas, Caviedes et al. 1994; Voets, Droogmans et al. 1996). The electrogenic Na^+/K^+-ATP-ase also contributes approximately −8 mV to the resting potential of EC (Daut, Standen et al. 1994; Oike, Droogmans et al. 1994).

Values of resting membrane potential are between 0 and −80 mV, the cell capacitance ranges between 30 and 80 pF and the input resistance of the cells varies between 1-10 GΩ in isolated non-confluent macrovascular EC (Nilius and Droogmans 2001). Confluent cells have a higher membrane capacitance (up to 160 pF) and lower input resistance (0.01-0.4 GΩ), which can be due to intercellular electrical coupling via gap junctions (Nilius, Viana et al. 1997).

Endothelial K^+ channels are said to be responsible for setting the membrane potential and their role in endothelium-dependent vasodilatation has been widely implicated. Different types of K^+ channels have been described in EC using various culturing and recording conditions: inwardly rectifying K^+ channel (K_{ir}), large conductance Ca^{2+} activated K^+ channel (BK_{Ca}), small- and intermediate-conductance Ca^{2+} activated K^+ channel (SK_{Ca} and IK_{Ca1} respectively), ATP-sensitive K^+ channels (K_{ATP}). K_{ir} channels are the major class of ion channels setting the resting membrane potential, and quite heterogeneously expressed in different EC types. The gating of K_{ir} channels is also regulated by the $[K^+]_{ec}$, the increase of extracellular K^+ activates these channels, which leads to hyperpolarization, thus relaxation of the vascular smooth muscle (VSM) (Knot, Zimmermann et al. 1996; Haddy, Vanhoutte et al. 2006). In addition to serving as extracellular K^+ sensors, these channels act as amplifiers of hyperpolarization initiated by the opening of other K^+ channels (Jackson 2005). K_{ir} channels also play an important role in shear-stress induced hyperpolarization of EC, whereas vasoconstrictors (angiotensin II, vasopressin, endothelin and histamine) have been reported to inhibit K_{ir} channels by G-protein dependent mechanism (Nilius and Droogmans 2001).

Ca^{2+} activated K^+ channels (BK_{Ca}, IK_{Ca1} and SK_{Ca}) are activated by the increase of $[Ca^{2+}]_i$ and have been described in freshly isolated EC and as well as EC in primary culture (Rusko, Tanzi et al. 1992; Haburcak, Wei et al. 1997; Kamouchi, Trouet et al. 1997). The inhibition of these channels interferes with NO release (Busse, Fleming et al. 1993), but understanding their physiological roles requires further studies. K_{ATP} channels were observed in rat aorta and brain mircrovessel EC during ischemic/hypoxic condition, but their contribution to EC function has been challenged on many studies (Nilius, Viana et al. 1997). Delayed rectifier K^+ current has been observed (probably Kv1.5) in freshly isolated EC from resistance vessels. These channels` functions still remains to be hypothetical, they supposedly have effect on the oscillation of membrane potential and $[Ca^{2+}]_i$ (Nilius and Droogmans 2001) **(Figure 4).**

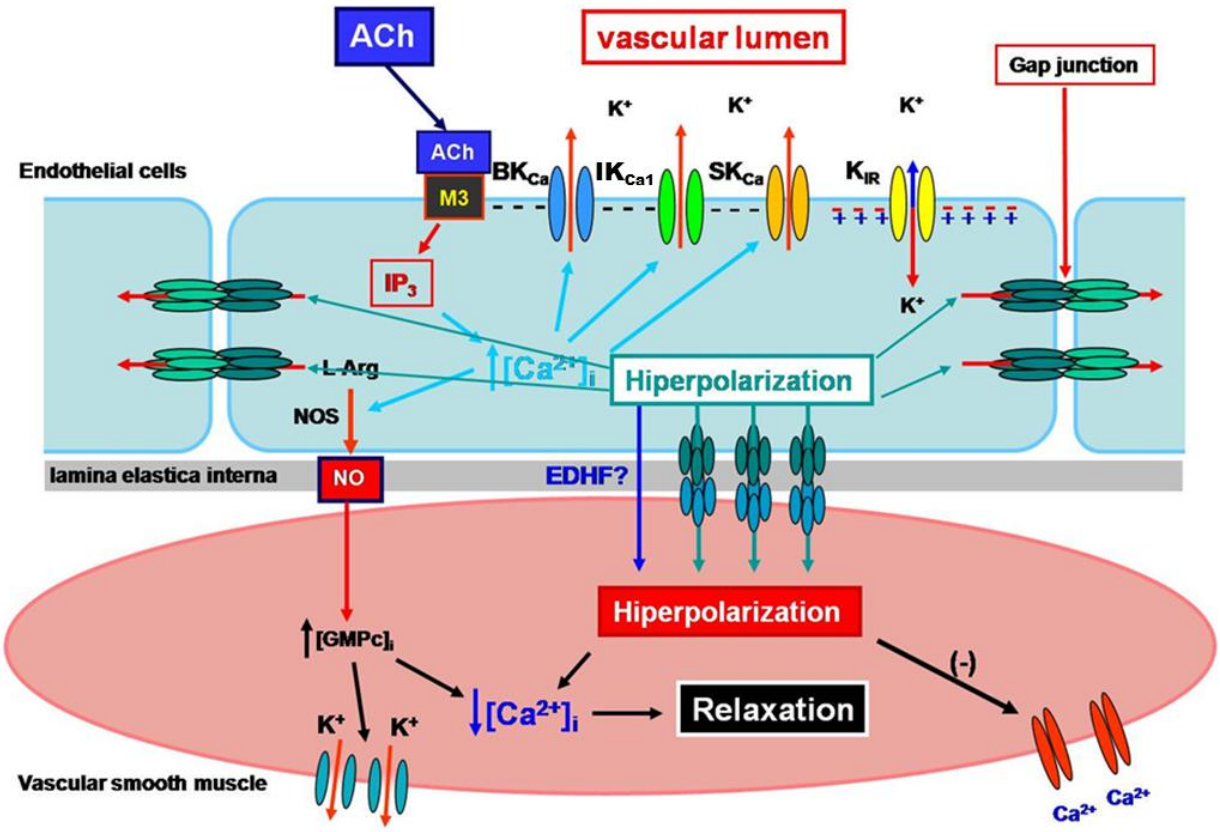

Figure 4 Role of K_{ir}, K_{Ca} and gap junctions in the regulation of vascular tone

K_{ir} channels are the major class of ion channels setting the resting membrane potential and the expression of these channels is inversely proportional with the diameter of the arteries, thus they are more abundant on autoregulatory vascular beds. The gating of K_{ir} channels is also regulated by the $[K^+]_{ec}$, the increase of extracellular K^+ activates these channels, which leads to hyperpolarization and relaxation of the VSM (Knot, Zimmermann et al. 1996; Haddy, Vanhoutte et al. 2006). The Ca^{2+} activated K^+ channels (BK_{Ca}, IK_{Ca1}, SK_{Ca}) are activated by the increase of $[Ca^{2+}]_{i,}$, and their opening also hyperpolarize EC. This response is transmitted to the smooth muscle cells by direct electrical coupling through myoendothelial gap junctions (MEGJ) and by the accumulation of K^+ in the intercellular myoendothelial space (Rusko, Tanzi et al. 1992; Haburcak, Wei et al. 1997; Kamouchi, Trouet et al. 1997).

Like most mammalian cells, EC also express anion channels, which are mainly permeable for Cl^- and activated during cell swelling. Among the Cl^- channels, high-conductance Cl^- channels, volume-regulated anion channels (VRAC), Ca^{2+}-activated Cl^- channels and cystic fibrosis transmembrane conductance regulator channels have been identified (Tousson, Van Tine et al. 1998). They play pivotal role in cell volume regulation, adjustment of cell shape for mechanical forces (shear stress, biaxial tensile stress) (Nilius, Viana et al. 1997; Barakat

1999; Nakao, Ono et al. 1999) and they seem to regulate the transport of amino acids, organic osmolytes and HCO_3^-, which is important for regulation of the intracellular pH in EC.

Several studies demonstrate the presence of voltage-gated Na^+ channels in both cultured and freshly isolated EC. Voltage-gated TTX- and STX-sensitive Na^+ channels have been described in human umbilical vein, rat pulmonary artery and in microvascular EC (Gordienko and Tsukahara 1994; Walsh, Wolf et al. 1998). However the majority of these channels are inactivated at normal resting potential. Although activation of PKC increases the magnitude of this current, it does not change the voltage-dependence of gating of the channels therefore the contribution of the Na^+ channels to the resting membrane must be negligible (Walsh, Wolf et al. 1998).

It is known that vascular endothelium has the ability to sense mechanical forces, such as stretch and pressure. In vivo EC are constantly exposed to wall shear stress generated by the streaming blood. Early responses to elevated shear stress include the elevation of $[Ca^{2+}]_i$, and the synthesis of NO, EDHF, and PGI_2. Later responses include endothelial remodeling and modulation of gene expression levels such as connexins (Cx), adhesion molecules, cyclooxigenase (COX) and endothelial nitric oxide synthase (eNOS) (Brakemeier, Kersten et al. 2003). In this process ion channels serve as effective mechanosensors to transform mechanical forces into electrical responses. Still it is not clear how ion channels may be directly involved in the responses to mechanical forces; however it has been shown recently that shear stress stimulation leads to an increase of IK_{Ca1} functions is human umbilical vein EC (Brakemeier, Kersten et al. 2003). IK_{Ca1} and SK_{Ca} have been implicated in EDHF mediated dilatation as they induce hyperpolarization and changes in $[Ca^{2+}]_i$. VRAC or VRAC-like channels may also contribute to the shear stress induced vascular responses, as they can be activated by shear stress and membrane stretch, induced by positive pressure in the patch pipette (Nilius, Viana et al. 1997; Barakat 1999; Nakao, Ono et al. 1999).

Stretch-activated non-selective Ca^{2+} permeable cation channels (NSC) with a conductance of 20–30 pS for monovalent cations and 10–20 pS for Ca^{2+} and Ba^{2+} have also been described in endocardial endothelium and microvascular EC (Popp, Hoyer et al. 1992; Hoyer, Distler et al. 1994). Activation of these channels induces an increase in $[Ca^{2+}]_i$ that is sufficient to activate Ca^{2+} activated K^+ channels and hyperpolarize the membrane.

2. Gap junctions in the vascular response

Endothelium gap junctions are frequently observed between EC of small and large arteries. Gap junctions are cell-to-cell high conductance low resistance channels (**Figure 5**) that allow direct electrical and metabolic communication between EC, EC and smooth muscle cells (SMC) - myoendothelial junction-, and also between EC and lymphocytes/monocytes (Davies, Olesen et al. 1988). Gap junctions form clusters of various hundreds of units in the EC membranes. These cluster formation facilitates interactions and enhances intercellular signaling (Bukauskas, Jordan et al. 2000). Three isoforms of connexins (Cx37, -40, -43) have been described in EC, and they have been shown to be involved in the regulation of vascular tone. Connexin 40 is the most frequently observed, and could coexist with Cx 37 or 43. Signals for vasoconstriction and vasodilatation travel rapidly along the vessel network through gap junctions, thus EC as well as vascular SMC behave as an electrical syncytium (De Wit 2004; Figueroa, Isakson et al. 2004; Haefliger, Nicod et al. 2004) .

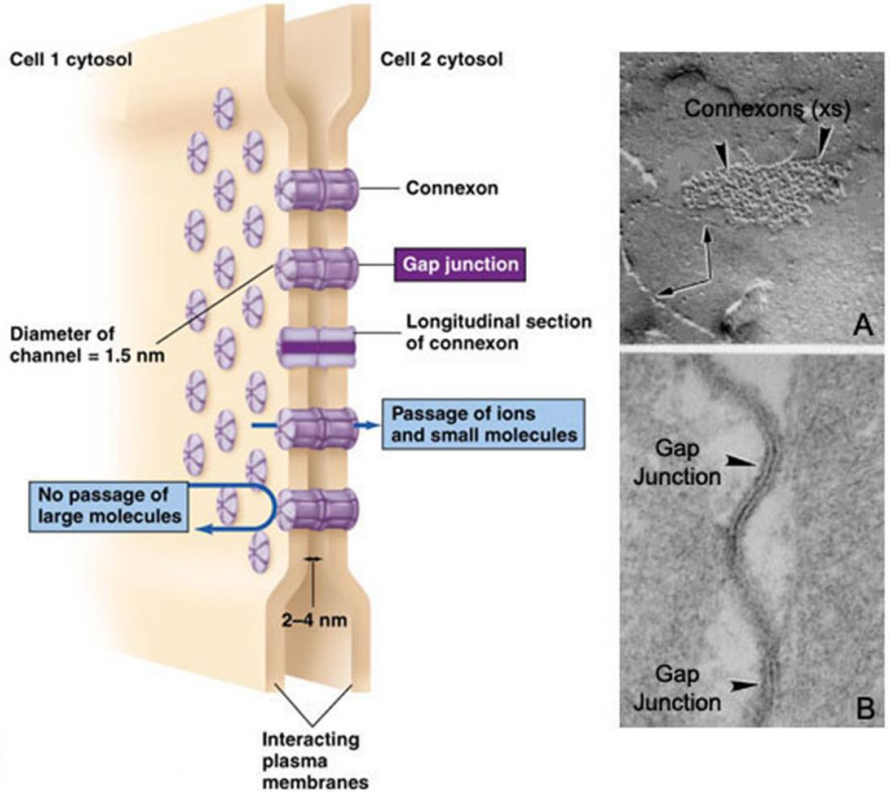

Figure 5 Structure of Gap Junction

Gap junctions unite EC and VSM and provide a pathway for the radial and longitudinal communication. They coordinate changes in membrane potential, intracellular Ca^{2+} and IP_3 (De Wit 2004; Figueroa, Isakson et al. 2004).

3. Polarity of the vascular bed

EC are generally considered to be non-excitable cells, however, the abundance of ion channels that have been described in these cells has raised significant attention regarding the functional role of these channels. Most of the described channels have only been detected in cultured or in freshly isolated EC, but very few measurements were done *in vivo* in blood vessels. It is known that ion channels in EC adapt their appearance to external conditions, and gene expression can vary with the cell isolation, culture and growth condition (Hewett, Murray et al. 1993). Therefore the *in vivo* functional impact of the described channels is still a matter of controversy.

Recently several studies focused on the importance of membrane polarity of endothelial and epithelial cells. The exchange of substances between higher organism and the environment takes place across these cells. To perform this function, endothelial and epithelial cells have to form thigh junctions that seal the extracellular space meanwhile they are polarized into an apical and a basolateral domain, with entirely different structural, biochemical and physiological properties (Gibson and Perrimon 2003). Polarized epithelia are equipped with markedly distinct populations of channels, carriers and pumps, for example the polarized distribution of renal Na^+/K^+ ATPase, the asymmetrical Cl^- conductances of respiratory epithelia or the gastric H^+/K^+ ATPase (Caplan 1997; Dunbar and Caplan 2001). While polarized epithelial cells show a high degree of spatial sorting of junctional complexes, EC organizes their junctions randomly (Aurrand-Lions, Johnson-Leger et al. 2002). For this reason the nature of endothelial contacts may be highly adaptable to the need of permeability and leukocyte transmigration. Breakdown of this barrier allows access of growth factors in the luminal fluid to their receptors on the basal lateral cell membranes. This property have an adaptive value for epithelial tissues in general as a response to injury, but may also promote cancer formation in premalignant epithelia tissues in which the tight junctions have become chronically leaky to growth factors (Mullin 2004).

To maintain a polarized state is also essential for migrating cells (during embryogenesis, inflammation, wound healing or in metastatic cascade). By setting the correct cell volume, ion channels and transporters create an intracellular milieu that is required for rapid cytoskeletal operation. Voltage dependent K^+ channels (Kv1.3, Kv.1.4 and Kv.3.1), IK_{Ca1} channels, Na^+/H^+ and Cl_2/HCO_3 exchangers have been related to migration. These

transporters are clustered at the leading edge of the lamellipodium contributing to its protrusion by inducing local cell swelling (Schwab 2001). The functional properties of these cells depend on the differentiation and the appropriately polarized cell organization, which is reliant upon extracellular signals generated from cell-cell or cell-matrix interactions. To retain the ultrastructure of the original tissue, the ion transport properties or the gene expression, optimal conditions have to be provided. Hence the use of non-polarized, poorly differentiated primary cultures or immortalized cell lines is suboptimal for endothelial/epithelial cell research (Schwab 2001; Lavender, Pang et al. 2005). To overcome this problem several co-culture systems have been developed lately to study EC-VSMC interactions. These include the culture of VSMC and EC on the opposite sides of membranes, culture of EC on collagen gels containing VSMC or the culture of EC directly on VSMC (Lavender, Pang et al. 2005). Existing co-culture systems are able to bring EC and VSMC within 10-50 μm of each other, and in this case VSMC can make contact with EC and can modulate phenotypic changes and cell replication. The development of a functional, adherent endothelium is not only important for endothelial researches, but it is also the major limiting factor for the successful development of tissue engineered vascular grafts (Nachman and Jaffe 2004; Lavender, Pang et al. 2005). Tissue engineering represents a promising approach to treat a number of cardiovascular problems including atherosclerosis, damaged valves and heart failures, but yet the attachment of endothelial cells on cultured blood vessels is often suboptimal, and adherent EC are usually pro-coagulant (Lavender, Pang et al. 2005).

Summarizing all the difficulties of vascular research and the complexity of EC's physiology, the aim of our study was to set up a method that allows identifying and characterizing the activity of ion channels present on EC '*in situ*', thereby avoid the alterations induced by cell isolation methods or cell culture.

III. Aims

A. General aims

In our study we focused on the characterization of ion channels on two different cell types, the human DC and the EC of the arteria mesenterica superior in rats. In both cases our goal was to characterize the ion channels under the most physiologic circumstances. Further, we aimed to compare the ion channel expression pattern on IDC, MDC and the DC model cell line KG-1 in unstimulated and stimulated state.

B. Specific aim 1: Characterizing the ion channels expressed on IDC, MDC and KG-1 cells

We aimed to identify and compare the expression and functional activity of voltage-gated ion channels in DC generated *in vitro* from human peripheral blood monocytes using patch-clamp technique. We hypothesized that differentiation/maturation of monocyte-derived DC is accompanied by a change in the ion channel repertoire, which could contribute to the distinct functional activities of these cells associated with their different maturation states. We also aimed to compare the ion channels expression pattern of activated and non-activated KG-1 cells to our measurements obtained on DC. To test this hypothesis we carried out the following experiments:

1. Characterization of ion channels on IDC and MDC:

i. performing whole-cell measurements on IDC and MDC and comparing the obtained currents
ii. biophysical and pharmacological characterization of the obtained currents on IDC and MDC using whole cell patch clamp technique and high affinity toxins
iii. confirmation of the presence of characterized channels on IDC and MDC using molecular biology techniques (real time Q-RT-PCR, Western blott)

2. Characterizing the ion channels in a DC model KG–1:

i. performing whole-cell measurements on unstimulated and stimulated KG-1 cells and comparing the obtained currents
ii. biophysical and pharmacological characterization of the currents on KG-1 cells

C. Specific aim 2: In situ characterization of the ion channels expressed in EC

We aimed to set up a method that allows identifying and characterizing the activity of ion channels present on EC '*in situ*' and thereby avoiding the alterations induced by cell isolation and culturing. We used single microvascular myograph to adjust the vessel diameter combined with patch clamp technique to measure the whole cell currents. The development of the method consisted of the following steps:

1. Vessel preparation and identification of EC for optimal electrophysiological measurements

2. Electrophysiological studies on EC

i. to perform whole cell blind patch clamp experiments on EC layer and characterize the obtained currents (biophysical and pharmacological properties)
ii. to study the effect of Ach and gap junction blockers on obtained current

IV. Materials and Methods

A. Dendritic cells

1. Dendritic cell preparation

Human myeloid DC were generated from blood monocytes isolated from Buffy Coats by Ficoll-Pacque (Amersham Biosciences, Uppsala, Sweden) gradient centrifugation (Thurner, Roder et al. 1999). Monocytes were separated by positive selection with anti-CD14-coated magnetic beads (Miltenyi Biotech, Bergisch Gladbach, Germany) from peripheral blood mononuclear cells. Purified monocytes ($\geq$95%) were plated at $2x10^6$ cell/ml concentration and cultured in serum free AIMV medium (Invitrogen, Paisley, Scotland) in the presence of 100 ng/ml IL-4 and 75 ng/ml GM-CSF (Peprotech EC, London, UK) given on days 0 and 2. Activation of IDC was induced by an inflammatory cocktail containing 10 ng/ml TNF-α, 5 ng/ml IL-1β, 20 ng/ml IL-6, 75 ng/ml GM-CSF (Peptrotech EC) and 1 μg/ml prostaglandin E2 (Sigma, St Louis, MO, USA). MDC were identified by flow cytometry using anti-CD83 mAb (Immunotech, Marseille, France) as described elsewhere (Gogolak, Rethi et al. 2003).

2. Dendritic cell line KG-1 cell culture

KG-1 cells were obtained from the American Type Culture Collection (Manassas, VA, USA) and were cultured in IMDM (Gibco, BRL, Grand Island, NY, USA) supplemented with 20% fetal calf serum (Gibco), 1 mM L-glutamine (Gibco), 80 μg/ml gentamicin (Chinoin, Budapest, Hungary). Cell suspensions were grown in a humidified incubator at 37^{o}C in an atmosphere containing 5% CO_2. Cell counts were adjusted to an optimal concentration of 1×10^5 cells/ml and the cells were fed every other day. KG-1 cells were stimulated with 10 ng/ml PMA (Sigma-Aldrich, Steinheim, Germany) and 100 ng/ml ionomycin (Sigma-Aldrich) for 4 days as described previously (St Louis, Woodcock et al. 1999).

3. Protein Extracts and Western Blotting

Dendritic cells were washed twice in cold phosphate-buffered saline (PBS) and lysed on ice with lysis solution (50mM Tris-HCl, 150 mM NaCl, 1 mM EDTA, 1% Triton X-100, pH7.4) supplemented with 2 μM Pepstatin A, 2 μM leupeptin, 2 μg/ml Aprotinin and 1mM

phenylmethylsulfonyl fluoride as protease inhibitors. Cell lysates were centrifuged at 10,000×g for 10 min at 4 ^{o}C, and the protein content of the supernatant was determined using Bradford protein assay. Samples were separated into aliquots and stored at −80 °C. Protein samples (50 μg) were boiled in Laemmli SDS loading buffer and separated on 10% SDS-PAGE. Other details of the western blotting were as described elsewhere (Vicente, Escalada et al. 2006) using antibodies against Kv1.5 (1/500, Alomone Labs, Israel). As a loading and transfer control, a monoclonal anti-β-actin antibody (1/5000, Sigma) was used. The specificity of the Kv1.5 antibody was tested with a control antigen peptide provided by the manufacturer. Raw 264.7 macrophages and HEK-293 cells were grown and HEK-293 cells were transienltly transfected with Kv1.5 cDNA as described elsewhere (Vicente, Escalada et al. 2006). Samples were analyzed 24 hours after transfection. Protein biochemistry was done in Prof. Felipe's laboratory (Molecular Physiology Laboratory, Department of Biochemistry and Molecular Biology, Institute of Biomedicine, University of Barcelona, Barcelona, Spain).

4. Electrophysiology of dendritic cells

Patch-clamping. Standard whole-cell patch-clamp techniques were used, as described previously (Hamill, Marty et al. 1981). Whole-cell measurements were carried out using Axopatch-200 and Axopatch-200A amplifiers connected to personal computers using Axon Instruments Digidata 1200 data acquisition boards (Molecular Devices, Sunnyvale, CA USA). For data acquisition and analysis the pClamp8 software package (Molecular Devices) was used. Pipettes were pulled from GC 150 F-15 borosilicate glass capillaries (Clark Biomedical Instruments, Pangboume, UK) in five stages and fire-polished to gain electrodes of 2-3 MΩ resistance in the bath. Series resistance compensation up to 85% was used to minimize voltage errors and achieve good voltage clamp conditions (V_{err}<5mV).

Solutions for DC. The normal bath or extracellular solution was (in mM): 145 NaCl, 5 KCl, 1 $MgCl_2$, 2.5 $CaCl_2$, 5.5 glucose, 10 HEPES (pH 7.35, 305 mOsm/kg). 145 mM choline-Cl substituted for NaCl in the choline-extracellular bath solution (pH 7.35, 305 mOsm/kg). NaCl was replaced by equimolar tetraethylammonium chloride (TEA) in the 10 mM TEA-extracellular solution. The composition of the pipette solution for current recording in MDC was (in mM): 140 KF, 11 K_2EGTA, 1 $CaCl_2$, 2 $MgCl_2$, and 10 HEPES (pH 7.20, ~295 mOsm/kg). This pipette solution was supplemented with 5 mM NaCl for recording currents in IDC.

Solutions for the KG-1 cells. The normal bath or extracellular solution and the KF-based pipette filling solution were the same as for MDC. The composition of the 1 μM [Ca^{2+}]-containing pipette solution was (in mmol): 130 K-aspartate, 10 K_2EGTA, 8.7 $CaCl_2$, 2 $MgCl_2$, and 5 HEPES (pH 7.20, 295 mOsm).

Test substances for DC or KG-1 recording. Toxins (tetrodotoxin, charybdotoxin and margatoxin) were dissolved in the standard extracellular solution supplemented with 0.1 mg/ml BSA (Sigma, Budapest, Hungary) to suppress nonspecific binding of the toxins to the wall of the tubes and to the Petri dish. Bath perfusion around the measured cell with different test solutions was achieved using a gravity-flow perfusion setup with 8 input lines and PE10 polyethylene tube output tip having flanged aperture to reduce the turbulence of the flow. Excess fluid was removed continuously.

5. Electrophysiological protocols and data analysis

a) Inactivation kinetics of the Na^+ and the K^+ current

Cells were depolarized to evoke whole-cell currents and the decaying parts of current traces were fitted using a single-exponential function:

$$I(t) = I_i \times e^{-\frac{t}{\tau_{in,x}}} + I_{ss} \qquad \text{(eq. 1)}$$

where I_i is the amplitude of the decaying current component, $\tau_{in,x}$ is the inactivation time constant for either the Na^+ ($\tau_{in,Na}$) or the K^+ ($\tau_{in,K}$) current, and I_{ss} is the steady-state value of the current at the end of depolarizing pulse.

b) Current-voltage relationship for Na^+ current

To study the voltage dependence of steady-state activation of the Na^+ conductance a family of 40-ms-long depolarizing test pulses ranging from −50 mV to +100 mV were applied every 15 s. A P/5 online leak subtraction protocol was used to minimize capacitance artifacts. The peak currents were determined, plotted as a function of the following equation:

$$I(V) = G \times V \times \frac{1 - e^{-(V - E_{rev})/25mV}}{1 - e^{-V/25mV}} \frac{1}{1 + e^{-(V - V_{m,a})/s_a}} \qquad \text{(eq. 2)}$$

where G is the whole-cell peak Na^+ conductance, E_{rev} is the reversal potential for Na^+ ions. The free parameters of the last term of the equation, $V_{m,a}$ and s_a, are the midpoint and the slope factor of the voltage-dependence of steady-state activation, respectively. Current-voltage relationships were individually fitted for each cell and the free parameters (G, E_{rev}, $V_{m,a}$ and s_a) were averaged to obtain the characteristic values.

c) Steady-state inactivation of Na^+ current

To elucidate the voltage dependence of steady-state inactivation of the Na^+ current in IDC 5–s-long prepulse potentials (V_p) ranging between –120 mV and 0 mV were applied followed by a test potential to 0 mV for 20 ms. The inward peak currents were normalized to the maximal peak currents recorded at V_p=–120 mV to express the fraction of channels which were not inactivated by the prepulse ($I_{norm}(V_p)$). $I_{norm}(V_p)$ was plotted as a function of the prepulse potential for each cell separately, and the Boltzmann function was fit to each data series, with values $V_{m,i}$ and s_i corresponding to the midpoint and the slope factor of the voltage dependence of steady-state inactivation, respectively:

$$I_{norm}(V_p) = \frac{1}{1 + e^{-(V - V_{m,i})/s_i}} \qquad \text{(eq. 3)}$$

$V_{m,i}$ and s_i obtained for individual cells were averaged to report the characteristic values.

d) Recovery from inactivation of Na^+ currents

A conventional two-pulse protocol was used to determine the kinetics of recovery from inactivation of Na^+ channels at a hyperpolarized potential. A pair of depolarizing pulses from –120 mV to 0mV for 50 ms was delivered separated by the interpulse interval (IPI). IPI was varied between 1 to 20 ms and the membrane potential was held at –120 mV during IPI. The degree of recovery from inactivated state at a given IPI was characterized by the Recovered Fraction (RF) of the Na^+ current: RF= $(P_2\text{-}I_{ss1})/(P_1\text{-}I_{ss1})$ where P_1 and P_2 denote the peak

currents obtained during the first and the second depolarizing pulses, respectively, and I_{ss1} represents the current at the end of the first depolarizing pulse. RF was plotted as a function of IPI and a single exponential rising function was fitted to the data resulting in the time constant for recovery from inactivation (τ_r):

$$RF(t) = 1 - e^{-\frac{t}{\tau_r}} \qquad \text{(eq. 4)}$$

The τ_r was determined separately for each cell and averaged to give the characteristic value reported.

e) Voltage-dependence of steady-state activation of K^+ current in MDC

MDC were held at −120 mV and depolarized to the test potentials ranging from −70 mV to +60 mV for 800 ms every 90 s. Peak whole-cell conductance (G(*V*)) at each test potential was calculated from the peak current (I_p) at test potential *V* and the K^+ reversal potential (E_r) using $G(V)=I_p/(V-E_r)$. G(*V*) values were normalized to the maximal K^+ conductance of the cell, the resulting $G(V)_{norm}$ data were plotted as a function of test potential. Data points were fitted using the Boltzmann function to obtain the midpoint ($V_{1/2}$) and the slope (k) of the voltage-dependece of steady-state activation:

$$G(V)_{norm} = \frac{1}{1 + e^{-\left(\frac{V - V_{1/2}}{k}\right)}} \qquad \text{(eq. 5)}$$

$V_{1/2}$ and k were determined separately for each cell and averaged to give the characteristic values reported.

f) Dose-response curves

The extent of current inhibition by various inhibitors was defined by the remaining current fraction (RCF) which is calculated as I/I_0 where I and I_0 are the peak currents in the presence and absence of a blocker (e.g. TTX), respectively. RCF values obtained at different toxin

concentrations were plotted and the Hill equation assuming 1:1 channel-toxin stoichiometry was fitted to the data points to obtain the equilibrium dissociation constant (K_d):

$$RCF = \frac{I}{I_0} = \frac{K_d}{K_d + [T]} \qquad \text{(eq. 6)}$$

where [T] is the concentration of the toxin applied. Where indicated, K_d was estimated form RCF obtained at a single toxin concentration using eq. 6.

g) Analysis of the IK_{Ca1} current in KG-1 cells

Families of whole-cell current traces were recorded from unstimulated and stimulated KG-1 cells in response to depolarizing pulses from a holding potential of −80 mV to different test potential ranging from −70 to +50 mV in 10 mV increments. Since the free Ca^{2+} concentration is in the nanomolar range when using KF-containing internal solution, we substituted fluoride ions with aspartate, and adjusted the EGTA and Ca^{2+} concentration in the pipette solution to result in 1μM free Ca^{2+} concentration during the measurement of IK_{Ca1} currents – and calculated the reverse potential of the whole-cell current using the Nernst-equation. The voltage protocol in the latter case consisted of 200 ms-long voltage ramps from −120 mV to +50 mV.

6. Cloning and sequencing

To prepare cDNA for cloning of Na^+ channels, monocyte-derived IDC or MDC were collected on day 5 and 6, respectively and total RNA was isolated with TRI Reagent (Sigma). Reverse transcription was performed at 42°C for 60 min from 500 ng of total RNA using Superscript II reverse transcriptase (Promega Corporation, Madison, WI, USA). The DNA, encoding a conserved region of the Na^+ channels was amplified from cDNA with polymerase chain reaction (PCR), using high fidelity *Pfu* polimerase (Promega) and degenerate primers:

5`-GATTTCCAGGGAGATAAGACAAGCAG-3` and
5`-GAAGCAGAGGCTGAACCTATGAA TT-3`.

Specific PCR products were gel-purified, ligated into the PCR Blunt vector (Invitrogen) and transformed into the *E. coli* strain TOP10 by the standard heat shock method. Plasmid DNAs obtained from 20 single bacterial colonies were first analyzed by restriction digestion. Inserts of 5 randomly picked clones were fully sequenced on an ABI Prism 310 Automatic Sequencer (Applied Biosystems, Warrington, UK). All five selected constructs carried the same insert.

7. Real time Q-RT-PCR

To quantify the expression of voltage-gated ion channel genes, we applied the TaqMan PCR system using the 5700 Sequence Detector (Applied Biosystems). Gene-specific TaqMan PCR assays for human Kv1.3 and Kv1.5; and Nav1.7 channels were purchased from Applied Biosystems, whereby each probe was synthesized with a fluorescent 5'-reporter dye (FAM: 6-carboxy-fluorescein) and a 3'-quencher dye (TAMRA: 6-carboxy-tetramethyl-rhodamine). Parallel TaqMan PCR assays for each gene target were performed with cDNA samples. To quantify the relative expression of voltage-gated channel expression 8 ng reverse transcribed RNA was used in a 25 µl reaction volume. As an internal control, 36B4 was used. The PCR reaction was performed at 94°C, 1 min followed by 40 cycles at 94°C, 12 s and 60°C, 1 min. The PCR product was analyzed on a real-time PCR cycler (SDS 5700, Applied Biosystems). The relative amounts of individual channel transcripts are given in relation to those of 36B4. A "no-RT control" with untranscribed RNA and a "no-template control" with water were performed parallel in all experiments. Each series of experiments were performed in triplicates. The relative expression of the target gene was calculated using the comparative method ($2^{-\Delta\Delta Ct}$) (Livak and Schmittgen 2001). Cloning and RT PCR experiments were done in Prof. Rajnavölgyi's laboratory in the Dept. of Immunology, University of Debrecen.

B. Endothelial cells

1. Mesenteric artery preparation

Adult male Wistar rats (250-300g) were used. All experimental procedures were carried out according to the guidelines of the European Union and by following protocols approved by the corresponding local ethics committee. Rats were stunned and bled, then the mesenteric vascular bed was immediately removed and dissected free of the adhering fat and connective tissue. The vascular bed was placed in a Petri dish containing chilled (4ºC) physiological salt solution (PSS), for composition see below. Segments from the proximal part, between aorta and the first branch of the superior mesenteric artery, were dissected away under binocular microscope. Vascular segments were mounted as ring preparations (*ca*. 2 mm in length) on a single wire myograph 310-A (DMT A/S, Aarhus, Denmark) onto two 40 µm wires, by fixing one wire to an isometric force transducer and the second wire to a micrometer screw (**Figure 6**). Vessel segments were allowed to equilibrate for 30 minutes and were continuously superfused with PSS (37ºC) at 3 ml min^{-1}. The PSS was equilibrated with a mixture of 95% O_2 and 5% CO_2, resulting a pH of 7.4. A U-shape was cut out on the dorsal wall of the arterial segment at one end in order to allow direct access to the EC layer underneath (Stankevicius, Lopez-Valverde et al. 2006).

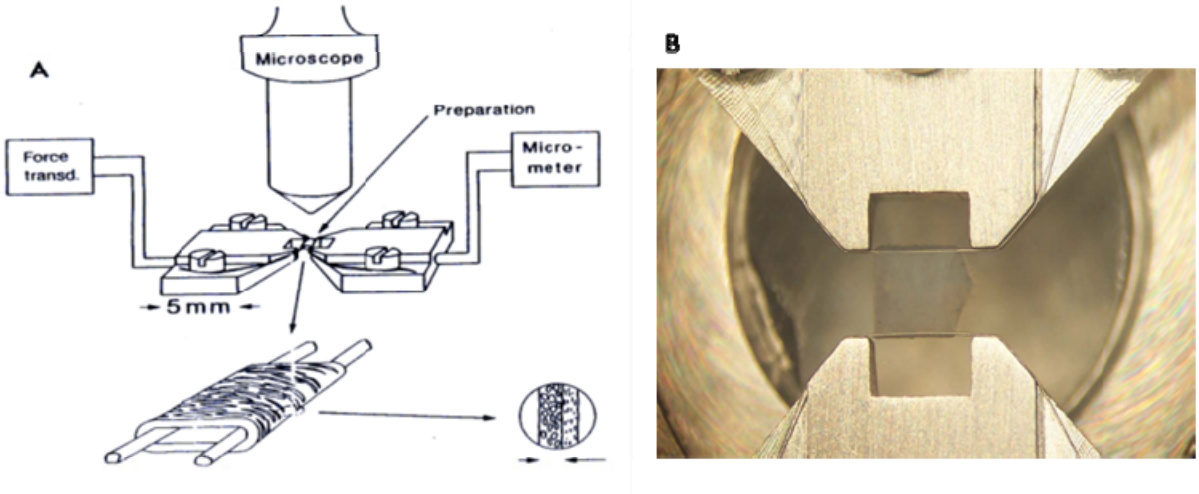

Figure 6 The schematic diagram (A) and a picture (B) of the experimental apparatus and the arrangement of the isolated vessel segment

The micrometer on the right hand side of panel A was used to adjust the vessel diameter. The bottom part of panel A and panel B shows the arrangement of the mounting wires and the blood vessel.

2. Application of physiological wall tension to isolated vessel segments

It is known that the sensitivity of ring preparations to agonist depends on the degree of stretch. Because of this it is necessary to determine the relation between resting wall tension and internal circumference, and set vessels to an internal circumference which gives the maximum response. From this relationship the internal circumference (L_{100}) corresponding to a transmural pressure of 100mm Hg (13.3 kPa) for a relaxed vessel '*in situ'* was calculated (Mulvany and Nyborg 1980).

In practice, this experiment was performed by distending the vessel stepwise and measuring sets of micrometer screw readings (μm) and of tension (mN / mm) on the display box of the myograph amplifier (**Figure 7**).

The internal circumference of the vessel was calculated from the measured distance between the wires and the known diameter of the mounting wires. The exact wall length of the vessel was determined using a calibrated eyepiece with the dissecting microscope. The wall tension was the measured force divided by the wall length. The Laplace relation was used to determine the *effective pressure*, P_i, given by

$$P_i = \frac{\text{wall tension}}{\frac{\text{internal circumference}}{2\pi}} \qquad \text{(eq. 7)}$$

Effective pressure is thus an estimate of the pressure, which would be necessary to extend the vessel to the measured internal circumference.

Each pair of readings was keyed into a programmable calculator, and having entered the relevant calibrating factors, the effective pressure corresponding to each distension was calculated. The stepwise distension was stopped when the effective pressure was brought near 100 mmHg. An exponential curve was then fitted to the internal circumference–pressure data and, using Laplace's equation, the internal circumference corresponding to 100 mmHg was determined and denoted L_{100}. Having found this, the internal circumference was set to L_1 = 0.9 x L_{100}, since preliminary experiments showed that force development is almost maximal at this internal circumference (**Figure 7**). Effective luminal diameter (l_1) was determined using the following formula (Mulvany and Nyborg 1980):

$$l_1 = L_1 \pi^{-1} \qquad \text{(eq. 8)}$$

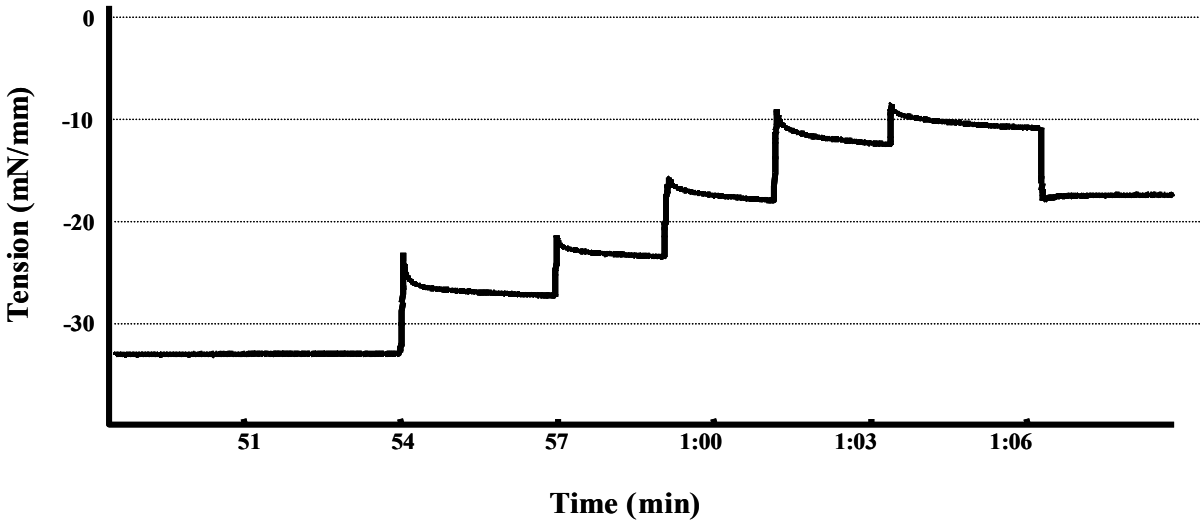

Figure 7 Record showing the output from the force transducer during the procedure

The abscissa indicates the time while the vessel was stretched. The ordinate shows the tension in mN /mm. The chart illustrates the tension after stretching immediately and its decrease during the 1 min waiting period. These values (after 1min) were used together with the corresponding micrometer settings to determine the internal circumference.

3. Procedure for verifying the functional integrity of endothelium

The purpose of the procedure is to provide indirect evidence that the endothelium has not been damaged during dissecting or mounting. Through the procedure the contracting and relaxing function of the endothelium were checked.

Figure 8 shows the one representative experiment. The circumference of the vessel was set to $L_1 = 0.9 \times L_{100}$ and 100 nM phenylephrine was administered by bath perfusion. As expected form a functional vessel wall, the recorded tension increased significantly and reached a plateau within 60 - 120 s. Subsequently, 10 µM ACh was added into the myograph chamber. ACh induced the relaxation of the vessel wall, indicating that the signaling pathways leading to NO release form the endothelium are intact. Upon removal of the endothelium no relaxation to ACh could be seen (data not shown). The phenylephrine/Ach application procedure was always performed following the determination of the optimal vessel wall tension (see above) to ensure that the vessel is viable before starting the patch clamp experiments (**Figure 8**).

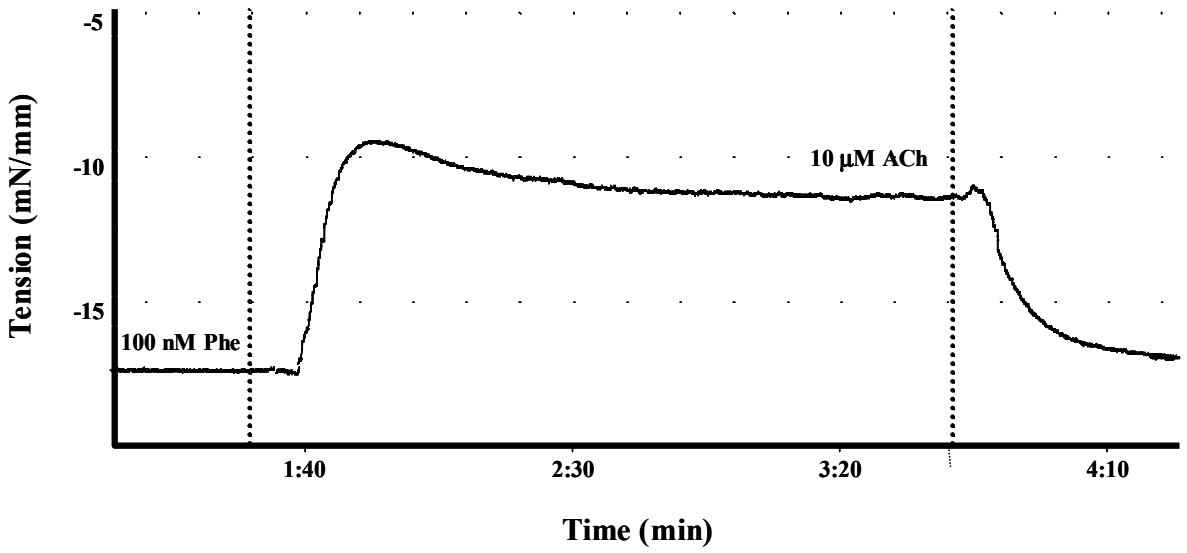

Figure 8 Verifying the functional integrity of the endothelium

The figure shows the changing of the vascular wall tension recorded after 100 nM phenylephrine (Phe) and 10 µM ACh added to the bath solution (vertical dashed lines). The wall tension increased significantly after the application of Phe, while Ach induced relaxion due to the release of NO from the intact endothelium.

4. "In situ" patch-clamp recording

Dissection stereomicroscope (Wild M3Z, Wild Heerbrung, Switzerland) at 40x magnification, which did not allow to distinguish individual EC, was used. Macroscopic K^+ currents were recorded '*in situ*' from EC under whole-cell configuration of the patch-clamp technique. Mechanical micromanipulator (Leica Microsystems GmbH, Wetzlar, Germany) was attached to the myograph stage, allowing '*in situ*' recording of the EC with patch clamp microelectrodes via the U-shaped cut (**Figure 9**).

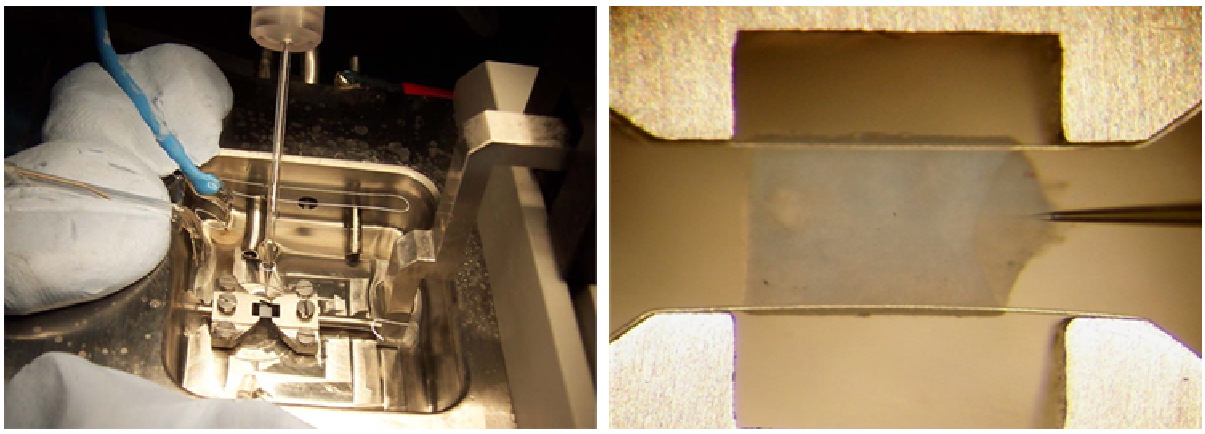

Figure 9 Patch clamp set-up

Picture on the left side shows the set-up with the bath containing the vessel on the microvascular myograph as well as the pipette and the reference electrode. The picture on the right side shows the pipette on the vessel segment during patch clamp experiment.

The electrode was connected to an Axon Multiclamp 700A amplifier (MDS Analytical Technologies Sunnyvale, CA, USA). Patch pipettes were made of borosilicate glass capillaries (WPI Inc. FL, USA) pulled in two steps on a vertical pipette Narishige PP 830 puller (Narishige, Tokyo, Japan). Pipettes were then backfilled with intracellular (IC) solution. Pipette resistance was in the range of 4-8 MΩ. Seal resistance was ≈5 GΩ. We corrected routinely for the liquid junction potential. Cell capacitance and series resistance ranging from 10 MΩ to 20 MΩ were automatically compensated through the amplifier's circuitry.

Generation of holding (V_h) and command (V_p) potentials and on-line data acquisition were achieved using a personal computer connected to the PowerLab system (PowerLab/8SP - ADInstruments Pty Ltd, Castle Hill, Australia). Macroscopic K^+ currents were evoked by either families of hyper- or depolarizing steps, over 400 ms in 20 mV increments, either from −60 mV to −200 mV or from −60 to 140 mV, respectively. Pulses were separated by 10 s intervals at the holding potential of -60 mV. Membrane current was also monitored by an A/D storage oscilloscope (HAMEG HM507, Hameg Instruments, Mainhausen, Germany). Data were first sampled at 0.2-10 kHz after low-pass filtering with an appropriate cut-off frequency for each sampling rate, and were digitized by a 16-bit A/D converter and stored in a 'PowerLab Scope v3.6.4' Software package for off-line analysis.

5. Intracellular injection of neurobiotin

In order to ensure that we were recording from EC and for identification purposes, EC were iontophoretically filled with the marker neurobiotin according to the protocol described by Germain et al. (Germain, Fernandez et al. 2003). The tip of the patch pipette was backfilled with IC solution containing 3% neurobiotin (Vector, Burlingame, CA, USA) in 0.1 mol/L Tris buffer (pH 7.4). The tip resistance was 4-8 MΩ. Once the whole cell configuration was established on an EC, and due to the fact that neurobiotin carries positive charges, neurobiotin was iontophoresed into the cell by injecting positive square current pulses (10 pA, delivered at a rate of 1Hz, 500 ms duration). After labeling the cell for approximately 15 min, the patch electrode was detached from the cell and the arterial segment was slit open and pinned with the luminal surface upward onto the bottom of the chamber. The vessel was then equilibrated in Ames medium for 30 min. The segment was fixed in 4% paraformaldehyde in 0.1M phosphate buffer (PB) pH 7.4 at 22º C for 2 h. The vessels were then rinsed in PB, cryoprotected in 30% sucrose in PB and stored at −18ºC for further processing. The arterial segments were defrosted at room temperature and rinsed in PB. The vessels were then incubated for 10 min in 0.2% albumin and 0.1% Triton X-100 in 0.1 mol/L PB to avoid non-specific labeling. After several rinses in PB they were incubated with 1% ethanol and 0.15% H_2O_2 in PB for 15 min. The arteries were then incubated for 2 h in avidin-biotin complex solution (ABC kit, Vectastatin, Vector, Burlingame, CA, USA). After incubation the mesenteric artery segments were rinsed in PB and incubated in the dark with 0.05% diaminobenzidine for 20 min. Neurobiotin was visualized after adding 0.03% H_2O_2 to the solution. The artery segments were then rinsed and dehydrated through an ascending ethanol series and mounted in DEPEX mounting medium.

6. Statistics

We obtained electrophysiological data from 61 EC *in situ*. Unsuccessful experiments and cells with incomplete data are not included in the analysis. Depolarizing and hyperpolarizing currents were measured and normalized for the maximal currents obtained in control conditions (I/Imax) using GraphPad software (GraphPad, Institute for Scientific Information, San Diego, Ca, USA).The Remaining Fraction of the current (RF) was calculated as $RF=I/I_0$ where I and I_0 are the peak currents in the presence and absence of a blocker, respectively, at a given membrane potential. The results are expressed as means ± SEM of at least four independent measurements done under identical conditions, unless otherwise indicated.

Differences between means were analyzed using Student's *t*-test for paired and unpaired observations as appropriate with differences considered statistically significant at $p<0.05$.

7. Solutions and drugs for EC electrophysiology

The composition of the extracellular PSS was (in mM): 119 NaCl, 4.6 KCl, 1.2 $MgCl_2$, 24.9 $NaHCO_3$, 11 glucose, 1.5 $CaCl_2$, 1.2 KH_2PO_4 and 0.027 EDTA (etylenediamineteraacetic acid). The PSS was continuously superfused at a rate of 3ml min^{-1}. In order to investigate the expression of the different K^+ currents the composition of the IC pipette solution was (in mM): 141 KCl, 5 Na_2ATP, 0.6 $CaCl_2$, 3 $MgCl_2$, 10 HEPES (N-2-hydroxyethylpiperadine-*N*-*2*-ethanesulphonic acid) and 0.1 EGTA (ethyleneglycol-*bis*-(β-aminoether) *N, N, N', N'*-tetraacetic acid), titrated to pH 7.4 with Tris base.

Drugs used. Acetylcholine HCl (Ach) , apamin, barium chloride, 18β-glycyrrhetinic acid (18β-gly), iberiotoxin (IbTx), tetraethylammonium (TEA), TRAM34 ([1-[(2-chlorophenyl) diphenylmethyl]-1H-pyrazole) and TRIS-Cl, - all from Sigma-Aldricht Co. (St Louis, MO, USA). Stock solutions of the drugs were prepared in distilled water except TRAM34, which was first dissolved in dimethyl sulfoxide and further diluted in distilled water. The final concentration of dimethyl sulfoxide was <0.1%, a concentration which did not affect the electrophysiological activity of EC. Drugs were applied to the recording chamber either via perfusion pump or by direct application into the chamber with micropipette. Due to the extracellular volume in the recording chamber (>5 ml) and since it takes a long period of time, usually around 60-90 min, washout of the applied blockers were not successful in the majority of the cases. In these cases after each recording, a new vascular segment was used. Solutions were either made up freshly for each experiment or were prepared from aliquots stored at -18º C.

V. Results

A. Dendritic cells

1. TTX-sensitive Na^+ current in immature dendritic cells

Figure 10 A shows whole-cell currents measured in a single IDC in response to a voltage-ramp from –100 mV to +50 mV. The record shows the activation of a marked inward current at membrane potentials more depolarized than –30 mV. This inward current is voltage-gated and potentially can be attributed to the influx of either Na^+ or Ca^+ ions or even both. To clarify the nature of the charge carrier, ion substitution experiments were performed by changing the normal extracellular bath solution for Na^+-free choline extracelluar solution. As shown in **Figure 10** B the robust inward current recorded at 0 mV test potential in the Na^+-containing solution completely disappears in the Na^+-free choline based solution. The loss of the Na^+ current in choline-extracellular solution was quickly reversed by perfusing the bath with normal extracellular bath solution (**Figure 10** B, dashed line). The inset shows that the peak current was reduced to ~0 pA between two consecutive pulses upon changing to choline-extracellular and recovered to the control value upon changing to normal extracellular bath with a similar rate, i.e., between two consecutive pulses. These experiments demonstrated that the decrease of the inward current is due to the replacement of Na^+ with the impermeable monovalent choline ion, and thus, strongly argue for the presence of Na^+ channels in the membrane of IDC. The peak Na^+ current density at 0 mV test potential was quite variable ranging between –15.1 pA/pF and –110 pA/pF with median and mean current densities of –56.8 pA/pF and –61.9±7.3 pA/pF (n=20), respectively.

To characterize the Na^+ current in IDC we utilized TTX, a ubiquitous inhibitor of voltage-gated Na^+ channels. **Figure 10** C shows typical current traces recorded in the absence and in the presence of 100 nM TTX. The effect of the toxin was rapid and reversible, the peak current was reduced to ~37% of the control upon perfusion with TTX-containing normal-extracellular bath and recovered to the control value within a few pulses following a switch to the toxin-free normal-extracellular bath (see inset). The effect of TTX was concentration dependent and the dose-response data were fit with the Hill equation (eq. 6) resulting in a K_d value of 55 nM (**Figure 10** D). These results revealed that the inward current detected in IDC is mediated by TTX-sensitive voltage-gated Na^+ channels.

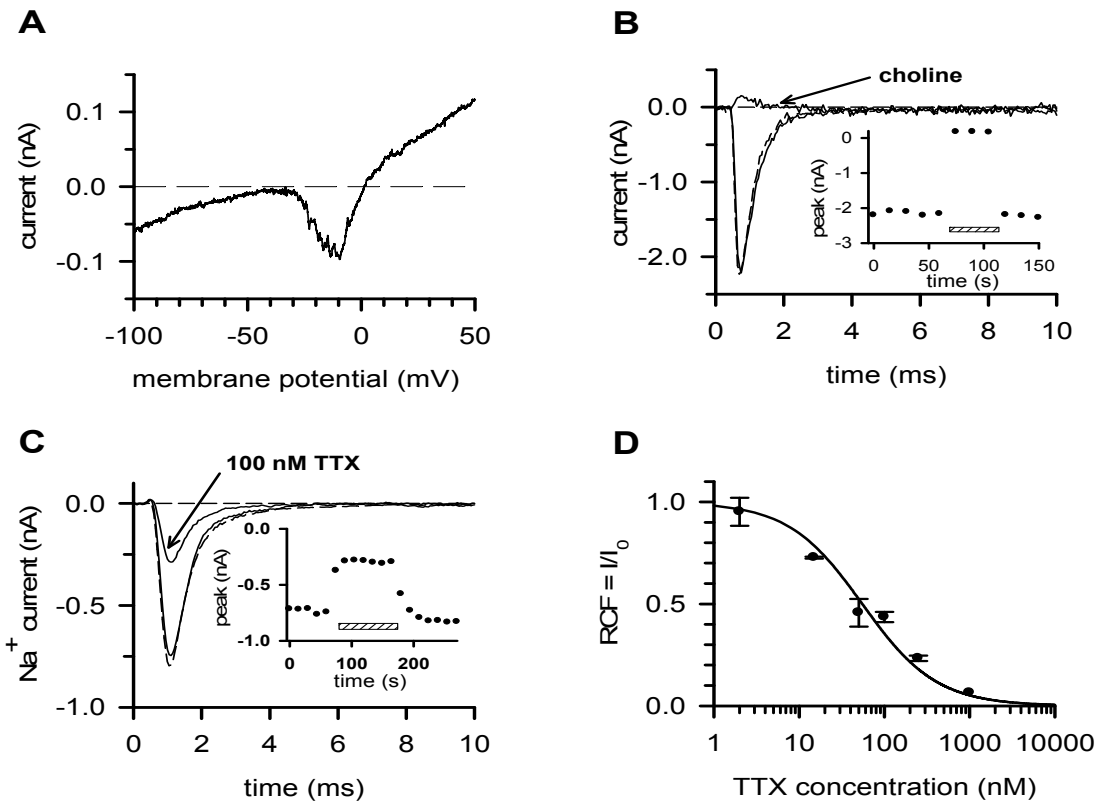

Figure 10 Voltage-gated, TTX sensitive sodium current is expressed in IDC

(Panel A) The representative whole-cell current trace was recorded in an IDC bathed in normal extracellular solution. A 150-ms-long voltage-ramp protocol ranging from –100 mV to +50mV was delivered. The horizontal dashed line indicates the zero current level on each panel in this study, where applicable. **(Panel B)** The inward current disappears upon perfusing the cells with Na^+-free choline extracellular solution. The cell was whole-cell clamped and depolarized to 0 mV from –120 mV for 50 ms every 15 s (solid line: control; dashed line: washout; trace recorded in choline bath is indicated by the arrow). P/5 online leak subtraction was applied. Inset: The wash-in and wash-out time course of the choline extracellular solution. Peak currents were determined from a series of records shown in Panel B and plotted as a function of time. The right-hatched bar indicates the perfusion with choline extracellular solution. **(Panel C)** Reversible inhibition of the inward current by TTX. Representative traces show the inward current before the application of the toxin (solid line: control), after the equilibration of the block in the presence of 100 nM TTX (as indicated by the arrow) and after full recovery from block during the perfusion of the bath with toxin-free solution (dashed line: wash-out). Currents were evoked by the same pulse protocol as described in the panel B. Inset: Time-course of the development and the removal of the current block. Peak currents were determined from a series of records shown in Panel C and plotted as a function of time. Right-hatched bar indicates the duration of perfusion with 100 nM TTX. **(Panel D)** Dose-response of the inhibition of the inward current by TTX. The remaining fraction of the current (RCF) was defined by the ratio of I and I_0 where I and I_0 are the peak currents measured at 0 mV depolarization in the presence and absence of TTX. The Hill equation (eq. 6) assuming 1:1 channel-toxin stochiometry was fitted to the data points resulting a K_d value of 55 nM (n=3). Error bars indicate SEM.

2. Biophysical characterization of the Na^+ current in immature dendritic cells

To further characterize the Na^+ channel expressed in IDC we determined the biophysical characteristics (equilibrium and kinetic properties) of the whole-cell Na^+ current gating. In general, VGSCs are closed at hyperpolarized potentials, open quickly upon depolarization and then get inactivated. Recovery from the inactivated state into the closed state takes place at negative membrane potentials and is necessary for re-populating the closed, activable channel pool. Thus we used the simplest model that was proposed and worked out by Hodgkin and Huxley in 1952 (Hodgkin and Huxley 1952) as a working-hypothesis of our further experiments. **Figure 11** A shows a family of currents recorded by depolarizing an IDC from the holding potential of –120 mV to various test potentials (for additional details see the figure legend and the Materials and Methods). The peak current at each test potential was determined and plotted as a function of the test potential in **Figure 11** B. The peak current-voltage relationship shows that the activation threshold of the current is around –50 mV, and the current reverses close to +60 mV. The current-voltage relationship is non-linear at depolarized test potentials, thus, eq. 2 was used to characterize the voltage-dependence of steady-state activation of the Na^+ channels. The superimposed solid line in **Figure 11** B displays the best fit of eq. 2 to the data points. This cell is characterized by a peak whole-cell Na^+ conductance (G) of 3.5 nS, and a reversal potential (E_{rev}) of +62.6 mV for the Na^+ current. Parameters describing the voltage-dependence of steady-state activation, i.e., the test potential at which 50% of the Na^+ channels are activated (midpoint, $V_{m,a}$) and the slope of voltage-dependent gating (s_a) were –24.8 mV and 9.1 mV, respectively. Characteristic values for the parameters of eq. 2 were obtained by fitting individual I-V relationships cell-by-cell and averaging the obtained values. This resulted in G=4.1±1.2 nS, E_{rev}=+64.4±4.2 mV, $V_{m,a}$= –19.8 ± 3.0 mV and s_a= 10.0±0.7 mV (n=5).

The voltage dependence of steady-state inactivation was studied using the pulse protocol shown in **Figure 11** C. The cell was held at different prepulse potentials (V_p) for 5s and then depolarized to 0 mV to evoke whole-cell Na^+ currents with magnitudes proportional to the fraction of Na^+ channels not inactivated by the preceding prepulse. The resulting family of current records is shown in **Figure 11** C. The peak currents normalized to the maximal values

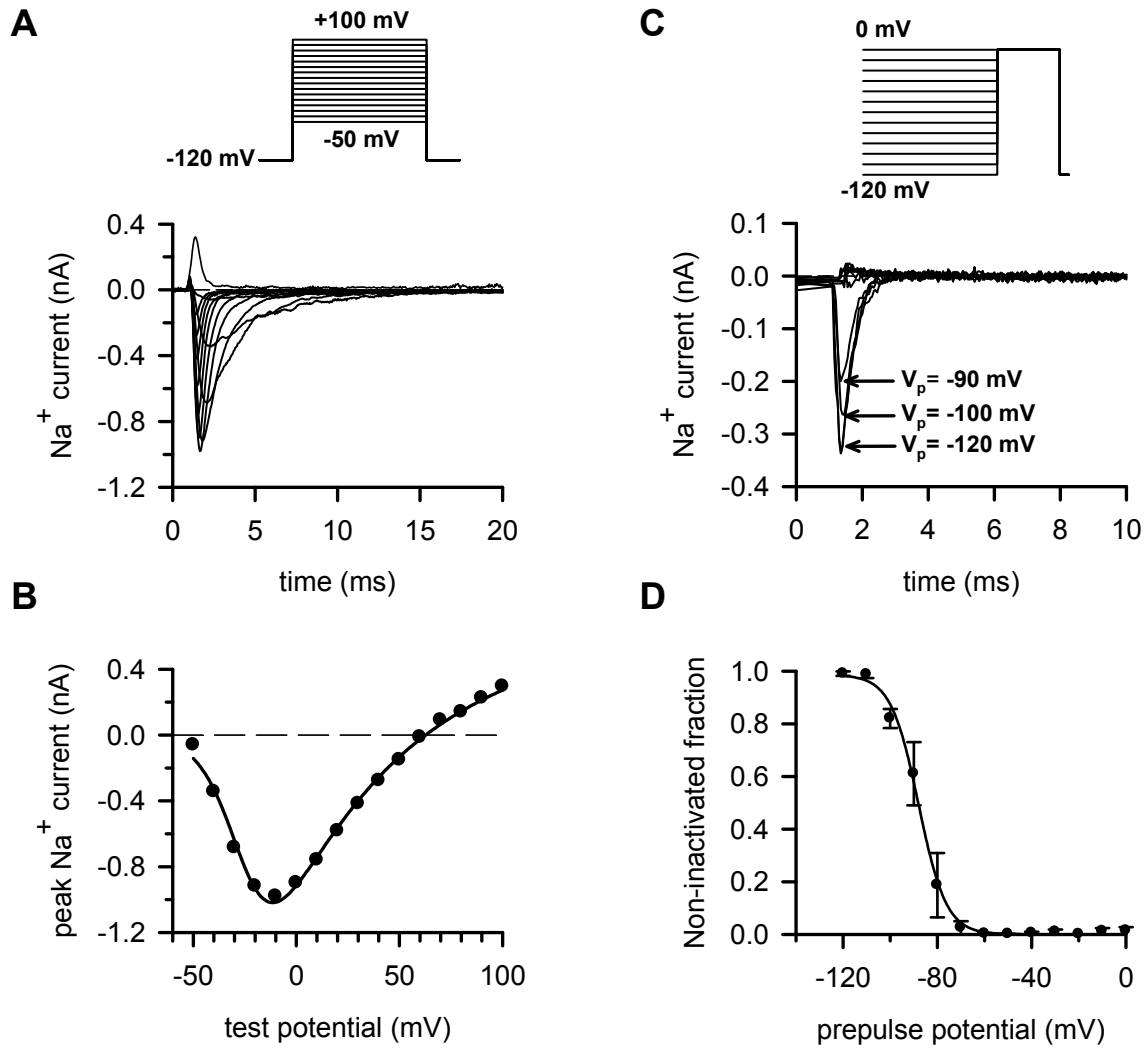

Figure 11 Steady-state parameters of activation and inactivation for Na^+ current in IDC.

(Panel A) Voltage-dependence of Na^+ current activation. 50-ms-long depolarizing step pulses ranging from −50 mV to +100 mV were applied to the cells every 15 s in 10 mV increments from the holding potential of −120 mV (pulse protocol is shown on the top, P/5 online leak subtraction was applied). 20–ms-long segments of the current traces evoked by depolarizations between −50 mV and +50 mV and to +100 mV are shown for clarity of the figure and for the emphasis of the fast kinetics. **(Panel B)** Voltage-dependence of Na^+ current activation. Peak whole-cell current (●) at each test potential was determined from the currents shown in Panel A. The superimposed solid line shows the best fit of eq. 2 to the data points with G=3.5 nS, E_{rev}=62.6 mV, $V_{m,a}$ =−24.8 mV and and s_a= 9.1 mV. **(Panel C)** Voltage-dependence of steady-state inactivation of the Na^+ current. The cell was held for 5 s at various pre-pulse potentials (V_p) ranging between –120 mV and 0 mV then depolarized to 0 mV (test pulse) for 20 ms (pulse protocol is shown on the top). Prepulse/test pulse sequences were separated by 15 s at the holding potential of −120 mV. The gradual loss of the current with depolarizing prepulses (indicated with arrows) demonstrate steady-state inactivation of Na^+ channels. **(Panel D)** The inward peak currents recorded following prepulse potential V_p were normalized to the maximal peak current recorded following a −120 mV prepulse potential to express the fraction of channels which were not inactivated by the prepulse ($I_{norm}(V_p)$). The fraction of non-inactivated channels was averaged and plotted as a function of the prepulse potential (n=3). The superimposed solid line is the best fit of the Boltzmann function (eq. 3) to the data points with $V_{m,i}$= −88.0 mV and s_i=−5.9 mV. Error bars indicate SEM.

were plotted vs. V_p cell-by-cell, and the Boltzmann function (eq. 3) was fitted to the data points. The characteristic values of the voltage-dependence of steady-state inactivation, i.e., the membrane potential at which 50% of the channels are inactivated was $V_{m,i}= -87.6\pm3.3$mV (n=3), and the slope was $s_i= -5.1\pm0.1$ mV (n=3). The voltage-dependence of steady-state inactivation is represented in **Figure 11** D as the average of the fraction of non-inactivated channels at different prepulse potentials for n=3 independent experiments along with the best fit Boltzmann function.

Figure 12 represents the kinetic features of the Na^+ current. As shown in **Figure 10** and **Figure 11** the Na^+ current activates and inactivates quickly upon the depolarization of the membrane. The inactivation kinetics of the current was characterized by the inactivation time constant ($\tau_{i,Na}$). $\tau_{i,Na}$ was determined by fitting a single exponential function (eq. 1) to the decaying part of the currents (see Materials and Methods). The dash-dot lines (red) superimposed over the Na^+ currents in **Figure 12** A indicate the best fits to eq. 1 at four test potentials. The voltage dependence of $\tau_{i,Na}$ is shown in **Figure 12** B, which indicates that inactivation kinetics of the current is getting faster with increasing depolarization.

Following a full inactivation of the current the membrane has to be hyperpolarized to allow recovery of the channels from inactivation. The kinetics of recovery from inactivation was studied using a conventional two-pulse protocol (see Materials and Methods) where the time between two consecutive depolarizing pulses (IPI) is gradually increased thereby resulting in larger and larger currents during the second pulse (**Figure 12** C). The recovered fraction (RF) of the current as a function IPI was plotted for individual cells and a single exponential function was fitted to the individual datasets (eq. 4, see Materials and Methods) resulting in the time constant for recovery from inactivation of $\tau_r=4.9\pm0.9$ ms (n=3). The kinetics of recovery from inactivation is represented in **Figure 12** D as the average of the RF at different interpulse intervals for n=3 independent experiments along with the best fit of eq. 4 to the data points.

These results show that IDC express TTX-sensitive rapidly inactivating Na^+ channels. Depolarization up to +100 mV and 50 ms in duration failed to elicit any other type of inward or outward current under our experimental conditions (n>20).

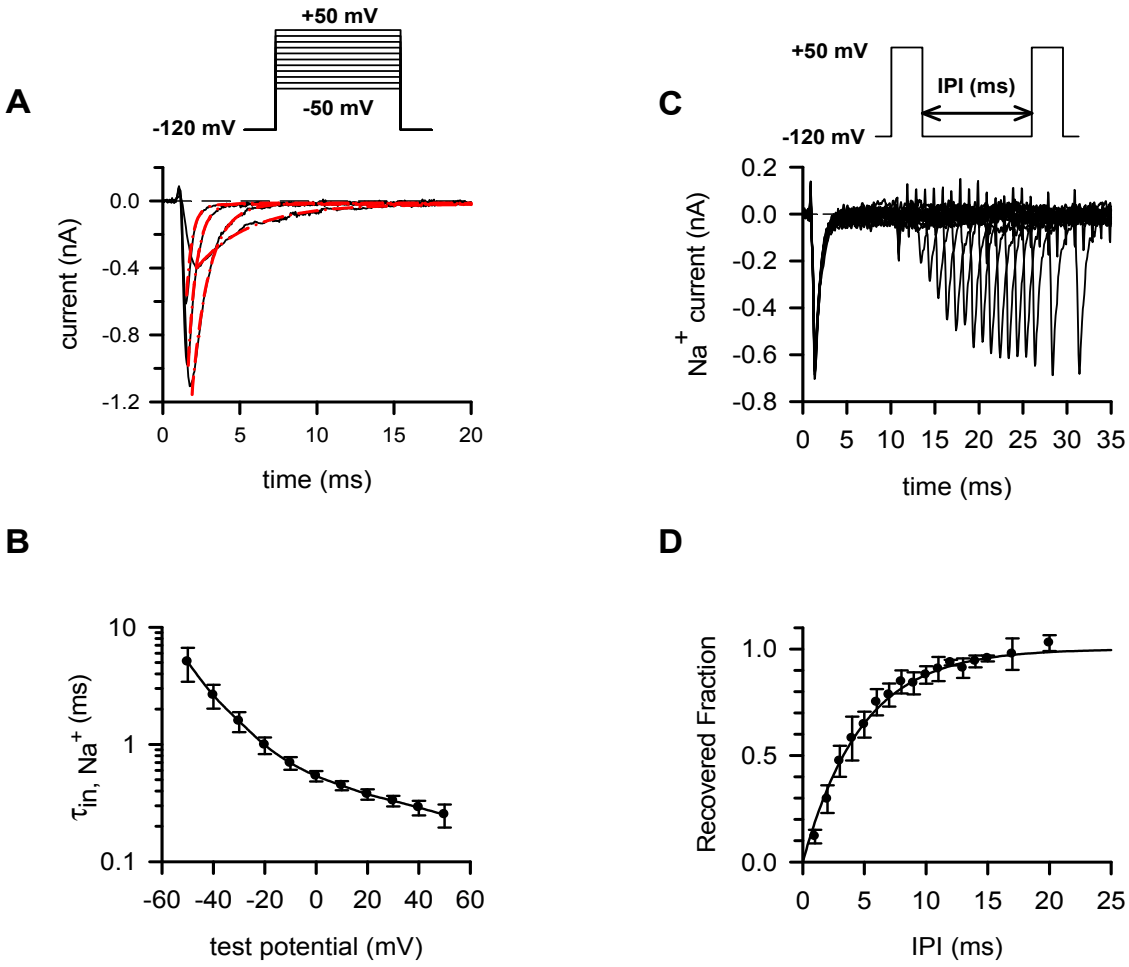

Figure 12 Kinetic parameters of inactivation and recovery from inactivation for Na^+ current in IDC.

(**Panel A**) Whole-cell currents were evoked by the same protocol as in Figure 11 A. The superimposed dash-dot lines indicate the best fit of a single exponential decay function (eq.1) to the data points. Selected traces evoked by depolarizations to −40, −20, 0 and +20 mV are shown for clarity having inactivation time constants of 3.39, 1.10, 0.58 and 0.39 ms, respectively.

(Panel B) The voltage-dependence of the inactivation time constant for the whole cell Na^+ currents in IDC. Inactivation time constants were determined at different test potential as described in Panel A. Data points are given as the average of four independent measurements. Please note the logarithmic scaling of the ordinate. Error bars indicate SEM.

(Panel C) Representative whole-cell current traces used to characterize the time course of the recovery from inactivation of the Na^+ current in an IDC Pairs of depolarizing step pulses from –120 mV to 0mV for 10 ms were separated by interpulse intervals (IPI) ranging from 1 to 20 ms. The membrane potential was set to –120 mV during the IPI.

(Panel D) Recovered Fraction (RF) of the Na^+ current was calculated as $(P_2\text{-}I_{ss1})/(P_1\text{-}I_{ss1})$ where P_1 and P_2 denote the peak currents obtained at the first and the second pulses, respectively, and I_{ss1} represents the steady-state current at the end of the first depolarizing pulse. RF was at each IPI was calculated and averaged for n=3 independent experiments and plotted as a function of IPI. A single exponential rising function (eq. 4) was fitted the data points to result in 4.76 s for the time constant of recovery from inactivation (τ_r). Eq. 4. was also fitted to RF–IPI relationships obtained for individual cells and the resulting τ_r was 4.9±0.9 ms (n=3). Error bars indicate SEM.

3. Outward K^+ current in mature dendritic cells

The activation of IDC by an inflammatory cytokine cocktail (see Materials and Methods) induced a dramatic change in the electrophysiological properties of the cells. The voltage ramp experiment in **Figure 13** A indicates that the inward current characteristic of IDC disappeared in MDC, furthermore, a voltage-gated outward current is activated at membrane potentials more depolarized than –30 mV.

A similar approach, used for the biophysical characterization of the Na^+ channels, was applied to specify the type(s) of channels generating the outward current, including the determination of the current-voltage relationship, the voltage-dependence of steady-state activation, the inactivation kinetics and the pharmacological properties of the current.

Figure 13 B illustrates a series of current traces evoked by 800-ms-long step depolarization pulses to different test potentials from a holding potential of –120 mV in every 90 s. The records show that the activation threshold of the current is between –40 and –30 mV, the current quickly activates and almost completely inactivates with a relatively slow kinetics. The leak-corrected peak current at each test potential was determined and plotted as a function of the test potential in the inset of **Figure 13** B. This I_p-V relationship shows that extrapolated reversal potential of the current is more negative than –60 mV, and that the voltage-dependence of the activation of the channels is very steep above –40 mV. Based on these characteristics the expression of voltage-gated K^+ channels is predicted in MDC. The peak K^+ current density at +50 mV test potential varied between 6.7 pA/pF and 111.9 pA/pF with median and mean current densities of 38.6 pA/pF and 48.1±9.4 pA/pF (n=13), respectively.

The I_p-V relationships were used to calculate the K^+ conductance of the membrane at each test potential and the normalized conductance-test potential (G_{norm}-V) relationships were generated for each cell individually as detailed in the Materials and Methods, and the Boltzmann function (eq. 5) was fitted to the data points (**Figure 13** C). The fits resulted in –25.0± 0.8 mV for the midpoint and 5.2 ± 0.4 mV for the slope of the voltage-dependence of steady state activation (n=4). The G_{norm}-V relationships are represented in **Figure 13** C as the average of the G_{norm} at different test potentials for n=4 independent experiments along with the best fit of the Boltzmann function (eq. 5) to the data points.

As **Figure 13** B shows that the whole-cell K^+ current in MDC displays inactivation. The superimposed dashed lines in **Figure 13** B indicate the best fit single exponential functions (eq. 1) to the decaying part of the current traces (red dashed line). The resulting time

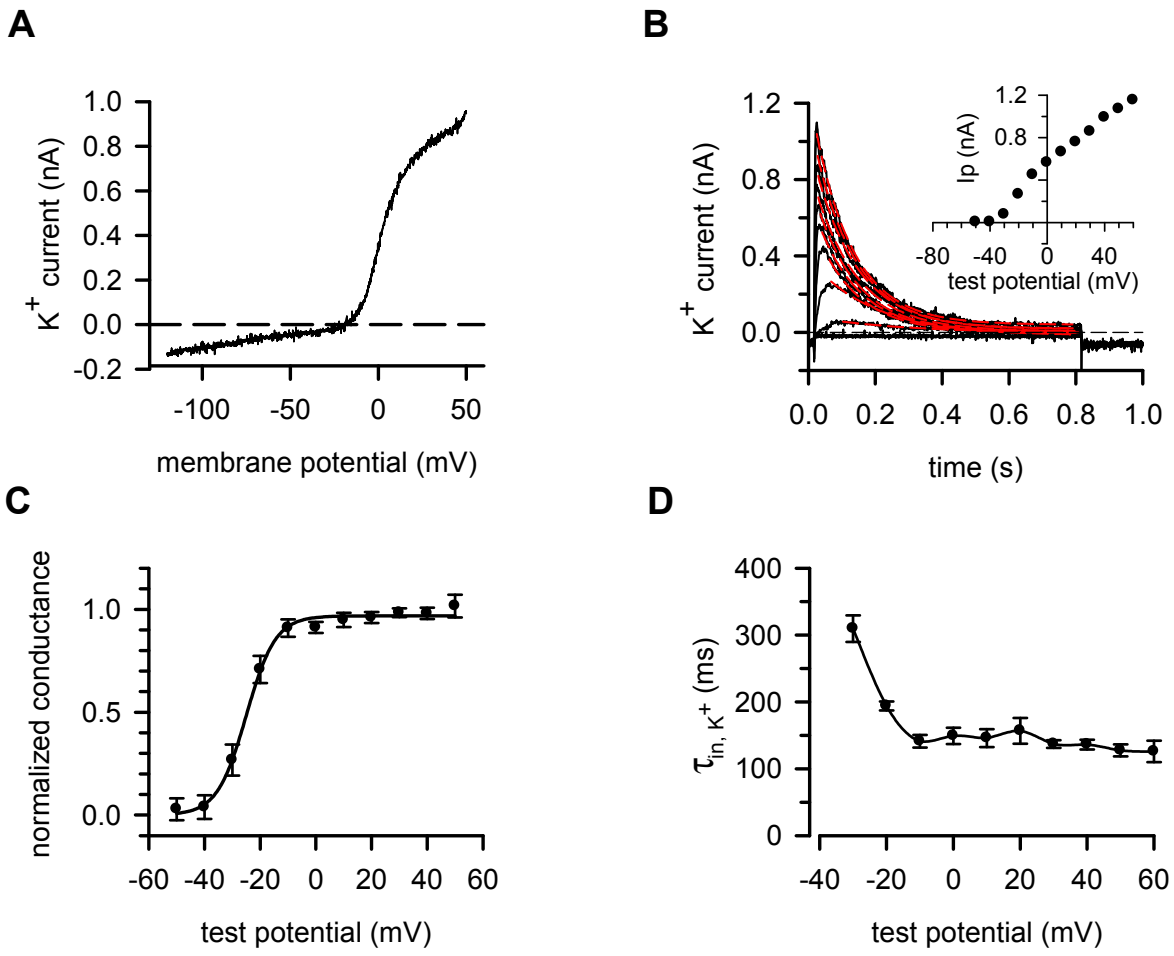

Figure 13 Depolarization-activated, outward, potassium current is present in MDC

(**Panel A**) The representative whole-cell current trace was recorded in an MDC in normal extracellular solution. A 150-ms-long voltage-ramp protocol ranging from –120 mV to +50mV was delivered. Horizontal dashed line represents the zero current level. (**Panel B**) Voltage-gated outward K^+ current in an MDC. The cell was held at –120 mV and depolarized to the test potentials between –70 mV to +60 mV for 800 ms every 90 s in 10 mV increments. The peak currents were used to construct the current-voltage relationship (see inset) whereas the decay of the curves was analyzed to characterize the inactivation kinetics. The superimposed dashed lines (red) indicate the best fit of a single exponential decay function (eq.1) to the data points (see **Panel D**). Inset: The peak current (I_p) at each test potential was determined from the records in Panel B and plotted as a function of the test potential to obtain the current-voltage relationship. **(Panel C)** Voltage-dependence of steady-state activation of the K^+ current in MDC. Peak whole-cell conductance (G(V)) at each test potential was calculated from the I_p at test potential V and the K^+ reversal potential (E_r) using $G(V)=I_p/(V-E_r)$. G(V) values were normalized to the maximum conductance, averaged for n=4 independent experiments (error bars indicate SEM.) and plotted as a function of test potential along with the best fit Boltzmann-function (eq. 5). The resulting $V_{½}$ and k values were –25.0 mV and 5.2 mV, respectively. Fitting eq. 5 to individual normalized conductance-test potential relationships (cell-by-cell) resulted in –25.0± 0.8 mV for the midpoint and 5.2 ± 0.4 mV for the slope of the voltage-dependence of steady-state activation. (**Panel D**) The voltage-dependence of the inactivation time constant for the whole cell K^+ currents ($\tau_{in,K}$) in MDC. Inactivation time constants were determined at different test potential as described in Panel A. Data points are given as the average of 3 independent measurements, error bars indicate SEM.

constants ($\tau_{i,K}$) were used to characterize inactivation kinetics of the K^+ current. $\tau_{i,K}$ at +50 mV was 127.4 ± 9 ms (n=3), the inactivation kinetics showed negligible voltage-dependence at membrane potentials more positive than –10 mV (**Figure 13** D).

The biophysical characteristics of the current, especially the inactivation kinetics, narrows significantly the range of ion channels suitable to produce the whole-cell currents in MDC. Based on these and the predominant expression of Kv1.3 channels in various cell types of the immune system we hypothesized that Kv1.3 channels may be expressed in MDC. To test this hypothesis we applied peptide and non-peptide ion channel blockers.

4. Pharmacological characterization of the outward K^+ current

Kv1.3 channels inactivate by the slow (P/C-type) inactivation mechanism which is characterized by the ability of extracellularly applied TEA to inhibit the current and to slow the inactivation process simultaneously by the foot-in-the-door mechanism (Grissmer and Cahalan 1989). This feature is demonstrated in **Figure 14** for the whole-cell K^+ current recorded in MDC. The figure shows that the amplitude of the whole-cell K^+ current is reduced to ~55% of the control in the presence of 10 mM TEA, the single-point estimate of the equilibrium dissociation constant from eq. 6 is 12.4±0.7 mM (n=3, see Materials and Methods). The figure also demonstrates that the inactivation kinetics of the current is slower in the presence of TEA, the time constants were 189 ms for control and 282 ms in the presence of 10 mM TEA.

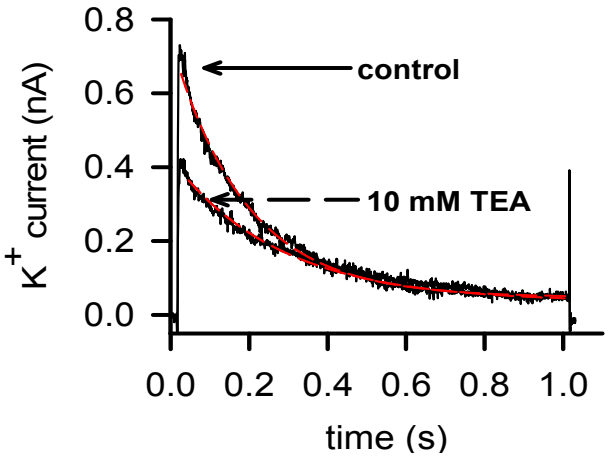

Figure 14 TEA blocks the K^+ current in MDC and slows the inactivation kinetics

K^+ currents in a whole-cell voltage-clamped MDC were evoked by 1000-ms-long depolarizations to +50 mV from a holding potential of –120 mV every 90s. The representative traces were recorded in normal extracellular solution (control) and in the presence of 10 mM TEA, as indicated. The peak current was reduced to 55% of the control by 10 mM TEA. The best fitting single exponential curves (eq. 1) are shown with dashed lines (red). The inactivation time constants were 189 ms in control solution and 282 ms in the presence of 10 mM TEA.

Two peptide toxins with different affinities and selectivities for Kv1.3, ChTx and MgTx, were used in subsequent pharmacological experiments. **Figure 15** A shows typical current traces recorded in the absence and in the presence of 2 nM ChTx. The effect of the toxin was reversible; the peak current was reduced to ~50% of the control upon perfusion with ChTx-containing normal-extracellular bath and recovered to the control value following a switch to the toxin-free normal-extracellular bath (washout). ChTx reduced the K^+ current in a dose-dependent manner (**Figure 15** B). The Hill equation (eq. 6) was fit to the dose-response data resulting in an equilibrium dissociation constant of 3.4 nM (**Figure 15** B). The inhibition of the whole-cell K^+ current by MgTx, a Kv1.3 specific toxin, is shown in **Figure 15** C. The trace recorded 300s after the start of the perfusion with toxin-containing (50 pM) extracellular solution indicates the equilibrium block of the current by MgTx. The dose-response of the current inhibition by MgTx is shown in **Figure 15** D. Fitting the Hill equation to the data points resulted in an equilibrium dissociation constant of 39.8 pM, which is characteristic of the inhibition of Kv1.3 channels. The wash-out of the toxin was extremely slow requiring 20-30 min for significant recovery from block (data not shown). Based on the biophysical and pharmacological data we propose that the channel responsible for the outward K^+ currents in MDC is Kv1.3.

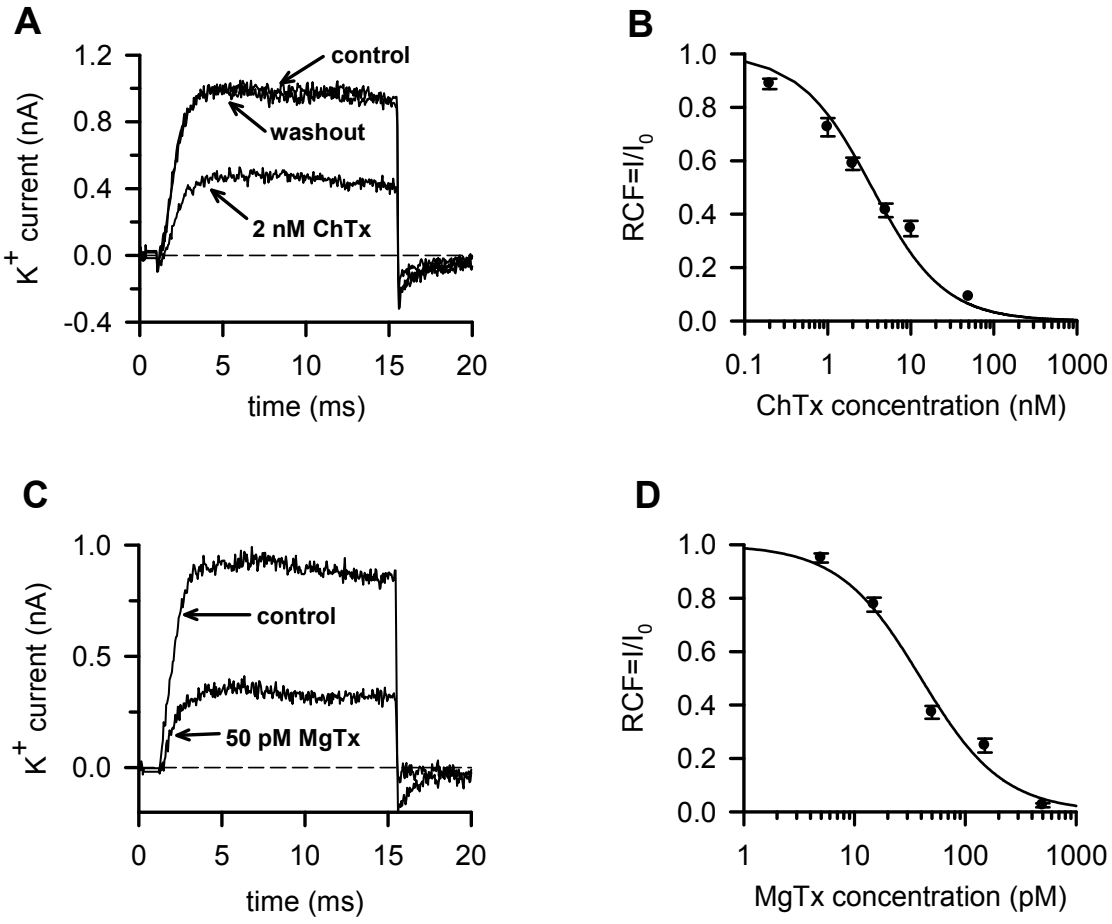

Figure 15 Inhibition of the K^+ current in MDC by ChTx and MgTx

(Panel A) Reversible inhibition of the whole-cell K^+ current by ChTx in an MDC. Representative traces show the K^+ current before the application of the toxin (control), after the equilibration of the block in the presence of 2 nM ChTx (as indicated by the arrow) and after full recovery from block during the perfusion of the bath with toxin-free solution (washout). The peak current was reduced by ChTx to 50% of the control. Currents were evoked by depolarizations to +50 mV for 15 ms every 30 s from a holding potential of –120 mV.

(Panel B) ChTx inhibits the outward K^+ current in a dose-dependent manner. The remaining fraction of the current (RCF) was calculated as I/I_0 where I and I_0 are the peak currents in the presence and absence of ChTx. The voltage protocol and toxin application procedure were the same as in Panel A. RCF at each toxin concentration was calculated from n≥4 independent experiments and plotted as a function of ChTx concentration. Error bars indicate SEM. The Hill equation (eq. 6) assuming 1:1 channel-toxin stochiometry was fitted to the data points to give a K_d of 3.4 nM.

(Panel C) Margatoxin inhibits the K^+ current with high affinity. Currents were evoked by the same protocol as in Panel A. Representative traces show the K^+ current before the application of the toxin (control) and after the equilibration of the block in the presence of 50 pM MgTx (as indicated by the arrow). The toxin in 50 pM concentration reduced the peak current to ~40% of the control.

(Panel D) MgTx inhibits the outward K^+ current in a dose-dependent manner. RCF was calculated as in Panel B, voltage protocol and toxin application procedure were the same as in Panel A. RCF at each toxin concentration was calculated from n≥4 independent experiments and plotted as a function of MgTx concentration. Error bars indicate SEM. The Hill equation (eq. 6) assuming 1:1 channel-toxin stochiometry was fitted to the data points to give a K_d of 39.8 nM.

5. Identification of the electrophysically characterized voltage-gated Na^+ channel of immature dendritic cells

A PCR-based strategy was used to identify the TTX-sensitive VGSC responsible for the Na^+ current detected in the membrane of IDC. Prior to this study, no Na^+ channel-related DNA sequences of DC were known, thus we probed a cDNA library using degenerate primers based on a conserved sequence common to all VGSCs. Using these degenerate primers, a 387-bp portion of the gene was amplified, cloned and sequenced, as described in the Materials and Methods. The nucleotide sequence of five out of twenty cloned constructs fitted perfectly to the human gene SCN9A (GenBank accession number NM_002977), which encodes for the voltage-gated Na^+ channel 1.7 α subunit. Sequences corresponding to Nav channels other than Nav1.7 were not found in either of the clones. These findings indicate that the molecular identity of the channels responsible for the inward Na^+ currents in of IDC is Nav1.7.

6. Expression of mRNAs for voltage-gated ion channels in differentiating monocyte-derived dendritic cells

In order to quantify the relative expression of the identified voltage-gated ion channels we measured mRNA expression levels by real time RT-PCR in IDC and MDC activated by an inflammatory cocktail. As several cell types of myeloid origin also express Kv1.5 channel subunits the mRNA expression level for Kv1.5 was also determined along with that of the Nav1.7 and the Kv1.3 channel. To compare the relative expression of these mRNA transcripts in IDC and MDC the data were normalized to the expression of the housekeeping gene 36B4. In line with the results of the biophysical characterization the expression of Nav1.7 mRNA was the highest in IDC, whereas the MDC expressed Kv1.3 transcripts (**Figure 16** A,B). As compared to IDC the changes of the relative expression of Nav1.7 and Kv1.3 in MDC were 118-fold decrease and 38-fold increase, respectively, calculated using the comparative method (2-ΔΔCt). These data demonstrate the coordinated but opposing regulation of well-defined Nav1.7 and Kv1.3 channels in differentiating monocyte-derived DC.

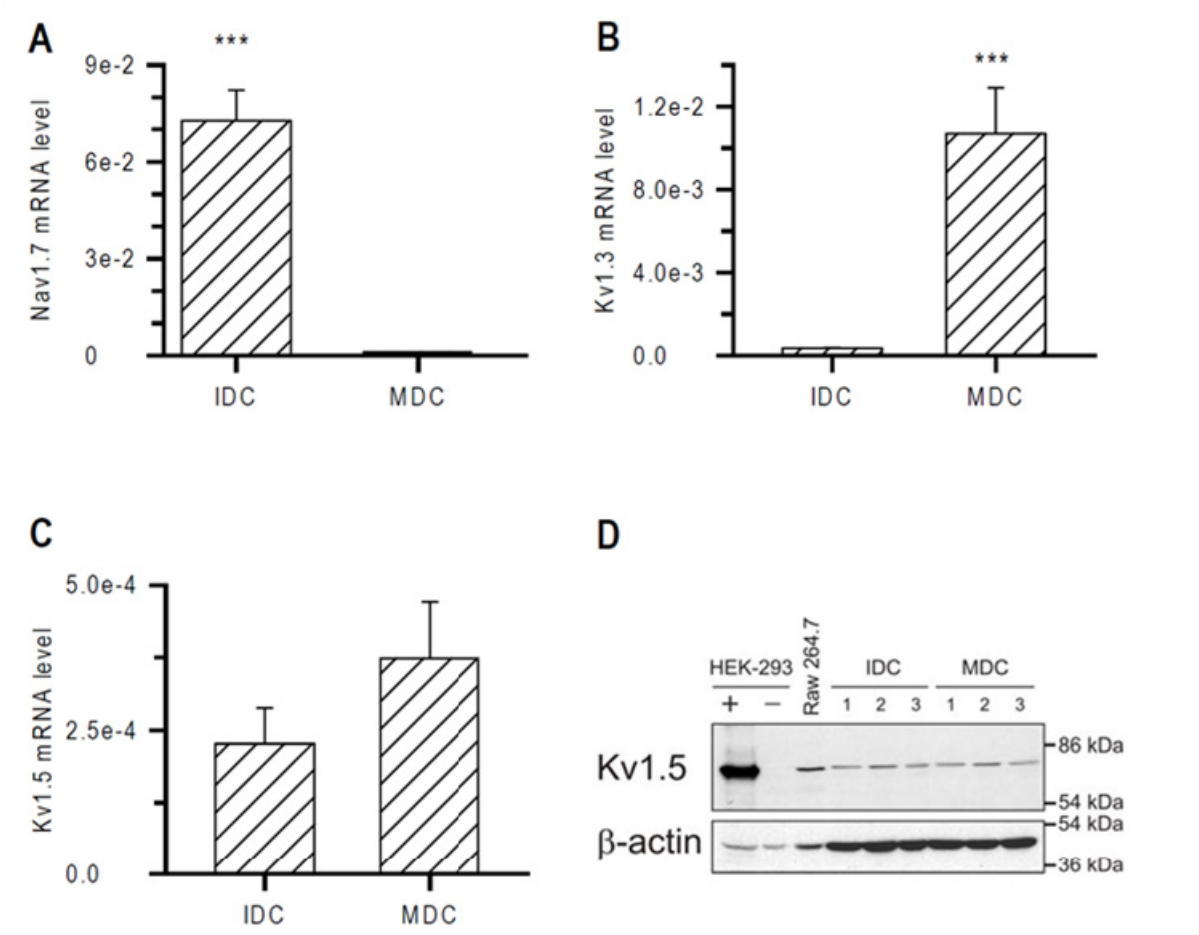

Figure 16 Expression of specific voltage gated channels in IDC and MDC

The relative mRNA expression of Nav1.7 (**Panel A**), Kv1.3 (**Panel B**) and Kv1.5 (**Panel C)** voltage-gated channels was measured by real-time RT-PCR in IDC and MDC stimulated by inflammatory cocktail. Values are expressed relative to the expression of the 36B4 housekeeping gene transcript (see details in the Material and Methods). Mean ± SEM of triplicate measurements of three independent experiments are shown. ***P < 0.001. (**Panel D)** Kv1.5 Western blot analysis. Lines loaded as indicated: HEK-293 (+): HEK -293 cells expressing Kv1.5; HEK-293 (–): control HEK-293 without transfection of Kv1.5; Raw 264.7 macrophages; IDC 1-3: immature dendritic cells from three independent isolations; MDC 1-3: mature dendritic cells from the same three independent isolations after maturation. Anti-β-actin was used as loading and transfer control.

Figure 16 C shows that Kv1.5 mRNA transcripts were also isolated from both IDC and MDC, however, at a lower level, with no significant change in the expression during differentiation. The presence of Kv1.5 mRNA and the functional absence of Kv1.5 subunits in the current records indicated Western blot experiments to assess the expression of this subunit in DC of various differentiation states. **Figure 16** D shows that the expression of the Kv1.5 subunit relative to that of β-actin is similar in both IDC and MDC. HEK-293 cells

transfected with Kv1.5 and Raw 264.7 macrophages, endogenously expressing the Kv1.5 subunit (Vicente, Escalada et al. 2006), were used to demonstrate the sensitivity of the assay. In addition, similar to Kv1.5 gene expression, the relative β-actin abundance and the fact that the same amount of protein was evaluated in each lane (group) indicate that the protein expression of Kv1.5 is much lower in either IDC or MDC than in Raw 264.7 macrophages.

7. Electrophysiological characterization of KG-1 cells

Figure 17 A and B show families of current traces obtained for an unstimulated and a stimulated KG-1 cell, respectively. Whole-cell currents were recorded in response to depolarizing pulses from a holding potential of −80 mV to different test potential ranging from −70 to +50 mV in 10 mV increments. The currents recorded in unstimulated and stimulated cells are qualitatively similar; they do not exhibit time-dependent gating. Current traces recorded at different test potentials run parallel to the voltage axis separated by approximately equal vertical distances. This picture is consistent with the presence of a linear leak conductance in these cells when KF-based solution was used in the pipette. The reversal potential of the current under these experimental conditions can be determined from currents recorded in response to a linear voltage ramp, as it is shown in panels C and D for unstimulated and stimulated KG-1, respectively. The reversal potential of the current is approximately 0 mV in both cell types which is characteristic to a non-specific leak current. The ohmic characteristics of the voltage ramp records shown in panels C and D also confirm the absence of a voltage-gated conductance in KG-1 cells.

The drawback of the KF-containing internal solution is that it does not allow the recording of K_{Ca} currents since the free Ca^{2+} concentration is in the nanomolar range in this solution. This is mainly due to the presence F^- in the pipette solution, which forms an insoluble precipitate with Ca^{2+}. Therefore, we substituted fluoride ions with aspartate, and adjusted the EGTA and Ca^{2+} concentration in the pipette solution to result in 1μM free Ca^{2+} concentration during the measurement of K_{Ca} currents. The whole-cell currents evoked by voltage ramps (control traces) in **Figure 17** E (unstimulated KG-1) and F (stimulated KG-1) reversed between −50 and −60mV when K-aspartate internal solution was used. This value is close to the equilibrium potential for K^+ ions (−83mV, calculated using the Nernst equation), which indicates that the whole-cell current is dominated by a K^+ selective conductance in this case. The deviation of the reversal potential from the theoretical value is due to the leak current:

the reversal potential for leak current is 0mV, which shifts the reversal potential of the whole-cell current to depolarized potentials (right shift along the voltage axis). Panels E and F of **Figure 17** also show that the whole-cell currents of unstimulated and stimulated KG-1 cells could be reversibly blocked by 10nM ChTx, a peptide inhibitor of several voltage-gated and K_{Ca} channels. The block of K_{Ca} channels resulted in a diminished slope of the current in the presence of ChTx, the current returned close to the control level after washing the recording chamber with toxin-free extracellular solution (washout). The magnitude of the K_{Ca} conductance calculated from the slope of the currents was relatively small in both cell types ~1.9 nS. On panel F the intersection of three curves (control, ChTx, washout) is below the zero current line, which is a consequence of a higher leak current during this measurement. In summary, the time- and voltage-independent but Ca^{2+}-dependent activation of the current and its sensitivity to ChTx point to the presence of K_{Ca} channels in both unstimulated and stimulated KG-1 cells.

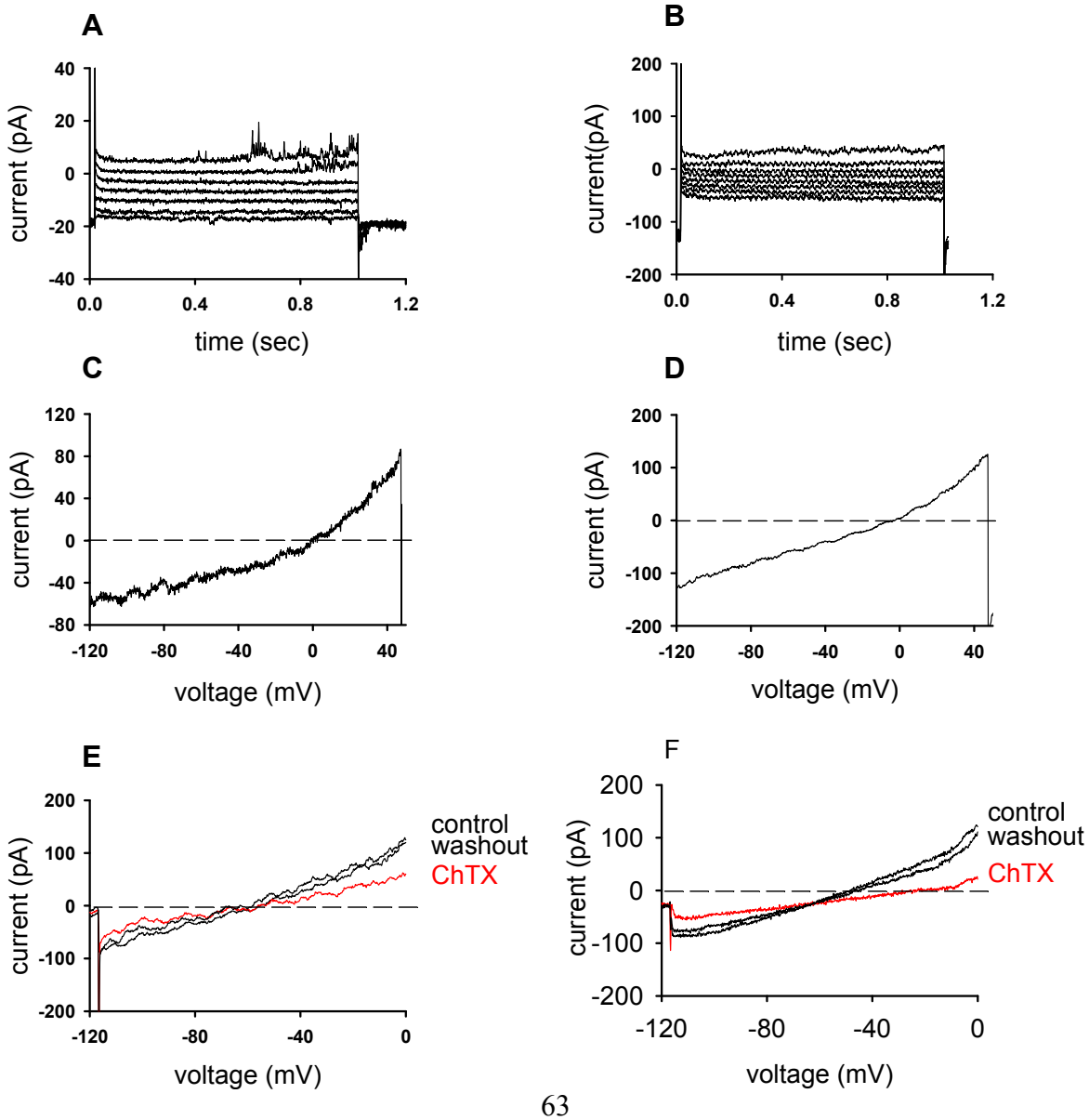

Figure 17 Ca^{2+}-activated ChTx sensitive K^+ current is expressed in KG-1 cells

Panels A and B: representative whole-cell current traces were recorded in an unstimulated (A) and a stimulated (B) KG-1 cell in normal extracellular solution using KF-based internal solution in the pipette. In this set of experiments a series of 1-s-long depolarizing step pulses ranging from −70 to +50 mV was applied to the cells from a holding potential of −80 mV. Selected traces are displaced for clarity of the graph. Panels C and D: a representative current recording in an unstimulated (C) and a stimulated (D) KG-1 cell evoked by a 200-ms-long voltage-ramp pulse ranging from −120 to +50 mV. The bath solution was normal extracellular solution and the pipette was filled with KF-containing internal solution. The dashed line indicates the zero current level throughout the whole graph. Panels E and F: representative current traces in an unstimulated (E) and a stimulated (F) KG-1 cell were evoked by 200-ms-long voltage-ramp pulse ranging from −120 to +0 mV in the absence (control, washout) and in the presence of 10 nM ChTx(red line). The pipettes were filled with Ca^{2+}-containing internal solution (1 μM free [Ca^{2+}]), and the bath solution was normal extracellular solution. Note the change in the slope of the current upon ChTx application.

B. Endothelial cells

1. Identification of EC with the diffusion of neurobiotin

In order to assure that the recorded currents were from EC and that these cells maintained their connection with their adjacent cells via gap junctions, the marker neurobiotin as a tracer was used. Injection of positive current (10 pA during 500 ms) was used to facilitate the diffusion of neurobiotin from the patch pipette into the cell under current clamp control (**Figure 17 A**). By using neurobiotin we showed that EC were homogeneously stained, indicating that they are electrically coupled to each other in both circumferential and longitudinal directions, thus creating a functional unit (**Figure 17**). Diffusion of neurobiotin from EC to VSMC was not observed, which is consistent with previous studies, that there is no heterocellular dye coupling between EC and VSMC in arterioles (Beny 1999; Yamamoto, Klemm et al. 2001). Due to the low resolution of the microscopic image we could not accurately measure the size of single EC, but in previous studies it was measured to be 20 - 40 µm (Yamamoto, Klemm et al. 2001).

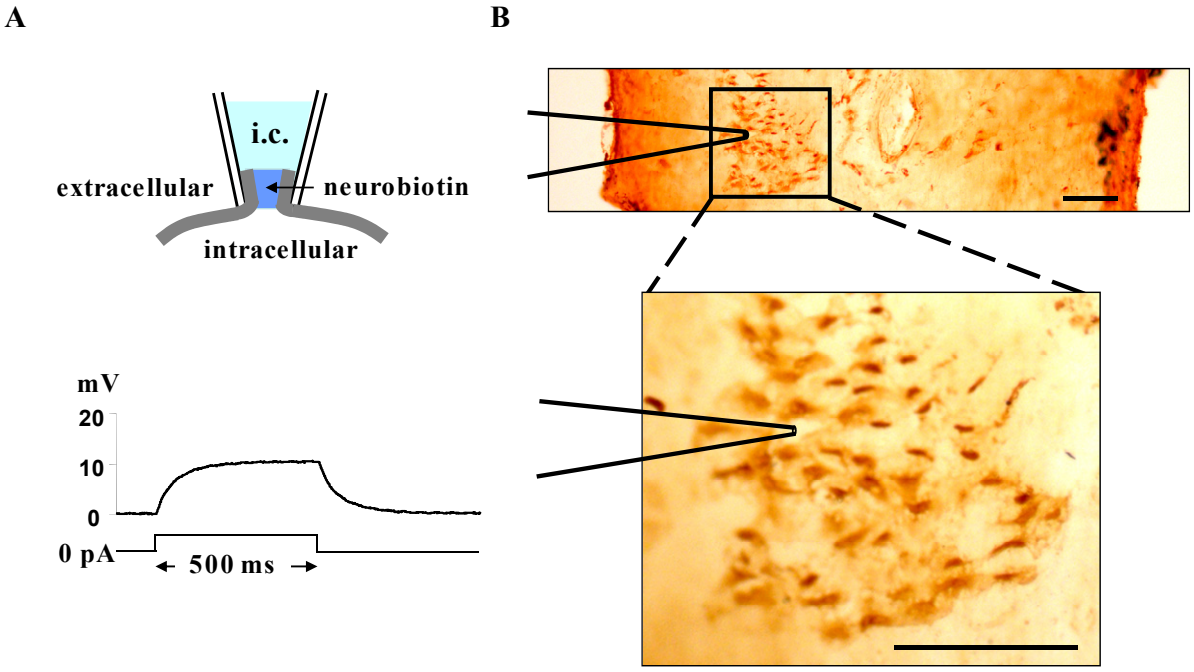

Figure 17 Identification of EC by neurobiotin tracer

A. Due to the fact that neurobiotin carries positive charges, neurobiotin was iontophoresed into the cell by injecting positive square current pulses (10 pA, delivered at a rate of 1Hz,500 ms duration- see protocol above, where the y axis represents the membrane potential change) and then to spread to neighboring cells via gap junctions. **B.** After labeling the cells for 15 min the patch electrode was removed and the arterial segment was fixed and processed. EC were homogeneously stained indicating that they are coupled to each other and could propagate messages along the artery. Calibration bar: 100 µm.

2. Identification of K_{ir} currents in EC

Previous electrophysiological studies have shown the expression of different K^+ channels in EC – such as $K_{ir,}$ BK_{Ca}, IK_{Ca1} and SK_{Ca} –, and the opening of these channels are said to be responsible for the regulation of vascular tone via membrane hyperpolarization (Nilius and Droogmans 2001).

We tested whether K_{ir} channels are expressed on intact EC. Families of hyperpolarizing voltage pulses from −60 mV to −200 mV (Vh=−60 mV) induced rectifying inward currents in intact EC (**Figure 19** Aa1). Hyperpolarizing voltage pulses induced rectifying non-inactivating inward currents in mesenteric EC. The pharmacological properties of the current were tested using a well-known blocker of K_{ir}, Ba^{2+} (Nilius and Droogmans 2001). Incubation with 30 µM Ba^{2+} inhibited the inward currents from −1148±189 to −573±211 pA at −200 mV, (p=0.008, n=8) and decreased current density from −34±7 to −20±3 pA/pF at -200 mV, (p=0.018, n=8) (**Figure 19** B_1, B_2) indicating that K_{ir} channels are expressed on intact rat mesenteric EC.

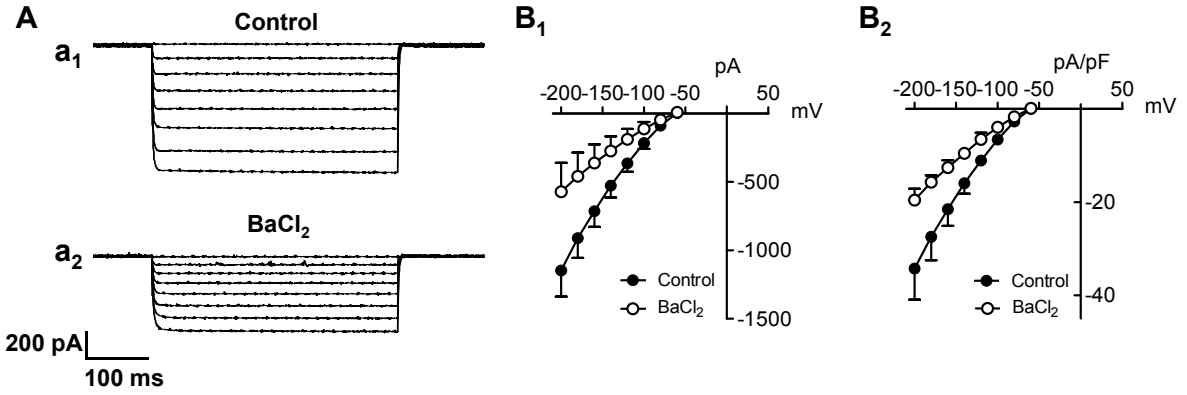

Figure 18 Expression of K_{ir} channels on EC of the rat superior mesenteric artery

A. Whole cell recording of K_{ir} currents in response to hyperpolarizing pulses from −60 mV to −200 mV over 400 ms in −20 mV increments, Vh=−60mV**.** Panels Aa1, Aa2 represent the whole cell K_{ir} current recording. Panels B_1 and B_2 represent the I-V relationship in control conditions (●) and after 30 µM Ba^{2+} (○) expressed as current amplitude (pA, B_1) or current density (pA/pF, B_2). Each point represents the mean±SEM., paired *t*-test of 8 cells.

3. Calcium activated potassium channels

Endothelial K_{Ca} have been reported in the rat superior mesenteric artery (Stankevicius, Lopez-Valverde et al. 2006), thus we tested whether outward K_{Ca} currents are expressed in intact EC. Cells were held at −60 mV and were subjected to families of depolarizing voltage pulses from −60 mV to 140 mV for 400 ms in 20 mV increments. Depolarizing pulses induced outwardly directed currents in mesenteric intact EC recorded '*in situ*' (**Figure 20** Aa1, Bb1). The voltage steps elicited non-inactivating outward currents up to test potentials of 140 mV (**Figure 20**). In order to investigate the nature of the currents we used TEA (10 mM), which significantly decreased the amplitude of these outward currents (**Figure 20** Aa_1 and Aa_2) from 1011±168 to 559±123 pA at 140 mV (p=0.028, n=5) and the current density from 35±7 to 16±4 pA/pF at 140 mV (p=0.004, n=5) (**Figure 20** A_1, A_2), indicating that K_{Ca} channels are expressed on intact EC (Ledoux, Werner et al. 2006).

We further characterize the different types of K_{Ca} channels using IbTx (**Figure 20** Bb_1, Bb_2) TRAM34 (**Figure 20** Aa_1, Aa_2) and apamin (**Figure 20** Bb_1, Bb_2), specific blockers of BK_{Ca}, IK_{Ca1} and SK_{Ca} currents, respectively. Blockade of SK_{Ca} channels with apamin (0.5 μM) had an inhibitory effect decreasing the amplitude of the currents from 453±51 to 206±74 pA at 140 mV (p=0.004, n=6) and current density from 29±6 to 12±5 pA/pF at 140 mV (p=0.004, n=6) (**Figure 20** B_1, B_2). Blockade of IK_{Ca1} channels with 0.1 μM TRAM34 (Wulff, Miller et al. 2000) reduced the outward currents from 1129±238 to 479±178 pA at 140 mV (p=0.002, n=5) and current density from 29±7 to 9±3 pA/pF at 140 mV (p=0.027,n=5) (**Figure 20** A_1, A_2). The blockade of BK_{Ca} currents with IbTx (0.1 μM) also had an inhibitory effect on the currents induced by depolarizing steps, decreasing the amplitude of the outward currents from 1040±93 to 639±75 pA at 140 mV pA (p=0.009, n=4) and current density from 36±4 to 23±5 pA/pF at 140 mV pA/pF (p=0.004, n=4) (**Figure 20** B_1, B_2).

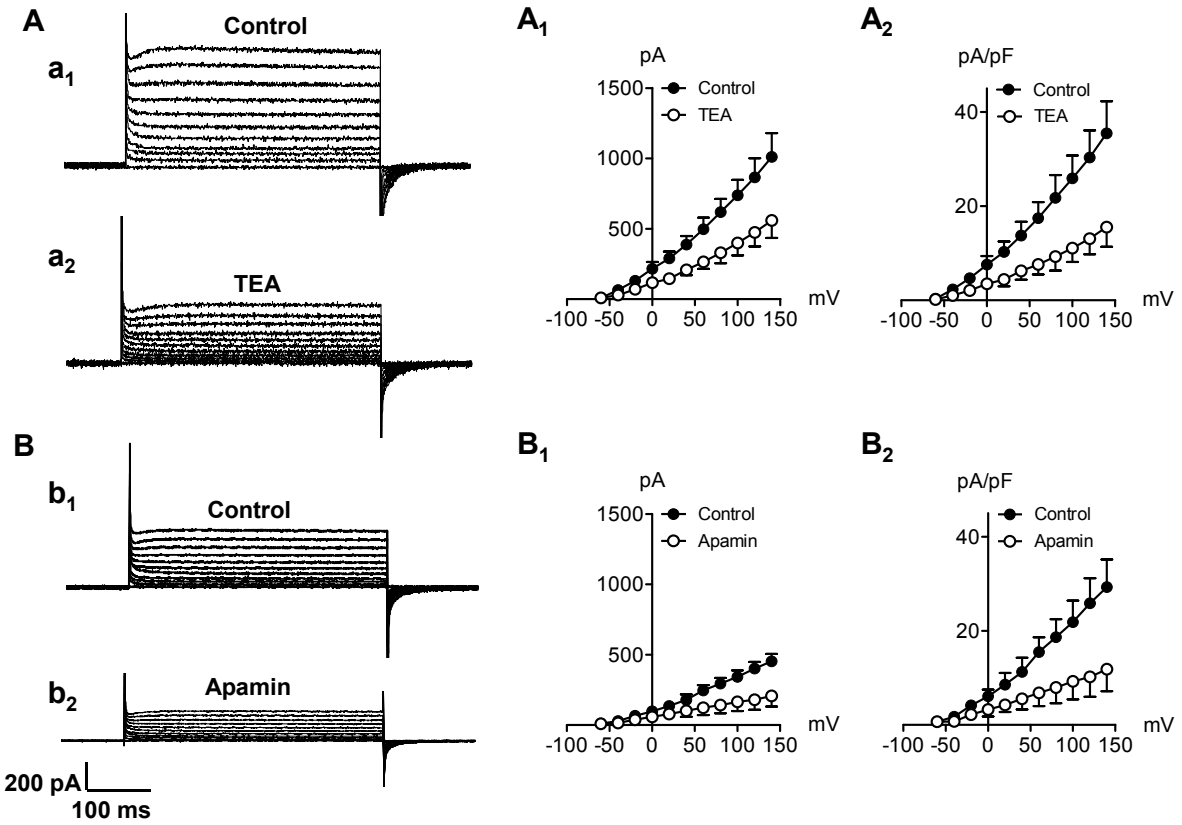

Figure 19 Patch clamp recording of K_{Ca} currents from the EC – identification of SK_{Ca}

A. Whole cell recording of outwardly directed K^+ currents in response to depolarizing pulses from −60 mV to 140 mV over 400 ms in 20 mV increments, Vh=−60mV. Panels Aa_1, Aa_2, represent the whole cell current recording. Panels A_1 and A_2 represent the I-V relationship in control conditions (●) and after 10 mM TEA (○) expressed as current amplitude (pA, A_1) and current density (pA/pF, A_2). Each point represents the mean±SEM., paired *t*-test of 5 cells. **B.** Patch clamp recording of apamin-sensitive SK_{Ca} currents. Panels Bb_1, Bb_2, represent the whole cell SK_{Ca} current recording. Panels B_1 and B_2 represent the I-V relationship generated from the voltage step protocol in control condition (●) and after 0.5 μM apamin (○) expressed as current amplitude (pA, B_1) and current density (pA/pF, B_2). Each point represents the mean±SEM., paired *t*-test of 6 cells.

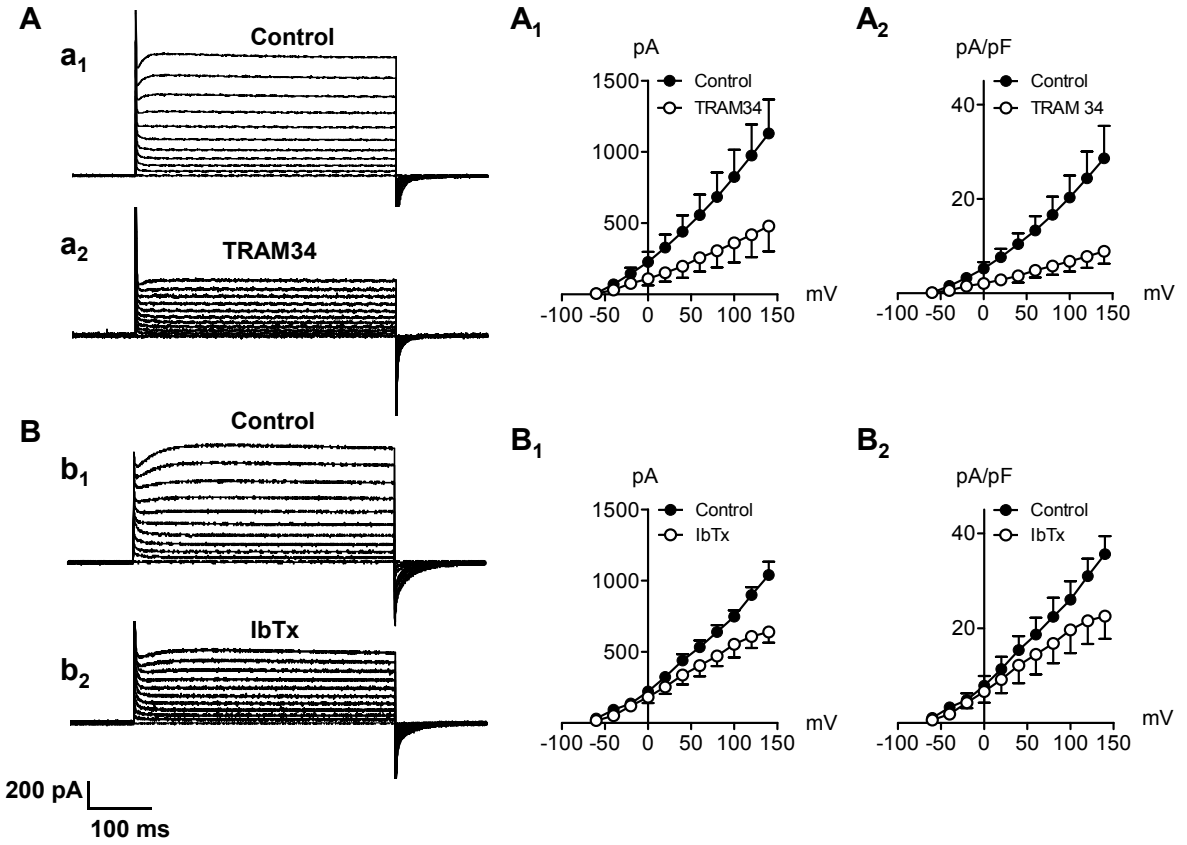

Figure 20 Patch clamp recording of K_{Ca} currents from intact EC – identification of IK_{Ca1} and BK_{Ca}

A Recording of TRAM34-sensitive IK_{Ca1} currents. Panels Aa_1, Aa_2, represent the whole cell IK_{Ca1} current recording. Panels A_1 and A_2 represent the I-V relationship generated from the voltage step protocol in control condition (●) and after 0.1 µM TRAM34 (○) expressed as current amplitude (pA, A_1) and current density (pA/pF, A_2). Each point represents the mean±SEM., paired t-test of 5 cells. **B.** IbTx-sensitive BK_{Ca} currents. Panels Bb_1, Bb_2, represent the whole cell BK_{Ca} current recording. Panels B_1 and B_2 represent the I-V relationship generated from the voltage step protocol in control condition (●) and after 0.1 µM IbTx (○) expressed as current amplitude (pA, (B_1) and current density (pA/pF, B_2). Each point represents the mean±SEM., paired t-test of 4 cells.

4. Effect of ACh on outward currents

It has been shown previously that Ach increases $[Ca^{2+}]_i$ by triggering Ca^{2+} release from the intracellular stores, evokes EC hyperpolarization by activation of membrane K_{Ca} channels, which promotes Ca^{2+} influx through an elevation of the electrochemical driving force for Ca^{2+} (Crane, Gallagher et al. 2003; Crane, Walker et al. 2003; Ledoux, Werner et al. 2006; Stankevicius, Lopez-Valverde et al. 2006). The rise of $[Ca^{2+}]_i$ will result in NO synthesis and release in EC, which will promote relaxation in the underlying VSMC .

We tested whether ACh has an effect on the whole cell currents described above. Cells were held at -60 mV and were subjected to either depolarizing voltage pulses from -60 mV to 140 mV over 400 ms in 20 mV increments or to depolarizing ramps from -60 to 140 mV over 100 ms. Under control conditions, depolarizing voltage pulses or ramps induced non-inactivating outward current (**Figure 22** a_1,a_2, a_3). ACh (10 μM) induced a significant increase in the amplitude of the outward currents from 689±122 to 995±170 pA at 140 mV (p=0.007, n=14) and in current density from 25±2 to 35±3 pA/pF at 140 mV (p=0.001, n=14). Incubation of the artery with 10 mM TEA significantly inhibited the Ach induced current from 995±170 to 399±137 pA at 140 mV (p=0.039, n=5), and decreased current density (from 35±3 to 14±6 pA/pF at 140 mV, p=0.001, n=14, n=5, unpaired t-test) (**Figure 22** A_1 and A_2). This indicates that K^+ channels are responsible for the ACh-mediated increase in outward currents, which may lead to NO release and thus endothelial cell hyperpolarization.

5. Effect of 18β-gly on inward and outward K^+ currents

Neurobiotin staining demonstrated that EC are electrically coupled to each other through gap junctions, which may facilitate electrical coupling between these cells. Thus, we tested whether homocellular gap junctions facilitate electrical spreading of the inward and outward K^+ currents. To block gap junction communication between EC we used 18β-gly (Tare, Coleman et al. 2002). Cells were held at −60 mV and subjected to either hyperpolarizing pulses from −60 mV to −200 mV over 400 ms in −20 mV increments or depolarizing voltage pulses from −60 to 140 mV over 400 ms in 20 mV increments (Vh=−60mV). 18β-gly (25 μM) decreased the inward and outward current amplitude (from −1032±122 to −622±126 pA at −200 mV, p=0.001, n=7; and from 1078±176 to 526±199 pA at 140 mV, p=0.007, n=6; respectively) (**Figure 23** Aa1, Aa2, A1; Bb1, Bb2; B1). Moreover, when data were expressed as current density, 18β-gly had not any significant effect (−29±3 vs −25±3 pA/pF at -200 mV, p=0.369, n.s., n=7; and 31±3 vs 33±6 pA/pF at 140 mV, p=0.409, n.s., n=6, respectively) (**Figure 23** A2, B2).

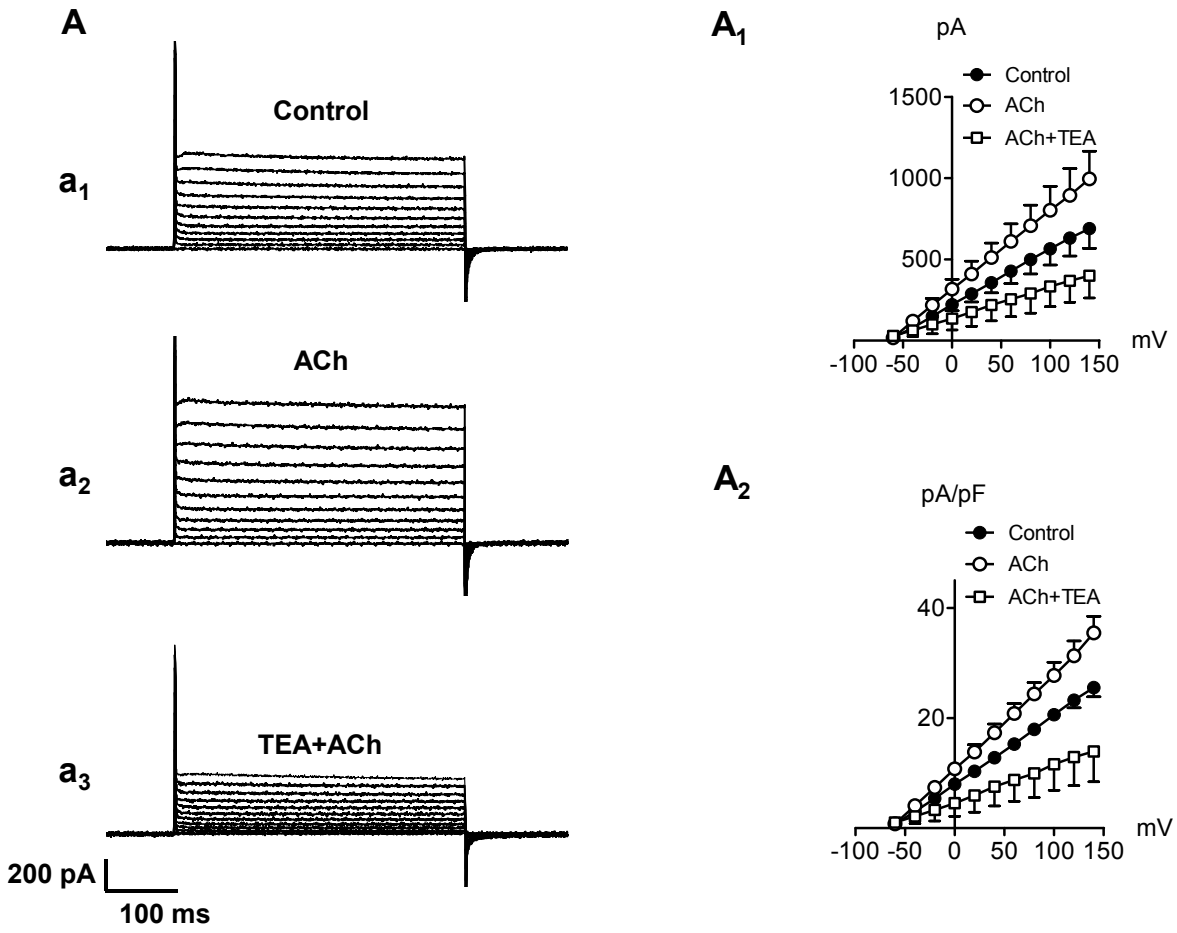

Figure 21 TEA inhibits the ACh-induced increase in the amplitude of outward currents in EC

A. Whole cell recording of outward K^+ currents in response to depolarizing pulses from −60 mV to 140 mV over 400 ms in 20 mV increments, Vh=−60mV. Panel Aa_1, a_2, a_3, represent the original whole cell K^+ current recording under control conditions, after 10 μM ACh, and after incubation with 10 μM ACh plus 10 mM TEA. Panels A_1 and A_2 represent the I-V relationship generated from the voltage step protocol in control condition (●), after ACh (○) and after ACh plus TEA (□) expressed as current amplitude (pA, A_1) and current density (pA/pF, A_2). Each point represents the mean±SEM., paired *t*-test of 14 cells ACh *vs* control, and the mean±SEM., unpaired *t*-test of 5 cells ACh *vs* TEA.

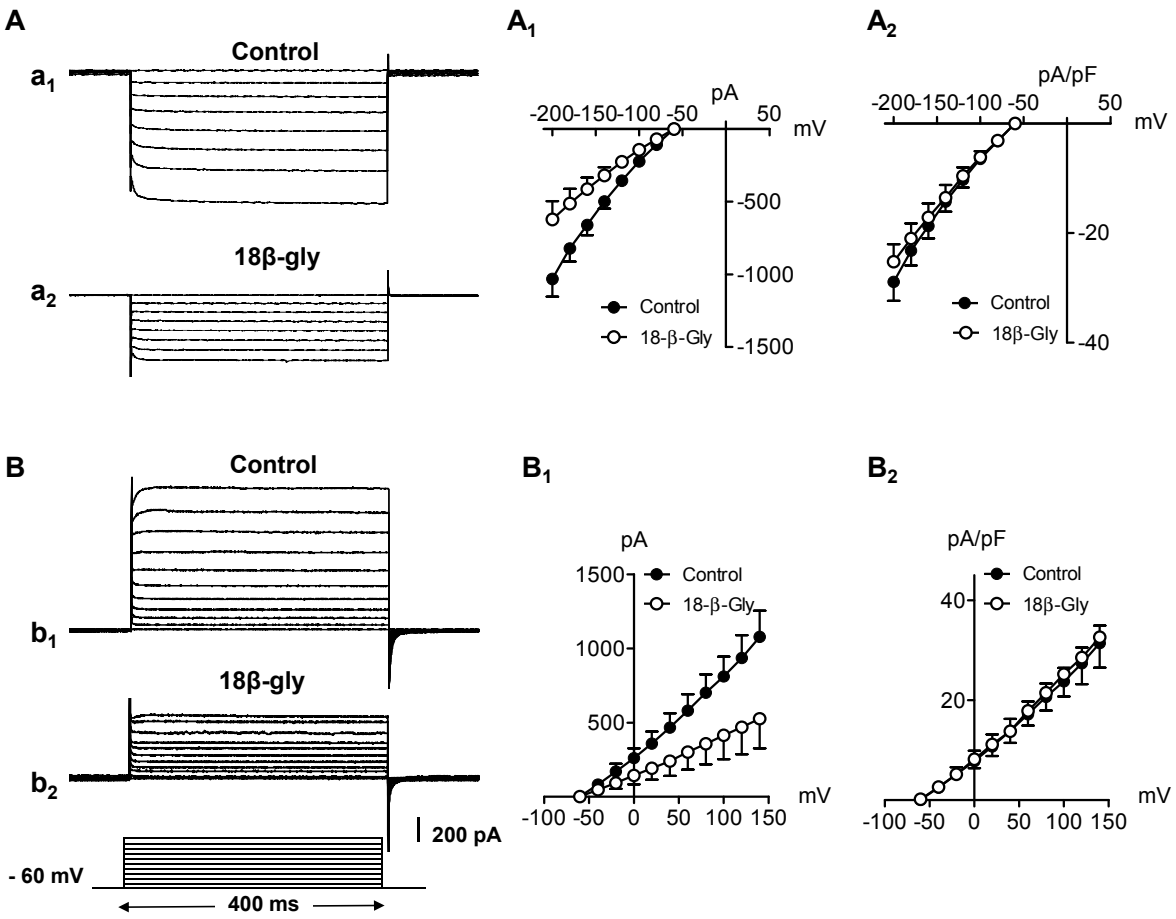

Figure 22 Effect of 18β-gly on inward and outward K^+ currents recorded from EC *"in situ"*

A. Whole cell recording of inward K+ currents in response to families of hyperpolarizing pulses from -60 mV to -200 mV over 400 ms in -20 mV increments, Vh=–60 mV. Panels Aa_1, Aa_2 represent the whole cell recording of inward K^+ currents in response to the voltage step protocol in control conditions and after 18β-gly 25 µM. Panel A_1 and A_2 represent the I-V relationship in control conditions (●) and after 18β-gly µM (○) expressed as current amplitude (pA, A_1) and current density (pA/pF, A_2). Each point represents the mean±SEM., paired *t*-test of 7 cells. **B.** Whole cell recording of outward K^+ currents in response to depolarizing pulses from –60 mV to 140 mV over 400 ms in 20 mV increments, Vh=–60 mV. Panels Bb_1, Bb_2 represent the whole cell recording of outward currents generated from the voltage step protocol in control conditions (●) and after 18β-gly 25 µM (○). Panels B_1 and B_2 represents the I-V relationship in control conditions and after 18β-gly expressed as current amplitude (pA, B_1) and current density (pA/pF, B_2). Each point represents the mean±SEM., paired *t*-test of 6 cells.

The data showed in **Figures 19-23** is summarized as a bar chart representing the effect of the different drugs on the inward and outward potassium currents **(Figure 23**)

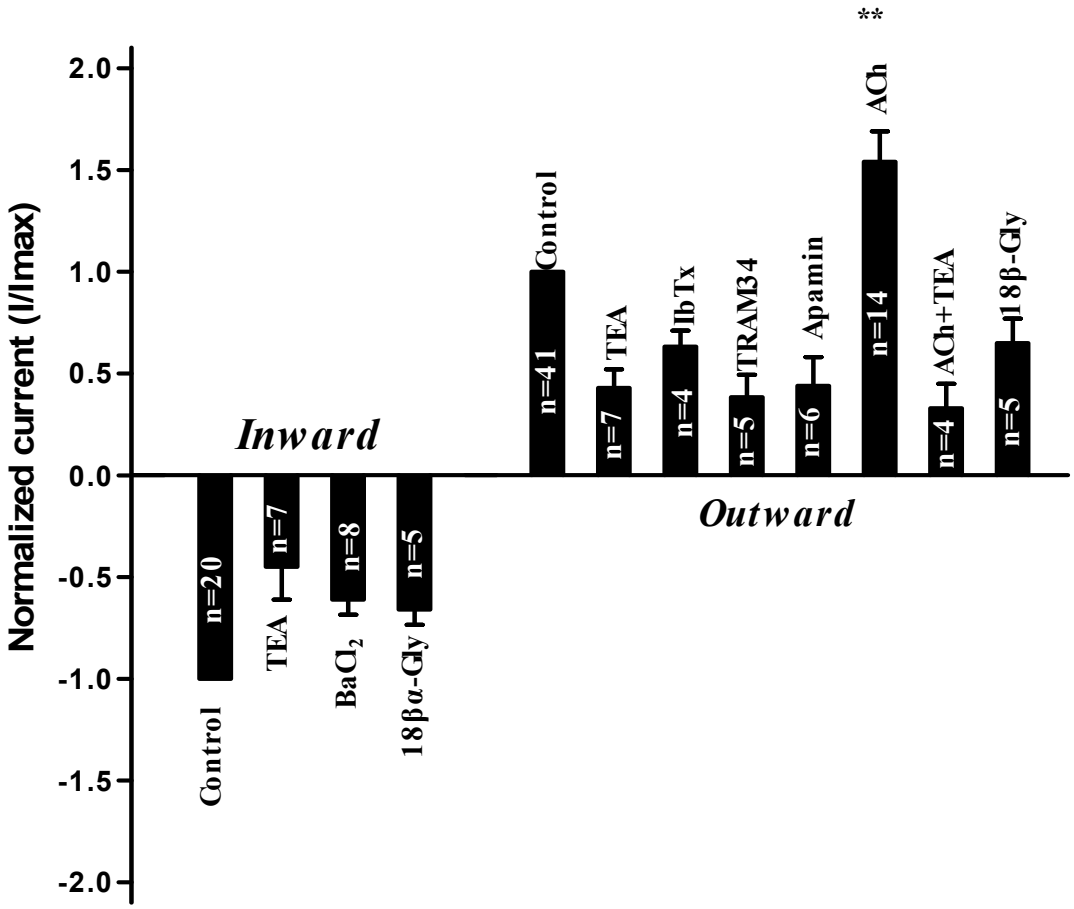

Figure 23 Effect of different K^+ channel blockers, ACh and 18 β-gly on inward and outward currents

Each bar corresponds to a different drug and bar amplitude represents the mean ± SEM. of the measurement normalized for the maximal effect obtained in control condition. The number of cells measured for each drug is located on each bar. For these experiments EC were superfused with PSS during control condition, and with 10 mM TEA; 30 μM Ba^{2+}; 25 μM 18 β-gly; 10 mM TEA; 500 nM apamin; 100 nM TRAM34; 100 nM IbTx; 10 μM ACh; 10 μM; ACh plus 10 mM TEA and 25 μM 18 β-gly, respectively.

VI. Discussion

A. Dendritic cells

Differentiation and maturation of DC from monocyte is linked to marked phenotypic, gene expression and functional changes (Gogolak, Rethi et al. 2003). The major function of IDC is to internalize exogenous soluble and particulate tissue components and collect stimuli associated with environmental changes for delivering this molecular information to lymph node T lymphocytes. Mobilization and maturation of DC to highly efficient antigen presenting cells with the unique capability to prime antigen-specific T lymphocytes in peripheral lymphoid organs requires inflammatory and danger signals. Activation-induced changes of DC include the down regulation of some endocytic/phagocytic receptors; upregulation of specific sets of chemokine receptors, adhesion and co-stimulatory molecules; changes in morphology, cytoskeleton, mobility; and reorganization of the endo-lysosomal and MHC class II-rich intracellular compartments (Flores-Romo 2001). Here we describe a dramatic change in the plasma membrane expression of two specific ion channels i.e. Nav1.7 and Kv1.3 in the course of monocyte-derived DC maturation.

First time in the literature we demonstrated the presence and activity of voltage-gated Na^+ channels in the plasma membrane of IDC. The identification of the channel being responsible for the whole-cell current required both electrophysiological and molecular biological approach. Using PCR-based cloning we identified the Na^+ channels expressed in IDC as Nav1.7 encoded by the SCN9A gene, the cloned sequence did not match the sequence of any other VGSC. The Nav1.7 channel is classified as TTX sensitive; it is inhibited by nanomolar concentrations of TTX (Klugbauer, Lacinova et al. 1995). Our results are consistent with this, however, the affinity of the channels for TTX is somewhat lower (K_d=55 nM) than reported by Klugbauer et al for human Nav1.7 expressed in oocytes (K_d=25 nM) and much lower than for rat Nav1.7 (K_d=4 nM) (Sangameswaran, Fish et al. 1997). Although we do not know the explanation for these differences it must be noted that the affinities of toxins for ion channels obtained in different expression systems vary significantly (Panyi, Possani et al. 2006).

Regarding the biophysical parameters of gating, the previously published values for the voltage-dependence of steady-state activation of Nav1.7 are between −20 and −25 mV for

the $V_{m,a}$, regardless of the expression system used (Klugbauer, Lacinova et al. 1995; Sangameswaran, Fish et al. 1997; Vijayaragavan, O'Leary et al. 2001; Cummins, Dib-Hajj et al. 2004) and our results in IDC are compatible with those ($V_{m,a}$=−19.8 ± 3.0 mV). Fast inactivation kinetics of Nav1.7 is characterized by time constants in the order of 1 ms at voltages where the current is maximal (−10 to 0 mV) (Vijayaragavan, O'Leary et al. 2001; Cummins, Dib-Hajj et al. 2004), however, biphasic current decay has also been reported (Rush, Brau et al. 1998). This fast inactivation kinetics has only been achieved by co-expressing the Nav1.7 subunits with the auxiliary β_1 subunit, which accelerates the inactivation kinetics as much as 10-fold (Vijayaragavan, O'Leary et al. 2001). The fast inactivation kinetics reported in this study (0.70±0.09 ms at −10 mV (at maximal inward current) indicate that Nav1.7 might be in complex with a β_1 subunit in IDC, furthermore, the small size of IDC allow better voltage-clamp conditions as compared to oocytes, thereby resulting in apparently faster kinetics. The midpoint for the voltage-dependence of steady-state inactivation ($V_{m,i}$) obtained in this study is slightly more negative than reported by Cummins et al. (−73.6 mV) (Cummins, Dib-Hajj et al. 2004) but significantly more negative than −60.5 mV reported by Klugbauer et al. (Klugbauer, Lacinova et al. 1995) for the human Nav1.7 expressed in HEK cells in both studies. In the latter study KCl was used in the pipette filling solution whereas in our study and in Cummins et al. F^- was used as the major anion and F^- is known to shift the voltage dependence of steady state inactivation of Nav1.9 channels in the hyperpolarizing direction (Rugiero, Mistry et al. 2003). Other factors explaining the discrepancies might be the difference in $V_{m,i}$ obtained in various expression system (Klugbauer, Lacinova et al. 1995; Vijayaragavan, O'Leary et al. 2001) and native cells (Rush, Brau et al. 1998) and the difference in the pulse protocols and holding potentials applied in various studies. In summary, apart from slight differences, the biophysical and pharmacological properties of Nav1.7 currents recorded in IDC agree well with those reported for Nav1.7 in other preparations.

The α subunits of the Nav1.7 channel are expressed in the dorsal root ganglion neurons, sympathetic neurons, Schwann cells and neuroendocrine cells (Catterall, Goldin et al. 2005). Their physiological functions include action potential initiation and transmission in peripheral neurons in response to nociceptive stimuli. These channels are mainly responsible for mechanosensation and for the development of inflammatory pain (Nassar, Stirling et al. 2004). IDC reside primarily within or beneath of epithelial surfaces such as the skin, bronchial and gastrointestinal mucosal layers (Banchereau and Steinman 1998) and are also concentrated at peripheral nerve endings and endoneurium, which may suggest a possible

relationship between nociceptive stimuli and DC functions (Nestle, Zheng et al. 1993; Weiss and Nickoloff 1993).

The presence of voltage-gated Na^+ channels has been previously confirmed in cells derived from precursors of the myeloid lineage. TTX-sensitive Nav1.6 channels were studied in brain macrophages (microglias) where the inhibition of these channels with TTX significantly reduced the phagocytic activity of these cells and lead to the improvement of neuroinflammatory diseases (Craner, Damarjian et al. 2005). In another study, intracellular localization of Nav1.5 (TTX-insensitive) and Nav1.6 channels was described in human monocyte-derived macrophages, with no detectable cell surface expression of either of these channels (Carrithers, Dib-Hajj et al. 2007). Nav1.5 was shown to localize in the late endosome and TTX inhibited the phagocytosis and certain endosomal functions in this cell type. Although monocyte-derived dendritic cells studied in our experiments, microglia and macrophages all originate from a common myeloid precursor; these data suggest that different VGSC and specific localization of these channels is required for their dedicated functions.

We also demonstrated that IDC challenged by inflammatory stimuli changed the cell surface expression of ion channels, and thus the MDC are characterized by another set of specific channels. Real time RT-PCR demonstrated the expression of transcripts for Kv1.3 and Kv1.5 in MDC. This raises the possibility that a mixture of Kv1.3 and Kv1.5 homoteramers and Kv1.3/Kv1.5 heterotetramers might be responsible for the whole cell currents observed in MDC, similarly to bone marrow-derived macrophages (Vicente, Escalada et al. 2006; Villalonga, Escalada et al. 2007) and MDC of the central nervous system (Mullen, Rozycka et al. 2006). Based on the following considerations we argue that Kv1.3 determines the properties of the whole-cell currents in our study. *i.*) The whole-cell current displays single-exponential inactivation kinetics with a time constant of ~127 ms at +50 mV (**Figure 13** B and D), which is characteristic of Kv1.3 (Panyi, Sheng et al. 1995). Kv1.5 homoterameric channels, on the contrary, have very slow and biphasic inactivation kinetics with time constants of ~450 ms and 5s (Grissmer and Cahalan 1989). Kv1.3/Kv1.5 heterotetramers should have intermediate inactivation kinetics depending on the subunit stoichiometry and calculated form the cooperative interaction between subunits (Panyi, Sheng et al. 1995). Thus, the whole-cell current carried by five different species of channels (homotertameric Kv1.3 and Kv1.5 and three types of heterotetramers should have complex decay kinetics with slow components in it (Panyi, Sheng et al. 1995), which was clearly not the case for whole-

cell currents in MDC and homotetrameric Kv1.5 channels are ~30-fold less sensitive to TEA than Kv1.3 homotetramers (Gutman, Chandy et al. 2005). As all four subunits contribute equally to the TEA binding site (Heginbotham and MacKinnon 1992) Kv1.3/Kv1.5 heterotetramers should have lower affinity for TEA than Kv1.3 homotetramers. Again, our results show the contrary, i.e., ~50% of the whole cell current is inhibited by 10 mM TEA (**Figure 14**), which is characteristic of Kv1.3 channels.

Kv1.5 channels are resistant to inhibition by scorpion toxins used in this study (ChTx, MgTx) (Grissmer, Nguyen et al. 1994). Kv1.3/Kv1.5 heterotetramers are less sensitive to MgTx inhibition, depending on the subunit stoichiometry 3 to 100-fold decrease in the affinity was reported by Felipe and colleagues (Vicente, Escalada et al. 2006; Villalonga, Escalada et al. 2007). Thus, a significant proportion of Kv1.5 homo- or heterotetramers would result in a residual toxin-insensitive current even at a high toxin concentration, which otherwise blocks almost completely Kv1.3 channels. In contrast, we measured higher than 90% blockage of the whole cell current at 50 nM ChTx concentration (**Figure 15 B**) and a full block at 500 pM MgTx concentration (**Figure 15** D). The presence of the mixture of homo- and heterotetrameric channels would result in a significant deviation of the dose-response relationship from a model (eq. 6), in which a single species of channels interacts with a single inhibitory peptide. On the contrary, our dose-response relationships showed K_d values of 3.4 nM and 39.8 nM, for ChTx and MgTx, respectively, which values are characteristic for inhibition of Kv1.3 (Gutman, Chandy et al. 2005), and eq. 6 fits perfectly to the dose-response relationships (**Figure 15** B,D), thereby arguing against the existence of Kv1.5 homotetramers and Kv1.3/Kv1.5 heterotetramers in MDC. In conclusion, although mRNA specific for Kv1.5 can be found in both IDC and MDC and Western blot analysis confirmed the expression of Kv1.5 subunits in these cells the protein expression level is too small to affect the properties of whole cell current.

We can exclude the contribution of IK_{Ca1} channels (the Ca^{2+}-activated K^+ channel, which is expressed in many lymphoid cells) to the whole-cell current by the lack of the elevated cytosolic free Ca^{2+} concentration required for the activation of these channels (i.e., the pipette filling solution contined 11 mM EGTA and 140 mM F^-) (Grissmer, Nguyen et al. 1993).

Based on these arguments we conclude that Kv1.3 channels are responsible for the whole-cell outward current in MDC, and the properties of the current agree with those reported in the literature for Kv1.3 in human T cells (Cahalan, Chandy et al. 1985). Kv1.3 is involved in the regulation of membrane potential and Ca^{2+} signaling in lymphocytes, macrophages and

monocytes (Kim, Silver et al. 1996; Cahalan, Wulff et al. 2001; Qiu, Campbell et al. 2002) The expression of Kv1.3 channels are important in the activation of macrophages, where their blockade inhibits the secretion of TNF-α and IL-8 cytokines (Qiu, Campbell et al. 2002). Brain macrophages express another type of voltage-gated channel, the Kv1.5, which was proven not to be functional in bone marrow-derived macrophages (Vicente, Escalada et al. 2003). A recent study, however proposed that the K^+ currents seen in bone marrow-derived macrophages are due to the expression of three voltage gated channels: Kv1.3, Kv1.5 and Kv1.3/Kv1.5 heteromeric channels (Vicente, Escalada et al. 2006; Villalonga, Escalada et al. 2007). The oligomeric composition of functional VGPCs could have a crucial effect on intracellular signaling events, determining the macrophage-specific response upon different physiological stimuli (Vicente, Escalada et al. 2006). The presence an outward rectifying K^+ conductance was described in dendritic cells isolated from murine spleen(Fischer and Eder 1995) but the ion channel responsible for that current was not identified. A recent study showed the existence of Kv1.3-like and Kv1.5 currents in MDC of the central nervous system (Mullen, Rozycka et al. 2006). The lack of a Kv1.5 current in monocyte-derived MDC and its presence in MDC in the central nervous system raises the question whether Kv1.5 expression could be linked to a special function and distribution of these latter cells.

Although significant efforts have been made to demonstrate the inhibition of different functions of IDC (pinocytosis and phagocytosis) and MDC (cytokine release and induction of T cell proliferation) by TTX and MgTx, respectively, we failed to inhibit any of these functions by the toxins (not shown). These negative results, however do not exclude the biological role of the channels described in this study. For example, currently unknown factors in the culture medium might mask the biological effects, but not the inhibition of the currents. A similar phenomenon was described earlier, where the inhibition of proliferation of T lymphocytes by ChTx could only be demonstrated in serum-free medium, but not in a culture medium containing human AB serum (Price, Lee et al. 1989). A detailed analysis of the components revealed that the presence of IL-2 in the culture media can overcome the antiproliferative effects of ChTx in cultured T cells.

The CD34+ erythroleukemia cell line KG-1 has been intensively studied as a potential model of IDC, which can be stimulated with various cytokine coctails that result in DC-like phenotype and function (Hulette, Rowden et al. 2001; Hajas, Zsiros et al. 2004). This DC-like phenotype was revealed not just by morphology but also by the appearance of specific DC receptors – like CD83 (Hulette, Rowden et al. 2001). PKC activation of KG-1 cells

induced maturation in these cells as they were shown to enhance allogenic T-cell proliferation, upregulate 4-1BB ligand, FcγRIIa (CD32), FcγRI (CD64), as well as downregulated Ox40 ligand and CD43, a cell surface sialoglycoprotein of immature DC (Hulette, Rowden et al. 2001). Even though there are many phenotypic and functional similarities described between DC and KG-1 cell line, we demonstrated several similarities and differences between these cells. Although stimulated KG-1 cells were able to induce T cell proliferation and TCR-mediated apoptosis and secrete inflammatory cytokines nearly as efficiently as monocyte derived DC unstimulated KG-1 cells were less efficient to internalize both soluble and particulate materials compared to IDC (Hajas, Zsiros et al. 2004). This latter was attributed to decreased phagocytic capacity and more restricted expression of receptors mediating internalization of special ligands such as immune complexes or apoptotic bodies (Hajas, Zsiros et al. 2004). Our electrophysiological assay also revealed striking differences in the ion channel expression of DC and KG-1. We showed biophysically and pharmacologically that the IK_{Ca1} type Ca^{2+}-activated K^+ channel is expressed in both unstimulated and stimulated KG-1cells. On the contrary, the voltage-gated Nav 1.7 and Kv1.3 channels which were the characteristic channel-type of IDC and MDC, respectively, were not present on the KG-1 model cell line.

These data altogether suggest that KG-1 cell line may be used as a model of professional myeloid antigen presenting cells owing to its overlapping phenotypic and functional characteristics with DC, however their ion channel expression profile was markedly different from DC. This sets limitations to the interpretation of the data obtained using KG-1 regarding the factors influencing IDC→MDC maturation and physiological functions of IDC.

In summary, we demonstrated that the inflammation-induced maturation of monocyte-derived DC is accompanied by a substantial change in the cell surface expression of VGSCs. Such alterations are common in the course of the terminal differentiation of immune cells, and the identification of two DC-related ion channels with restricted expression and linked but opposing regulation in MDC may have an impact on the targeted modulation of the cross-talk of immune cells (Panyi, Varga et al. 2004). The Nav1.7 channels are known to be abundantly expressed in the peripheral nervous system, but their presence in the plasma membrane of IDC is unique in the immune system. As VGSCs of non-excitable immune cells are considered to play a role in phagocytosis and migration, that are principal functions of IDC, the selective blockade of VGSCs can be a useful tool to modulate MDC functions. The presence of Kv1.3 channels in MDC is not surprising as Kv1.3 is probably responsible for

adjusting membrane potential, and through this may control Ca^{2+} signaling pathways during the activation of these cells. Further investigation of the specific function of these channels, as well as the regulation of intracellular Ca^{2+} signaling during the maturation process may open up new avenues for targeting DC-directed T lymphocyte activation, polarization and differentiation for immunomodulation.

B. Endothelial cells

Vascular endothelium forms a unique signal transduction surface as they pave the inner surface of the whole vascular tree. They create an ideal surface for the blood flow; they prevent blood clotting as well as they have thrombogenic activity. They are involved in the immune responses as they present antigens on their surface and facilitate the migration of inflammatory cells. Their regulatory effect on the underlying smooth muscle adjusts the vascular tone, and therefore controls the blood pressure. These multiple functions are mediated by the production and the release of variety of vasoactive compounds. In this process the control of $[Ca^{2+}]_i$ is one of the most important regulating factor. Although Ca^{2+} signaling is very well conserved throughout the phylogenetic tree, we still do not understand how this mechanism is able to rule specific EC responses. Ca^{2+} signal in EC is formed by the release of Ca^{2+} from intracellular Ca^{2+} stores as well as by the entry of Ca^{2+} via plasma membrane channels. A numbers of Ca^{2+} entry channels have been described (NSC, SOC, CCE), but their exact influence on the change is $[Ca^{2+}]_i$, is not known (Rusko, Tanzi et al. 1992; Haburcak, Wei et al. 1997). Ion channels contributing to the maintenance of the membrane potential are also abundantly present in EC. Their hypothetic role is the modulation of Ca^{2+} influx by changing the membrane potential in response to various external signals. The membrane potential is determined by K^+ and Cl^- channels, like K_{ir}, BK_{Ca}, IK_{Ca1}, SK_{Ca}, K_{ATP}, VRAC, Ca^{2+}-activated Cl^- channels, high-conductance Cl^- channels and CFTR (Nilius and Droogmans 2001).

Apart from the existence of numerous different studies describing ion-channels in EC, nowadays, the question about the role of these channels in vascular biology is still open. From a medical point of view there are certain diseases (e.g. atherosclerosis, hypertension, vascular inflammation, metastasic cascade) where pathophysiology could be answered through the better understanding of EC's physiology. Ion channels can serve as molecular

targets for new medications. To be able to use molecules acting on ion channels properly, we need to define clearly how these channels function under physiological circumstances. Knowing the fact how EC changes its ion channel and surface molecule expression in response to a slight change in the surrounding environment, in the future we need to focus on the development of new experimental setups, that would take us closer to physiological conditions. Physiologic conditions do not simply mean the culture EC with VSMC or with extracellular matrix, but there are several other factors that have to be considered during measurements. For instance mechanical forces associated with blood flow play an important role not just in the regulation of vascular tone, but also in vascular remodeling, and in the development of atherosclerosis. Endothelial cells are continuously exposed to mechanical stress and pressure as they play a key-role in shear-dependent vascular changes (Nakao, Ono et al. 1999; Brakemeier, Kersten et al. 2003). Shear stress can be involved in both physiologic and pathophysiologic vascular changes. Maintenance of a physiologic, laminar shear stress is known to be crucial for normal vascular functioning, which includes the regulation of vascular caliber as well as inhibition of thrombosis and inflammation of the vessel wall (Galbraith, Skalak et al. 1998). Non-laminar flow promotes changes to endothelial gene expression, cytoskeletal arrangement, wound repair, leukocyte adhesion, and because of these oscillatory flows are associated with atheroma formation and vessel wall remodeling. Thus, shear stress is critically important in regulating the atheroprotective, normal physiology as well as the pathobiology (Galbraith, Skalak et al. 1998).

Our experiments showed the expression and characteristics of different K^+ currents recorded '*in situ*' from the EC layer of the rat superior mesenteric artery. Many electrophysiological studies have been conducted on EC, but our goal was to provide an experimental approach that would lead to a better understanding of vascular electrophysiology by creating far more physiological circumstances. We demonstrated that using the patch clamp technique we were able to record ionic currents on a tissue, rather than in isolated EC. We set up and optimized the microvascular myograph for the studied vessels, where EC maintained their connections with each other as well as with the underlying VSMC. This set up may avoided potential alterations of ion channel expression induced by cell isolation or culturing.

Neurobiotin staining proved that we are recording currents from EC (**Figure 17**) and that EC remained electrically coupled through gap junctions to form a functional syncytium. Diffusion of neurobiotin from EC to VSMC was not observed, however the absence of

neurobiotin dye transfer to VSMC does not preclude electrical coupling between both cell types (Beny and Gribi 1989; Beny 1999; Yamamoto, Klemm et al. 2001). Due to the low resolution we could not accurately measure the size of single EC, but in previous studies it was measured to be around 20-40 μm (Yamamoto, Klemm et al. 2001).

Inhibition of gap junction channels with 18β-gly resulted in a significant decrease in the amplitude of inwardly and outwardly directed currents, which argues for a network of electrically coupled EC. Since gap junction functions as a low resistance - high conductance pathway, the EC layer form a functional syncytium, coordinating membrane potential changes along a segment of vessel, thus producing uniform cellular responses. Longitudinal signaling may be complemented by radial movement of currents between EC and VSMC cells via MEGJ located at the EC-VSMC interface and coordinates vasomotor tone (Figueroa, Isakson et al. 2004).

By using the '*in situ'* patch-clamp technique we identified electrophysiologically and pharmacologically different K^+ channels, such as K_{ir}, SK_{Ca}, IK_{Ca1} and BK_{Ca} in the rat superior mesenteric artery EC.

It is known from the literature that the expression of K^+ channels varies between different EC types, however one of the most widely described ion channel on EC is K_{ir} (Nilius, Viana et al. 1997; Nilius and Droogmans 2001; Crane, Walker et al. 2003; Haddy, Vanhoutte et al. 2006), which controls the resting membrane potential in non-stimulated cells. In our study we also demonstrated the presence of K_{ir}, which was evoked by voltage steps to hyperpolarizing potentials from the holding potential of −60 mV and was demonstrated to be sensitive to Ba^{2+} (**Figure 19**). The activation of the inward currents could be evoked by voltage steps to hyperpolarizing potentials from the holding potential of −60 mV. This is virtually in contrast to the behavior of K_{ir} channels which are conducting current at membrane potentials more negative than the equilibrium potential of K^+ (−87 mV in this study). The most important explanation for this inconsistency is that compensation for ohmic leak was not implemented in the records. Several non-voltage gated channels are expressed in EC which do not allow a clear reference voltage for leak subtraction. The presence of leak, in general, shifts the reversal potential of the whole cell currents to more positive values than the equilibrium potential for K^+ calculated from the Nernst equation. Another hallmark of K_{ir} is the lack of significant K^+ currents above the equlibrium potential of K^+. This feature of K_{ir} could not be demonstrated in this study due to the presence of other non-voltage gated K^+ channels, e.g. IK_{Ca1}. channels are characterized a quasi linear I-V relationship, i.e., outward K^+ current is

conducted by these channels above the equilibrium potential of K^+ thereby preventing the recording of an I-V relationship typical for K_{ir}.

In freshly isolated EC and VSMC of the rat mesenteric artery, K_{ir} currents are described to be exclusively expressed in EC, where they have a maximum amplitude of −190±16 pA at −150 mV (Crane, Walker et al. 2003). There have been few studies demonstrating the presence of Kir channels on isolated VSMC as well (especially on small arteries or arterioles) (Quayle, Nelson et al. 1997), however K_{ir} currents have been mostly reported on isolated EC. Crane et al. demonstrated that in the rat mesenteric artery the removal of endothelium eliminates the sensitivity to Ba^{2+} suggesting that in this vascular bed K_{ir} currents are expressed in the EC layer (Crane, Walker et al. 2003).

In our present multicellular preparation we also recorded K_{ir} currents with maximum amplitude of 1148±189 pA at -200 mV, and of 714±114 pA at -160 mV, which express sensitivity to Ba^{2+} as well. Taking into account the difference in the amplitude of currents, we might conclude that in the present multicellular preparation K_{ir} currents could spread through gap junctions from neighboring EC that are electrically coupled to the EC under recording. This conclusion is supported by **Figure 23** where the reduction of the total inward current is observed by uncoupling of the cells using 18β-gly without altering the capacitance-normalized current density.

The presence of SK_{Ca} and IK_{Ca1} channels on EC were recorded in our study, and they have also been widely reported on both cultured and freshly isolated small arteries in the past (Crane, Walker et al. 2003; Ledoux, Werner et al. 2006). In freshly isolated mouse aorta EC, the application of apamin plus ChTx inhibited a substantial fraction (44%) of the K^+ currents at +80mV (Ledoux, Bonev et al. 2008). In EC of the rat carotid artery, the selective IK_{Ca1} blocker TRAM34 reduced the current to 60-70% of the maximal current amplitude under control conditions (Eichler, Wibawa et al. 2003). These values are similar to those obtained in the present study, where the blockade with either apamin or TRAM34 inhibited the current to 55-60% and 60-70%, respectively, of the maximal current amplitude under control conditions, suggesting that a significant portion of the overall membrane K^+ conductance in intact EC is carried by SK_{ca} and IK_{Ca1} channels. Activation of these channels and/or EC hyperpolarization were demonstrated to elicit EDHF mediated responses in the past (Crane, Gallagher et al. 2003). Moreover, the ACh-mediated increase of TEA-sensitive K^+ currents

suggests the contribution and the activation of K_{Ca} currents significantly contributes to the overall membrane K^+ conductance.

In the rat mesenteric artery, ACh increases EC $[Ca^{2+}]_i$ by the release of Ca^{2+} from intracellular stores as well as by Ca^{2+} influx through plasma membrane leading to the activation of SK_{Ca} and IK_{Ca1} channels, which is followed by increased NOS activity and formation of NO (Stankevicius, Lopez-Valverde et al. 2006). In rat mesenteric artery, the expression of BK_{Ca} channels has been described to be restricted to VSMC (Mistry and Garland 1998), thereby the sensitivity of our outward current to IbTx could potentially imply either the presence of BK_{Ca} on EC or could imply that electrical coupling between EC and VSMC exist through MEGJ. This latter could indicate that membrane currents recorded from intact EC might be modulated by BK_{Ca} currents expressed in VSMC via MEGJ, which is in agreement with other previous reports that demonstrated bi-directionally coupling between the two cell layers (Beny 1999; Dora and Garland 2001). This communication could occur via direct spreading of depolarization and hyperpolarization or with the movement of other signaling molecules such as Ca^{2+} and IP_3 that can diffuse from one cell type to another (Dora and Garland 2001).

In conclusion, intact EC are coupled to each other through homocellular gap junctions to form a functional syncytium. K_{ir} as well as SK_{Ca}, and IK_{Ca1} channels coordinate membrane potential changes along the vessel wall and control VSM tone through MEGJ. Furthermore, our recorded BK_{Ca} currents on rat mesenteric artery could potentially arise from VSMC and can modulate EC membrane currents through MEGJ.

In summary the advantages of the experimental approach are the minimal disturbance of EC, which retain their fine relationship with their neighboring cells. Ion channels expression in EC make an important contribution to control the vascular tone *in vivo*; thus impaired function of these channels may play an important role in a range of diseases related to endothelial dysfunction and thus could blunt vasodilatation. Our results show that in the rat mesenteric artery, EC express K_{ir} currents that maintain membrane potential as well as SK_{Ca} and IK_{Ca1} currents, which could mediate the EC hyperpolarization. ACh increases TEA-sensitive K^+ currents, which are also involved in EC hyperpolarization. High conductance BK_{Ca} currents were recorded from the EC layer, which could indicate that the VSMC hyperpolarization is transmitted to the EC layer through MEGJ. Further, EC and

VSMC are in a sense both detectors and effectors, and the activation of each cell type leads to coordinated responses in the other (Figueroa, Isakson et al. 2004).

Our future goal is to further investigate the exact role of these channels in Ca^{2+} signaling and vasodilation. Although the complex function of EC along with the network of these cells creates challenges in circulatory research, with these *in situ* results we are confident that our work contributes significantly to the current understanding of EC physiology and the method described here will facilitate further electrophysiological and functional studies done on EC.

VII. Summary

Cells rapidly adjust their gene and ion channel expression upon the change of extracellular environment. To obtain valid measurements it is important to use models closest to the *in vivo* systems. In this work we focused on the characterization of ion channels on two different cell types, the human dendritic cells (DC) and the endothelial cells (EC) of the arteria mesenterica superior in rats in the most physiologic circumstances. We also used a DC model cell line (KG-1) during our electrophysiological studies to compare the obtained currents to that of DC. In the immune system VGPC, K_{ir}, and K_{Ca} channels have been described to play a major role in controlling the membrane potential and regulating intracellular Ca^{2+} signaling pathways required for proliferation and differentiation. In this study for the first time we described that immature monocyte-derived DC express voltage-gated Na^+ channels (Nav1.7). Transition from the immature to a mature state in DC however was accompanied by the down-regulation of Nav1.7 expression and the up-regulation of voltage-gated Kv1.3 K^+ channels. The presence of Kv1.3 is common for immune cells; hence, selective Kv1.3 blockers may emerge as candidates for inhibiting various functions of mature DCs that involve their migratory, cytokine-secreting, and T cell-activating potential. Both unstimulated and stimulated KG-1 cells expressed K_{Ca} only, which makes them not an ideal model for electrophysiological studies on DC.

EC function could be considerably altered during the process of isolation and cell culture. Previous electrophysiological studies on EC were conducted on isolated or cultured cells, ignoring the complex and fine network of EC and vascular smooth muscle. We developed a method that allows identifying and characterizing the ion channels of EC in their native environment. Rat mesenteric arteries mounted as ring preparations in a microvascular myograph for recording whole cell currents under '*blind*' patch clamp technique. Neurobiotin staining demonstrated that intact EC are electrically coupled through gap junctions and 18β-gly gap junction blocker decreased the outward and inward currents registered. We observed K_{ir} currents sensitive to $BaCl_2$, K_{Ca} currents of small (SK_{Ca}), intermediate (IK_{Ca1}) and high conductance (BK_{Ca}) that were sensitive to apamin, TRAM 34 and IbTx, respectively. Moreover, Ach increased outwardly directed K^+ currents that were sensitive to TEA. Under physiological circumstances K_{ir} current is involved in maintaining the resting membrane potential, where SK_{Ca} and IK_{Ca1} are mainly responsible for membrane hyperpolarization. The BK_{Ca} current reported in this study may arise from the vascular smooth muscle layer and potentially influence EC membrane potential via myoendothelial transfer of current.

VIII. Összefoglalás

A sejtek gyorsan alkalmazkodnak az extracelluláris környezet megváltozásához gén- és ioncsatorna expressziójuk módosításával. Élettani szempontból helytálló mérések végzéséhez fontos olyan modelleket alkalmazni, melyek az *in vivo* rendszerekhez a legközelebb állnak. Munkánkban két különböző sejttípus, a humán dendritikus sejt (DC sejt) és a patkány arteria mesenterica superiorból származó endotélsejt (EC sejt) ioncsatornáit jellemeztük élettani körülmények között. Elektrofiziológiai vizsgálataink során egy DC modellként használt sejtvonalat (KG-1) is vizsgáltunk, és az azon kapott áramokat összehasonlítottuk a DC sejteken mértekkel. Az immunrendszerben a feszültség-kapuzott K^+ csatornák a K_{ir}, és K_{Ca} csatornák határozzák meg a membránpotenciált és az intracelluláris Ca^{2+} jelátviteli útvonalak szabályozását, melyek a proliferációhoz és differenciálódáshoz szükségesek. Munkánkban elsőként írtuk le, hogy az éretlen monocita-eredetű DC sejtek feszültség-függő Na^+ csatornát expresszálnak (Nav1.7). Az éretlenből érett DC sejtté történő átalakulás azonban a Nav1.7 expresszió megszűnésével, és feszültség-függő Kv1.3 K^+ csatornák expressziójával jár. A Kv1.3 jelenléte gyakori immunsejtekben, így a kísérleteink alapján a szelektív Kv1.3 blokkolók szerephez juthatnak az érett DC sejtek különböző funkcióinak gátlásában, mint pl. migráció, citokin szekréció és T-sejt aktiváló képesség.. Nem-stimulált és stimulált KG-1 sejtek egyaránt csak K_{Ca} csatornát expresszálnak, emiatt elektrofiziológiai vizsgálatokhoz nem tekintjük a DC sejtek ideális modelljének. Az EC sejtek működését jelentősen befolyásolják az izolálás és a sejttenyésztés körülményei. A korábbi elektrofiziológiai mérések izolált vagy tenyésztett EC sejteken történtek, figyelmen kívül hagyva az EC sejtek és a vaszkuláris simaizomsejtek komplex és finoman összehangolt működését. Kifejlesztettünk egy olyan módszert, mely lehetővé teszi az EC sejtek ioncsatornáinak jellemzését azok természetes környezetében. Ehhez patkány mesenteriális artériát gyűrű preparátumként erősítettük mikrovaszkuláris miográfra, majd teljes-sejt (whole-cell) áramokat mértünk '*blind*' patch-clamp technikával. Neurobiotin jelöléssel bizonyosodtunk meg arról, hogy az intakt EC sejtek gap junction-on keresztül elektromos kapcsolatban állnak egymással. Az EC sejteken $BaCl_2$-ra szenzitív K_{ir} áramot, valamint kis (SK_{Ca}), közepes (IK_{Ca1}) és nagy konduktanciájú (BK_{Ca}) Ca^{2+}-aktivált K^+ áramokat mértünk melyek rendre apaminra, TRAM 34-re és IbTx-ra voltak érzékenyek. Élettani körülmények között az K_{ir} áramnak a nyugalmi membránpotenciál fenntartásában van szerepe, míg az SK_{Ca} és IK_{Ca1} főleg a membrán hiperpolarizációját okozza. A munkában leírt BK_{Ca} áram a vaszkuláris simaizomrétegből eredhet, és mioendoteliális transzferrel esetleg befolyásolhatja az EC sejtek membránpotenciálját.

IX. References

1. Ackerman, A. L. and P. Cresswell (2003). "Regulation of MHC class I transport in human dendritic cells and the dendritic-like cell line KG-1." J Immunol 170(8): 4178-4188.
2. Akagawa, K. S., N. Takasuka, et al. (1996). "Generation of CD1+RelB+ dendritic cells and tartrate-resistant acid phosphatase-positive osteoclast-like multinucleated giant cells from human monocytes." Blood 88(10): 4029-4039.
3. Andrews, D. M., C. E. Andoniou, et al. (2005). "Cross-talk between dendritic cells and natural killer cells in viral infection." Mol Immunol 42(4): 547-555.
4. Ardavin, C., d. H. Martinez, et al. (2001). "Origin and differentiation of dendritic cells." Trends Immunol. 22(12): 691-700.
5. Aurrand-Lions, M., C. Johnson-Leger, et al. (2002). "Junctional adhesion molecules and interendothelial junctions." Cells Tissues Organs 172(3): 152-160.
6. Banchereau, J. and R. M. Steinman (1998). "Dendritic cells and the control of immunity." Nature 392(6673): 245-252.
7. Barakat, A. I. (1999). "Responsiveness of vascular endothelium to shear stress: potential role of ion channels and cellular cytoskeleton (review)." Int.J.Mol.Med. 4(4): 323-332.
8. Bennett, S. R., F. R. Carbone, et al. (1998). "Help for cytotoxic-T-cell responses is mediated by CD40 signalling." Nature 393(6684): 478-480.
9. Beny, J. L. (1999). "Information Networks in the Arterial Wall." News Physiol Sci. 14: 68-73.
10. Beny, J. L. and F. Gribi (1989). "Dye and electrical coupling of endothelial cells in situ." Tissue Cell 21(6): 797-802.
11. Brakemeier, S., A. Kersten, et al. (2003). "Shear stress-induced up-regulation of the intermediate-conductance Ca(2+)-activated K(+) channel in human endothelium." Cardiovasc.Res. 60(3): 488-496.
12. Brent, L. H., B. Rubenstein, et al. (1996). "Transmembrane potential responses during HL-60 promyelocyte differentiation." J Cell Physiol 168(1): 155-165.
13. Bukauskas, F. F., K. Jordan, et al. (2000). "Clustering of connexin 43-enhanced green fluorescent protein gap junction channels and functional coupling in living cells." Proc Natl Acad Sci U S A 97(6): 2556-2561.
14. Busse, R., I. Fleming, et al. (1993). "Signal transduction in endothelium-dependent vasodilatation." Eur.Heart J. 14 Suppl I: 2-9.

15. Cahalan, M. D., K. G. Chandy, et al. (1985). "A voltage-gated potassium channel in human T lymphocytes." J Physiol 358: 197-237.
16. Cahalan, M. D., H. Wulff, et al. (2001). "Molecular properties and physiological roles of ion channels in the immune system." J Clin Immunol 21(4): 235-252.
17. Caplan, M. J. (1997). "Membrane polarity in epithelial cells: protein sorting and establishment of polarized domains." Am J Physiol 272(4 Pt 2): F425-429.
18. Carrithers, M. D., S. Dib-Hajj, et al. (2007). "Expression of the voltage-gated sodium channel NaV1.5 in the macrophage late endosome regulates endosomal acidification." J Immunol 178(12): 7822-7832.
19. Catterall, W. A., A. L. Goldin, et al. (2005). "International Union of Pharmacology. XLVII. Nomenclature and structure-function relationships of voltage-gated sodium channels." Pharmacol.Rev. 57(4): 397-409.
20. Caux, C., C. Dezutter-Dambuyant, et al. (1992). "GM-CSF and TNF-alpha cooperate in the generation of dendritic Langerhans cells." Nature 360(6401): 258-261.
21. Caux, C., C. Massacrier, et al. (1994). "Activation of human dendritic cells through CD40 cross-linking." J.Exp.Med. 180(4): 1263-1272.
22. Cella, M., D. Scheidegger, et al. (1996). "Ligation of CD40 on dendritic cells triggers production of high levels of interleukin-12 and enhances T cell stimulatory capacity: T-T help via APC activation." J.Exp.Med. 184(2): 747-752.
23. Cestele, S. and W. A. Catterall (2000). "Molecular mechanisms of neurotoxin action on voltage-gated sodium channels." Biochimie 82(9-10): 883-892.
24. Chandy, K. G., T. E. DeCoursey, et al. (1985). "Electroimmunology: the physiologic role of ion channels in the immune system." J.Immunol. 135(2 Suppl): 787s-791s.
25. Chandy, K. G., T. E. DeCoursey, et al. (1985). "Ion channels in lymphocytes." J.Clin.Immunol. 5(1): 1-6.
26. Chandy, K. G., H. Wulff, et al. (2004). "K+ channels as targets for specific immunomodulation." Trends Pharmacol Sci 25(5): 280-289.
27. Chevrier, P., K. Vijayaragavan, et al. (2004). "Differential modulation of Nav1.7 and Nav1.8 peripheral nerve sodium channels by the local anesthetic lidocaine." Br J Pharmacol 142(3): 576-584.
28. Crane, G. J., N. Gallagher, et al. (2003). "Small- and intermediate-conductance calcium-activated K+ channels provide different facets of endothelium-dependent hyperpolarization in rat mesenteric artery." J.Physiol 553(Pt 1): 183-189.

29. Crane, G. J., S. D. Walker, et al. (2003). "Evidence for a differential cellular distribution of inward rectifier K channels in the rat isolated mesenteric artery." J.Vasc.Res. 40(2): 159-168.
30. Craner, M. J., T. G. Damarjian, et al. (2005). "Sodium channels contribute to microglia/macrophage activation and function in EAE and MS." Glia 49(2): 220-229.
31. Cummins, T. R., S. D. Dib-Hajj, et al. (2004). "Electrophysiological properties of mutant Nav1.7 sodium channels in a painful inherited neuropathy." J.Neurosci. 24(38): 8232-8236.
32. Czerniecki, B. J., C. Carter, et al. (1997). "Calcium ionophore-treated peripheral blood monocytes and dendritic cells rapidly display characteristics of activated dendritic cells." J Immunol 159(8): 3823-3837.
33. Dauplais, M., A. Lecoq, et al. (1997). "On the convergent evolution of animal toxins. Conservation of a diad of functional residues in potassium channel-blocking toxins with unrelated structures." J Biol Chem 272(7): 4302-4309.
34. Daut, J., N. B. Standen, et al. (1994). "The role of the membrane potential of endothelial and smooth muscle cells in the regulation of coronary blood flow." J Cardiovasc Electrophysiol 5(2): 154-181.
35. Davies, P. F., S. P. Olesen, et al. (1988). "Endothelial communication. State of the art lecture." Hypertension 11(6 Pt 2): 563-572.
36. De Wit, C. (2004). "Connexins pave the way for vascular communication." News Physiol Sci. 19: 148-153.
37. DeCoursey, T. E., K. G. Chandy, et al. (1985). "Voltage-dependent ion channels in T-lymphocytes." J.Neuroimmunol. 10(1): 71-95.
38. Dora, K. A. and C. J. Garland (2001). "Properties of smooth muscle hyperpolarization and relaxation to K+ in the rat isolated mesenteric artery." Am.J.Physiol Heart Circ.Physiol 280(6): H2424-H2429.
39. Dunbar, L. A. and M. J. Caplan (2001). "Ion pumps in polarized cells: sorting and regulation of the Na+, K+- and H+, K+-ATPases." J Biol Chem 276(32): 29617-29620.
40. Eichler, I., J. Wibawa, et al. (2003). "Selective blockade of endothelial Ca2+-activated small- and intermediate-conductance K+-channels suppresses EDHF-mediated vasodilation." Br.J.Pharmacol. 138(4): 594-601.
41. Esper, R. J., R. A. Nordaby, et al. (2006). "Endothelial dysfunction: a comprehensive appraisal." Cardiovasc.Diabetol. 5: 4.

42. Figueroa, X. F., B. E. Isakson, et al. (2004). "Connexins: gaps in our knowledge of vascular function." Physiology.(Bethesda.) 19: 277-284.
43. Fischer, H. G. and C. Eder (1995). "Voltage-gated K+ currents of mouse dendritic cells." FEBS Lett 373(2): 127-130.
44. Fischer, H. G. and C. Eder (1995). "Voltage-gated K+ currents of mouse dendritic cells." FEBS Lett. 373(2): 127-130.
45. Flores-Romo, L. (2001). "In vivo maturation and migration of dendritic cells." Immunology 102(3): 255-262.
46. Fozzard, H. A. and D. A. Hanck (1996). "Structure and function of voltage-dependent sodium channels: comparison of brain II and cardiac isoforms." Physiol Rev 76(3): 887-926.
47. Galbraith, C. G., R. Skalak, et al. (1998). "Shear stress induces spatial reorganization of the endothelial cell cytoskeleton." Cell Motil.Cytoskeleton 40(4): 317-330.
48. Gallin, E. K. (1991). "Ion channels in leukocytes." Physiol Rev. 71(3): 775-811.
49. Gallin, E. K. and L. C. McKinney (1988). "Patch-clamp studies in human macrophages: single-channel and whole-cell characterization of two K+ conductances." J.Membr.Biol. 103(1): 55-66.
50. Galy, A., M. Travis, et al. (1995). "Human T, B, natural killer, and dendritic cells arise from a common bone marrow progenitor cell subset." Immunity 3(4): 459-473.
51. Garcia-Calvo, M., R. J. Leonard, et al. (1993). "Purification, characterization, and biosynthesis of margatoxin, a component of Centruroides margaritatus venom that selectively inhibits voltage-dependent potassium channels." J Biol Chem 268(25): 18866-18874.
52. Germain, F., E. Fernandez, et al. (2003). "Morphometrical analysis of dendritic arborization in axotomized retinal ganglion cells." Eur.J.Neurosci. 18(5): 1103-1109.
53. Ghanshani, S., H. Wulff, et al. (2000). "Up-regulation of the IKCa1 potassium channel during T-cell activation. Molecular mechanism and functional consequences." J.Biol.Chem. 275(47): 37137-37149.
54. Gibson, M. C. and N. Perrimon (2003). "Apicobasal polarization: epithelial form and function." Curr Opin Cell Biol 15(6): 747-752.
55. Gogolak, P., B. Rethi, et al. (2003). "Targeting dendritic cells for priming cellular immune responses." J Mol Recognit 16(5): 299-317.
56. Goldstein, S. A. and C. Miller (1993). "Mechanism of charybdotoxin block of a voltage-gated K+ channel." Biophys J 65(4): 1613-1619.

57. Gordienko, D. V. and H. Tsukahara (1994). "Tetrodotoxin-blockable depolarization-activated Na+ currents in a cultured endothelial cell line derived from rat interlobar arter and human umbilical vein." Pflugers Arch 428(1): 91-93.
58. Grissmer, S. and M. Cahalan (1989). "TEA prevents inactivation while blocking open K+ channels in human T lymphocytes." Biophys J 55(1): 203-206.
59. Grissmer, S., A. N. Nguyen, et al. (1994). "Pharmacological characterization of five cloned voltage-gated K+ channels, types Kv1.1, 1.2, 1.3, 1.5, and 3.1, stably expressed in mammalian cell lines." Mol Pharmacol 45(6): 1227-1234.
60. Grissmer, S., A. N. Nguyen, et al. (1993). "Calcium-activated potassium channels in resting and activated human T lymphocytes. Expression levels, calcium dependence, ion selectivity, and pharmacology." J Gen Physiol 102(4): 601-630.
61. Guerder, S. and P. Matzinger (1992). "A fail-safe mechanism for maintaining self-tolerance." J.Exp.Med. 176(2): 553-564.
62. Gutman, G. A., K. G. Chandy, et al. (2005). "International Union of Pharmacology. LIII. Nomenclature and molecular relationships of voltage-gated potassium channels." Pharmacol.Rev. 57(4): 473-508.
63. Haburcak, M., L. Wei, et al. (1997). "Calcium-activated potassium channels in cultured human endothelial cells are not directly modulated by nitric oxide." Cell Calcium 21(4): 291-300.
64. Haddy, F. J., P. M. Vanhoutte, et al. (2006). "Role of potassium in regulating blood flow and blood pressure." Am.J.Physiol Regul.Integr.Comp Physiol 290(3): R546-R552.
65. Haefliger, J. A., P. Nicod, et al. (2004). "Contribution of connexins to the function of the vascular wall." Cardiovasc.Res. 62(2): 345-356.
66. Hajas, G., E. Zsiros, et al. (2004). "New phenotypic, functional and electrophysiological characteristics of KG-1 cells." Immunol.Lett. 92(1-2): 97-106.
67. Hamill, O. P., A. Marty, et al. (1981). "Improved patch-clamp techniques for high-resolution current recording from cells and cell-free membrane patches." Pflugers Arch. 391(2): 85-100.
68. Hart, D. N. (1997). "Dendritic cells: unique leukocyte populations which control the primary immune response." Blood 90(9): 3245-3287.
69. Heginbotham, L. and R. MacKinnon (1992). "The aromatic binding site for tetraethylammonium ion on potassium channels." Neuron 8(3): 483-491.

70. Hewett, P. W., J. C. Murray, et al. (1993). "Isolation and characterization of microvessel endothelial cells from human mammary adipose tissue." In Vitro Cell Dev.Biol.Anim 29A(4): 325-331.
71. Himmel, H. M., A. R. Whorton, et al. (1993). "Intracellular calcium, currents, and stimulus-response coupling in endothelial cells." Hypertension 21(1): 112-127.
72. Hodgkin, A. L. and A. F. Huxley (1952). "A quantitative description of membrane current and its application to conduction and excitation in nerve." J Physiol 117(4): 500-544.
73. Hoshi, T., W. N. Zagotta, et al. (1990). "Biophysical and molecular mechanisms of Shaker potassium channel inactivation." Science 250(4980): 533-538.
74. Hoyer, J., A. Distler, et al. (1994). "Ca2+ influx through stretch-activated cation channels activates maxi K+ channels in porcine endocardial endothelium." Proc Natl Acad Sci U S A 91(6): 2367-2371.
75. Hsu, S., P. J. O'Connell, et al. (2001). "Fundamental Ca2+ signaling mechanisms in mouse dendritic cells: CRAC is the major Ca2+ entry pathway." J.Immunol. 166(10): 6126-6133.
76. Hulette, B. C., G. Rowden, et al. (2001). "Cytokine induction of a human acute myelogenous leukemia cell line (KG-1) to a CD1a+ dendritic cell phenotype." Arch.Dermatol.Res. 293(3): 147-158.
77. Hulette, B. C., G. Rowden, et al. (2001). "Cytokine induction of a human acute myelogenous leukemia cell line (KG-1) to a CD1a+ dendritic cell phenotype." Arch Dermatol Res 293(3): 147-158.
78. Inaba, K., M. Inaba, et al. (1992). "Generation of large numbers of dendritic cells from mouse bone marrow cultures supplemented with granulocyte/macrophage colony-stimulating factor." J.Exp.Med. 176(6): 1693-1702.
79. Jackson, W. F. (2005). "Potassium channels in the peripheral microcirculation." Microcirculation. 12(1): 113-127.
80. Jacob, R., J. E. Merritt, et al. (1988). "Repetitive spikes in cytoplasmic calcium evoked by histamine in human endothelial cells." Nature 335(6185): 40-45.
81. Jonuleit, H., E. Schmitt, et al. (2001). "Dendritic cells as a tool to induce anergic and regulatory T cells." Trends Immunol. 22(7): 394-400.
82. Ju, X., G. Clark, et al. (2010). "Review of human DC subtypes." Methods Mol Biol 595: 3-20.

83. Kalman, K., M. W. Pennington, et al. (1998). "ShK-Dap22, a potent Kv1.3-specific immunosuppressive polypeptide." J Biol Chem 273(49): 32697-32707.
84. Kamouchi, M., D. Trouet, et al. (1997). "Functional effects of expression of hslo Ca2+ activated K+ channels in cultured macrovascular endothelial cells." Cell Calcium 22(6): 497-506.
85. Kiertscher, S. M. and M. D. Roth (1996). "Human CD14+ leukocytes acquire the phenotype and function of antigen-presenting dendritic cells when cultured in GM-CSF and IL-4." J Leukoc Biol 59(2): 208-218.
86. Kim, S. Y., M. R. Silver, et al. (1996). "Ion channels in human THP-1 monocytes." J.Membr.Biol. 152(2): 117-130.
87. Klugbauer, N., L. Lacinova, et al. (1995). "Structure and functional expression of a new member of the tetrodotoxin-sensitive voltage-activated sodium channel family from human neuroendocrine cells." EMBO J 14(6): 1084-1090.
88. Knot, H. J., P. A. Zimmermann, et al. (1996). "Extracellular K(+)-induced hyperpolarizations and dilatations of rat coronary and cerebral arteries involve inward rectifier K(+) channels." J.Physiol 492 (Pt 2): 419-430.
89. Lanzavecchia, A. (1998). "Immunology. Licence to kill." Nature 393(6684): 413-414.
90. Lavender, M. D., Z. Pang, et al. (2005). "A system for the direct co-culture of endothelium on smooth muscle cells." Biomaterials 26(22): 4642-4653.
91. Ledoux, J., A. D. Bonev, et al. (2008). "Ca2+-activated K+ channels in murine endothelial cells: block by intracellular calcium and magnesium." J.Gen.Physiol 131(2): 125-135.
92. Ledoux, J., M. E. Werner, et al. (2006). "Calcium-activated potassium channels and the regulation of vascular tone." Physiology.(Bethesda.) 21: 69-78.
93. Leonard, R. J., M. L. Garcia, et al. (1992). "Selective blockers of voltage-gated K+ channels depolarize human T lymphocytes: mechanism of the antiproliferative effect of charybdotoxin." Proc Natl Acad Sci U S A 89(21): 10094-10098.
94. Lewis, R. S. (2001). "Calcium signaling mechanisms in T lymphocytes." Annu Rev Immunol 19: 497-521.
95. Liu, Q. H., H. Bohlen, et al. (1999). "Expression and a role of functionally coupled P2Y receptors in human dendritic cells." FEBS Lett 445(2-3): 402-408.
96. Liu, Y., M. E. Jurman, et al. (1996). "Dynamic rearrangement of the outer mouth of a K+ channel during gating." Neuron 16(4): 859-867.

97. Livak, K. J. and T. D. Schmittgen (2001). "Analysis of relative gene expression data using real-time quantitative PCR and the 2(-Delta Delta C(T)) Method." Methods 25(4): 402-408.

98. Logsdon, N. J., J. Kang, et al. (1997). "A novel gene, hKCa4, encodes the calcium-activated potassium channel in human T lymphocytes." J Biol Chem 272(52): 32723-32726.

99. Loots, E. and E. Y. Isacoff (1998). "Protein rearrangements underlying slow inactivation of the Shaker K+ channel." J Gen Physiol 112(4): 377-389.

100. Mistry, D. K. and C. J. Garland (1998). "Nitric oxide (NO)-induced activation of large conductance Ca2+-dependent K+ channels (BK(Ca)) in smooth muscle cells isolated from the rat mesenteric artery." Br.J.Pharmacol. 124(6): 1131-1140.

101. Mombouli, J. V. and P. M. Vanhoutte (1999). "Endothelial dysfunction: from physiology to therapy." J.Mol.Cell Cardiol. 31(1): 61-74.

102. Mueller, D. L. (2010). "Mechanisms maintaining peripheral tolerance." Nat Immunol 11(1): 21-27.

103. Mullen, K. M., M. Rozycka, et al. (2006). "Potassium channels Kv1.3 and Kv1.5 are expressed on blood-derived dendritic cells in the central nervous system." Ann.Neurol. 60(1): 118-127.

104. Mullin, J. M. (2004). "Epithelial barriers, compartmentation, and cancer." Sci STKE 2004(216): pe2.

105. Mulvany, M. J. and N. Nyborg (1980). "An increased calcium sensitivity of mesenteric resistance vessels in young and adult spontaneously hypertensive rats." Br J Pharmacol 71(2): 585-596.

106. Nachman, R. L. and E. A. Jaffe (2004). "Endothelial cell culture: beginnings of modern vascular biology." J Clin Invest 114(8): 1037-1040.

107. Nakao, M., K. Ono, et al. (1999). "Mechanical stress-induced Ca2+ entry and Cl-current in cultured human aortic endothelial cells." Am.J.Physiol 276(1 Pt 1): C238-C249.

108. Nassar, M. A., L. C. Stirling, et al. (2004). "Nociceptor-specific gene deletion reveals a major role for Nav1.7 (PN1) in acute and inflammatory pain." Proc.Natl.Acad.Sci.U.S.A 101(34): 12706-12711.

109. Nestle, F. O., X. G. Zheng, et al. (1993). "Characterization of dermal dendritic cells obtained from normal human skin reveals phenotypic and functionally distinctive subsets." J.Immunol. 151(11): 6535-6545.

110. Nilius, B. and G. Droogmans (2001). "Ion channels and their functional role in vascular endothelium." Physiol Rev. 81(4): 1415-1459.

111. Nilius, B., F. Viana, et al. (1997). "Ion channels in vascular endothelium." Annu.Rev.Physiol 59: 145-170.

112. O'Connell, P. J., V. A. Klyachko, et al. (2002). "Identification of functional type 1 ryanodine receptors in mouse dendritic cells." FEBS Lett 512(1-3): 67-70.

113. Oike, M., G. Droogmans, et al. (1994). "Amplitude modulation of Ca2+ signals induced by histamine in human endothelial cells." Biochim Biophys Acta 1222(2): 287-291.

114. Olcese, R., R. Latorre, et al. (1997). "Correlation between charge movement and ionic current during slow inactivation in Shaker K+ channels." J Gen Physiol 110(5): 579-589.

115. Pahapill, P. A. and L. C. Schlichter (1992). "Modulation of potassium channels in intact human T lymphocytes." J Physiol 445: 407-430.

116. Panyi, G. (2005). "Biophysical and pharmacological aspects of K+ channels in T lymphocytes." Eur Biophys J 34(6): 515-529.

117. Panyi, G., L. D. Possani, et al. (2006). "K+ channel blockers: novel tools to inhibit T cell activation leading to specific immunosuppression." Curr Pharm Des 12(18): 2199-2220.

118. Panyi, G., Z. Sheng, et al. (1995). "C-type inactivation of a voltage-gated K+ channel occurs by a cooperative mechanism." Biophys J 69(3): 896-903.

119. Panyi, G., Z. Varga, et al. (2004). "Ion channels and lymphocyte activation." Immunol.Lett. 92(1-2): 55-66.

120. Parekh, A. B. (2010). "Store-operated CRAC channels: function in health and disease." Nat Rev Drug Discov 9(5): 399-410.

121. Parekh, A. B. and J. W. Putney, Jr. (2005). "Store-operated calcium channels." Physiol Rev 85(2): 757-810.

122. Pickl, W. F., O. Majdic, et al. (1996). "Molecular and functional characteristics of dendritic cells generated from highly purified CD14+ peripheral blood monocytes." J.Immunol. 157(9): 3850-3859.

123. Poggi, A., A. Rubartelli, et al. (1998). "Involvement of dihydropyridine-sensitive calcium channels in human dendritic cell function. Competition by HIV-1 Tat." J Biol Chem 273(13): 7205-7209.

124. Popp, R., J. Hoyer, et al. (1992). "Stretch-activated non-selective cation channels in the antiluminal membrane of porcine cerebral capillaries." J Physiol 454: 435-449.

125. Prakriya, M. and R. S. Lewis (2006). "Regulation of CRAC channel activity by recruitment of silent channels to a high open-probability gating mode." J Gen Physiol 128(3): 373-386.

126. Price, M., S. C. Lee, et al. (1989). "Charybdotoxin inhibits proliferation and interleukin 2 production in human peripheral blood lymphocytes." Proc.Natl.Acad.Sci.U.S.A 86(24): 10171-10175.

127. Qiu, M. R., T. J. Campbell, et al. (2002). "A potassium ion channel is involved in cytokine production by activated human macrophages." Clin.Exp.Immunol. 130(1): 67-74.

128. Quayle, J. M., M. T. Nelson, et al. (1997). "ATP-sensitive and inwardly rectifying potassium channels in smooth muscle." Physiol Rev. 77(4): 1165-1232.

129. Rauer, H., M. Pennington, et al. (1999). "Structural conservation of the pores of calcium-activated and voltage-gated potassium channels determined by a sea anemone toxin." J Biol Chem 274(31): 21885-21892.

130. Reid, S. D., G. Penna, et al. (2000). "The control of T cell responses by dendritic cell subsets." Curr.Opin.Immunol. 12(1): 114-121.

131. Reschner, A., P. Hubert, et al. (2008). "Innate lymphocyte and dendritic cell cross-talk: a key factor in the regulation of the immune response." Clin Exp Immunol 152(2): 219-226.

132. Rodriguez de la Vega, R. C. and L. D. Possani (2004). "Current views on scorpion toxins specific for K+-channels." Toxicon 43(8): 865-875.

133. Romani, N., S. Gruner, et al. (1994). "Proliferating dendritic cell progenitors in human blood." J.Exp.Med. 180(1): 83-93.

134. Roy, M., T. Waldschmidt, et al. (1993). "The regulation of the expression of gp39, the CD40 ligand, on normal and cloned CD4+ T cells." J.Immunol. 151(5): 2497-2510.

135. Rugiero, F., M. Mistry, et al. (2003). "Selective expression of a persistent tetrodotoxin-resistant Na+ current and NaV1.9 subunit in myenteric sensory neurons." J Neurosci 23(7): 2715-2725.

136. Rush, A. M., M. E. Brau, et al. (1998). "Electrophysiological properties of sodium current subtypes in small cells from adult rat dorsal root ganglia." J Physiol 511 (Pt 3): 771-789.

137. Rusko, J., F. Tanzi, et al. (1992). "Calcium-activated potassium channels in native endothelial cells from rabbit aorta: conductance, Ca2+ sensitivity and block." J Physiol 455: 601-621.

138. Ryncarz, R. E. and C. Anasetti (1998). "Expression of CD86 on human marrow CD34(+) cells identifies immunocompetent committed precursors of macrophages and dendritic cells." Blood 91(10): 3892-3900.

139. Sallusto, F. and A. Lanzavecchia (1994). "Efficient presentation of soluble antigen by cultured human dendritic cells is maintained by granulocyte/macrophage colony-stimulating factor plus interleukin 4 and downregulated by tumor necrosis factor alpha." J.Exp.Med. 179(4): 1109-1118.

140. Salomonsson, M., C. M. Sorensen, et al. (2004). "Calcium handling in afferent arterioles." Acta Physiol Scand 181(4): 421-429.

141. Sangameswaran, L., L. M. Fish, et al. (1997). "A novel tetrodotoxin-sensitive, voltage-gated sodium channel expressed in rat and human dorsal root ganglia." J Biol Chem 272(23): 14805-14809.

142. Schuurhuis, D. H., N. Fu, et al. (2006). "Ins and outs of dendritic cells." Int.Arch.Allergy Immunol. 140(1): 53-72.

143. Schuurhuis, D. H., S. Laban, et al. (2000). "Immature dendritic cells acquire CD8(+) cytotoxic T lymphocyte priming capacity upon activation by T helper cell-independent or -dependent stimuli." J.Exp.Med. 192(1): 145-150.

144. Schwab, A. (2001). "Function and spatial distribution of ion channels and transporters in cell migration." Am J Physiol Renal Physiol 280(5): F739-747.

145. Sekhar, M., H. Kotani, et al. (1996). "Retroviral transduction of CD34-enriched hematopoietic progenitor cells under serum-free conditions." Hum Gene Ther 7(1): 33-38.

146. St Louis, D. C., J. B. Woodcock, et al. (1999). "Evidence for distinct intracellular signaling pathways in CD34+ progenitor to dendritic cell differentiation from a human cell line model." J.Immunol. 162(6): 3237-3248.

147. Stankevicius, E., V. Lopez-Valverde, et al. (2006). "Combination of Ca2+ -activated K+ channel blockers inhibits acetylcholine-evoked nitric oxide release in rat superior mesenteric artery." Br.J.Pharmacol. 149(5): 560-572.

148. Steinman, R. M. and Z. A. Cohn (1973). "Identification of a novel cell type in peripheral lymphoid organs of mice. I. Morphology, quantitation, tissue distribution." J.Exp.Med. 137(5): 1142-1162.

149. Steinman, R. M., D. Hawiger, et al. (2003). "Tolerogenic dendritic cells." Annu.Rev.Immunol. 21: 685-711.

150. Stockwin, L. H., D. McGonagle, et al. (2000). "Dendritic cells: immunological sentinels with a central role in health and disease." Immunol.Cell Biol. 78(2): 91-102.

151. Suciu-Foca Cortesini, N., F. Piazza, et al. (2001). "Distinct mRNA microarray profiles of tolerogenic dendritic cells." Hum Immunol 62(10): 1065-1072.

152. Tare, M., H. A. Coleman, et al. (2002). "Glycyrrhetinic derivatives inhibit hyperpolarization in endothelial cells of guinea pig and rat arteries." Am.J.Physiol Heart Circ.Physiol 282(1): H335-H341.

153. Terlau, H. and W. Stuhmer (1998). "Structure and function of voltage-gated ion channels." Naturwissenschaften 85(9): 437-444.

154. Thurner, B., C. Roder, et al. (1999). "Generation of large numbers of fully mature and stable dendritic cells from leukapheresis products for clinical application." J.Immunol.Methods 223(1): 1-15.

155. Tousson, A., B. A. Van Tine, et al. (1998). "Characterization of CFTR expression and chloride channel activity in human endothelia." Am.J.Physiol 275(6 Pt 1): C1555-C1564.

156. Trinchieri, G. (2007). "Pillars of immunology: The birth of a cell type." J.Immunol. 178(1): 3-4.

157. Van Kooten, C. and J. Banchereau (1997). "Functions of CD40 on B cells, dendritic cells and other cells." Curr.Opin.Immunol. 9(3): 330-337.

158. Vargas, F. F., P. F. Caviedes, et al. (1994). "Electrophysiological characteristics of cultured human umbilical vein endothelial cells." Microvasc Res 47(2): 153-165.

159. Vicente, R., A. Escalada, et al. (2003). "Differential voltage-dependent K+ channel responses during proliferation and activation in macrophages." J.Biol.Chem. 278(47): 46307-46320.

160. Vicente, R., A. Escalada, et al. (2005). "Pattern of Kv beta subunit expression in macrophages depends upon proliferation and the mode of activation." J.Immunol. 174(8): 4736-4744.

161. Vicente, R., A. Escalada, et al. (2006). "Association of Kv1.5 and Kv1.3 contributes to the major voltage-dependent K+ channel in macrophages." J.Biol.Chem. 281(49): 37675-37685.

162. Vijayaragavan, K., M. E. O'Leary, et al. (2001). "Gating properties of Na(v)1.7 and Na(v)1.8 peripheral nerve sodium channels." J Neurosci 21(20): 7909-7918.

163. Villalonga, N., A. Escalada, et al. (2007). "Kv1.3/Kv1.5 heteromeric channels compromise pharmacological responses in macrophages." Biochem.Biophys.Res.Commun. 352(4): 913-918.

164. Voets, T., G. Droogmans, et al. (1996). "Membrane currents and the resting membrane potential in cultured bovine pulmonary artery endothelial cells." J Physiol 497 (Pt 1): 95-107.

165. Walsh, K. B., M. B. Wolf, et al. (1998). "Voltage-gated sodium channels in cardiac microvascular endothelial cells." Am J Physiol 274(2 Pt 2): H506-512.

166. Wan, H. and M. Dupasquier (2005). "Dendritic cells in vivo and in vitro." Cell Mol Immunol 2(1): 28-35.

167. Weiss, S. W. and B. J. Nickoloff (1993). "CD-34 is expressed by a distinctive cell population in peripheral nerve, nerve sheath tumors, and related lesions." Am.J.Surg.Pathol. 17(10): 1039-1045.

168. Wulff, H., P. A. Calabresi, et al. (2003). "The voltage-gated Kv1.3 K(+) channel in effector memory T cells as new target for MS." J Clin Invest 111(11): 1703-1713.

169. Wulff, H., M. J. Miller, et al. (2000). "Design of a potent and selective inhibitor of the intermediate-conductance Ca2+-activated K+ channel, IKCa1: a potential immunosuppressant." Proc.Natl.Acad.Sci.U.S.A 97(14): 8151-8156.

170. Yamamoto, Y., M. F. Klemm, et al. (2001). "Intercellular electrical communication among smooth muscle and endothelial cells in guinea-pig mesenteric arterioles." J.Physiol 535(Pt 1): 181-195.

171. Yang, Y., Y. Wang, et al. (2004). "Mutations in SCN9A, encoding a sodium channel alpha subunit, in patients with primary erythermalgia." J Med Genet 41(3): 171-174.

172. Zhou, L. J. and T. F. Tedder (1996). "CD14+ blood monocytes can differentiate into functionally mature CD83+ dendritic cells." Proc Natl Acad Sci U S A 93(6): 2588-2592.

173. Zunkler, B. J., B. Henning, et al. (1995). "Electrophysiological properties of human coronary endothelial cells." Basic Res Cardiol 90(6): 435-442.

174. Zweifach, A. and R. S. Lewis (1993). "Mitogen-regulated Ca2+ current of T lymphocytes is activated by depletion of intracellular Ca2+ stores." Proc Natl Acad Sci U S A 90(13): 6295-6299.

X. Publication list

Jelölt: Zsíros Emese

Neptun kód: E6PUPE

Doktori Iskola: Molekuláris Orvostudomány Doktori Iskola

A PhD értekezés alapjául szolgáló közlemények

1. **Zsíros, E.**, Kis-Tóth, K., Hajdú, P., Gáspár, R., Bielansk, J., Felipe, A., Rajnavölgyi, É., Panyi, G.: Developmental switch of the expression of ion channels in human dendritic cells.
J. Immunol. 183 (7), 4483-4492, 2009.
IF:5.646
DOI: http://dx.doi.org/10.4049/jimmunol.0803003

2. Hajas, G., **Zsíros, E.**, László, T., Hajdú, P., Somodi, S., Réthi, B., Gogolák, P., Ludányi, K., Panyi, G., Rajnavölgyi, É.: New phenotypic, functional and electrophysiological characteristics of KG-1 cells.
Immunol. Lett. 92 (1-2), 97-106, 2004.
IF:2.136
DOI: http://dx.doi.org/10.1016/j.imlet.2003.11.021

További Közlemények

3. Balogh, Z., Fóris, G., Kosztáczky, B., Paragh, G., Seres, I., **Zsíros, E.**, Kónya, G.: The concentration dependent biphasic effect of leptin on endogenous cholesterol synthesis in human monocytes.
Peptides. 28 (10), 2081-2083, 2007.
IF:2.368
DOI: http://dx.doi.org/10.1016/j.peptides.2007.07.004

4. Kosztáczky, B., Fóris, G., Paragh, G., Seres, I., **Zsíros, E.**, Koncsos, P., Balogh, Z.: Leptin stimulates endogenous cholesterol synthesis in human monocytes: New role of an old player in atherosclerotic plaque formation.

DOI: http://dx.doi.org/10.1016/j.biocel.2007.04.012
IF:4.009

5. Petrohai, Á., Nagy, G., Bősze, S., Hudecz, F., **Zsíros, E.**, Paragh, G., Nyárády, Z., Németh, P., Berki, T.: Detection of citrate synthase-reacting autoantibodies after heart transplantation: An epitope mapping study.
Transpl. Int. 17 (12), 834-840, 2005.
DOI: http://dx.doi.org/10.1007/~00147-004-0794-4
IF:1.797

The Candidate's publication data submitted to the Publication Database of the University of Debrecen have been validated by Kenezy Life Sciences Library on the basis of Web of Science, Scopus and Journal Citation Report (Impact Factor) databases.

14 Feb, 2011

XI. Keywords

Ion channel, patch clamp, in situ patch clamp, dendritic cell, endothelial cell, voltage-gated sodium channel, voltage-gated potassium channel, inward rectifying K^+ channel, calcium activated potassium channel

Tárgyszavak:

Ion csatorna, patch clamp, in situ patch clamp, dendritikus sejt, endotél sejt, feszültség-függő nátrium csatorna, feszültség-függő kálium csatorna, inward rectifying K^+ csatorna, kalcium aktivált kálium csatorna

XII. ACKNOWLEDGEMENTS

First of all I would like to thank to my supervisors, to György Panyi and to Luis Rivera de los Arcos for their continuous support and never ending patient during whole my work!
I thank them both for teaching me all the techniques, starting from the basics of patch clamping to the dissection of the rats and the use of microvascular myograph through the blind patch clamp technique. All the interpretations and evaluation of my data were done under their supervision, including the writing my publications and my dissertation.

I am also grateful to Pedro de la Villa at the University of Alcalá, for helping and coordinating my work with Luis Rivera, and for teaching me patch clamping in his laboratory. Only with his work and help could I incorporate myself in the work of vascular laboratory in Madrid.

I also thank to Lola Prieto for her help in my teaching process with the myograph, and for her enthusiasm that encouraged us during the difficulties.

I cannot thank enough to the electrophysiology laboratory in the University of Debrecen, especially to Zoltán Varga, Sándor Somodi, Ferenc Papp, Miklós Bagdány, Zoltan Krasznai and Cecilia Nagy for all their support during all the years we have spent together working.

XIII. Adnexa

Attached Publications:

Zsiros, E., Kis-Toth, K., Hajdu, P., Gaspar, R., Bielanska, J., Felipe, A., Rajnavolgyi, E., & Panyi, G. (2009). Developmental switch of the expression of ion channels in human dendritic cells. *J.Immunol.* **183**, 4483-4492.

Hajas, G., Zsiros, E., Laszlo, T., Hajdu, P., Somodi, S., Rethi, B., Gogolak, P., Ludanyi, K., Panyi, G., & Rajnavolgyi, E. (2004). New phenotypic, functional and electrophysiological characteristics of KG-1 cells. *Immunol.Lett.* **92**, 97-106